NOTE TO USERS

This reproduction is the best copy available.

UMI®

MODELING OF ETHYLENE POLYMERIZATION WITH ZIEGLER-NATTA CATALYST IN A BUBBLING FLUIDIZED BED REACTOR

by

Neda Felorzabihi

Bachelor of Chemical Engineering

University of Tehran

Tehran, Iran, 1998

A thesis

presented to Ryerson University

in partial fulfillment of the

requirements for the degree of

Master of Applied Science

in the Program of

Chemical Engineering

Toronto, Ontario, Canada, 2004

© Copyright by Neda Felorzabihi (2004)

UMI Number: EC52931

INFORMATION TO USERS

The quality of this reproduction is dependent upon the quality of the copy submitted. Broken or indistinct print, colored or poor quality illustrations and photographs, print bleed-through, substandard margins, and improper alignment can adversely affect reproduction.

In the unlikely event that the author did not send a complete manuscript and there are missing pages, these will be noted. Also, if unauthorized copyright material had to be removed, a note will indicate the deletion.

UMI®

UMI Microform EC52931
Copyright 2008 by ProQuest LLC.
All rights reserved. This microform edition is protected against unauthorized copying under Title 17, United States Code.

ProQuest LLC
789 E. Eisenhower Parkway
PO Box 1346
Ann Arbor, MI 48106-1346

Ryerson University requires the signatures of all persons using or photocopying this thesis. Please sign below, and give address and date.

iii

MODELING OF ETHYLENE POLYMERIZATION WITH ZIEGLER-NATTA CATALYST IN A BUBBLING FLUIDIZED BED REACTOR

Neda Felorzabihi, 2004

Master of Applied Science

Chemical Engineering Department

Ryerson University

Abstract

In the present study, a new dynamic fluidized bed reactor (FBR) model is developed to account for the effect of bubble growth in the bed height on the dynamic behaviour of the reactor and the molecular properties of the polymer product. The model takes into account the existence of solid catalyst in both phases and consequently, the occurrence of polymerization reaction in both bubble and emulsion phases. A dynamic two-phase model is employed for predicting the key hydrodynamic parameters of the bed. A comprehensive kinetic model for ethylene polymerization in the presence of multiple-site Ziegler-Natta catalyst is considered to describe the number and molecular weight averages and molecular weight distribution of polymer in the FBR. The hydrodynamic model and the kinetic model have been coupled and solved simultaneously to simulate the performance of the fluidized bed reactor.

The study incorporates the effects of the most important reactor parameters such as superficial gas velocity, mean particle size, inlet gas temperature, bubble size, recycle stream and chain transfer agent on the steady-state behaviour of the FBR. The proposed dynamic model is capable of predicting both the performance of the reactor and the polymer physicochemical properties.

iv

Acknowledgments

Dedication

This thesis is dedicated to my loving husband, Mohammad Pouran and to my parents, Malihe and Bahman Felorzabihi. Mohammad has given me his love, friendship, support and encouragement throughout our marriage. I could not have accomplished so much without him. My parents have always encouraged me and have been a major influence in making me the person that I am today.

Table of Contents

viii

List of Tables

xiv

xvi

Nomenclature

A Reactor cross-sectional area, cm^2

$[A]$ Cocatalyst concentration

Ar Archimedes number

A_{sf}^{j} Fraction of metal with j^{th} catalyst active site, mol metal/mol potential active site

$C^{*}(j)$ Concentration of jth potential active site, mol/cm^3

Cp_{g}^{*} Molar specific heat capacity, cal/mol/K

Cp_{p} Specific heat capacity of polymer, cal/g/K

d Diameter, cm

d_{0} Initial bubble size, cm

d_{be} Equilibrium bubble size, cm

d_{bm} Maximum stable bubble size, cm

d_{p} Particle diameter, cm

D Reactor diameter, cm

D_{g} Gas self-diffusion coefficient, cm^2/s

D_{H2} Hydrogen self-diffusion coefficient, cm^2/s

D_{te} Hydraulic diameter of bed, cm

E Activation energy

g Gravitational acceleration, cm/s^2

h Random bed height, cm

H Bed height, cm

$[H_2]$ Hydrogen concentration, mol/cm^3

H_{bc} Bubble to cloud heat transfer coefficient, $cal/cm^3/s/K$

H_{ce} Cloud to emulsion heat transfer coefficient, $cal/cm^3/s/K$

H_{be} Bubble to emulsion heat transfer coefficient, $cal/cm^3/s/K$

$k_{d}(j)$ Rate constant of spontaneous deactivation for j^{th} site, 1/s

$k_f(j)$ Formation rate constant for jth site, cm^3/mol/s

k_g Gas thermal conductivity, cal/cm/s/K

$k_i(j)$ Rate constant of initiation of jth site by cocatalyst, cm^3/mol/s

$k_p(j)$ Propagation rate constant for jth site, cm^3/mol/s

$k_{tfA}(j)$ Rate constant of chain transfer by cocatalyst for jth site, cm^3/mol/s

$k_{tfH}(j)$ Rate constant of chain transfer by hydrogen for jth site, cm^3/mol/s

$k_{tfm}(j)$ Rate constant of chain transfer by monomer for jth site, cm^3/mol/s

$k_{tfs}(j)$ Rate constant of spontaneous chain transfer for jth site, 1/s

K_{bc} Bubble to cloud mass transfer coefficient, 1/s

K_{ce} Cloud to emulsion mass transfer coefficient, 1/s

K_{be} Overall bubble to emulsion mass transfer coefficient (for monomer), 1/s

$K_{be,H2}$ Overall bubble to emulsion mass transfer coefficient (for hydrogen), 1/s

$m(j)$ Mass fraction of polymer produced with jth site

n_{or} Number of nozzles on the distributor plate

N_s Total number of active sites

$[M]$ Monomer concentration, mol/cm^3

$\overline{M_n}$ Number average molecular weight of "bulk" polymer, g/mol

$\overline{M_w}$ Weight average molecular weight of "bulk" polymer, g/mol

Mw Molecular weight of monomer, g/mol

r The length (in polymer units) of a polymer chain

$R^{\bullet}(0,j)$ Concentration of uninitiated sites of type "j' produced by formation reaction, mol/cm^3

$R^{\bullet}(r,j)$ Concentration of live polymer chains of length r at site j, mol/cm^3

$R_A^{\bullet}(1,j)$ Concentration of jth site produced by transfer to cocatalyst, mol/cm^3

$R_d(j)$ Concentration of deactivated jth site, mol/cm^3

$R_H^{\bullet}(0,j)$ Concentration of uninitiated jth site produced by transfer to hydrogen, mol/cm^3

$P(r, j)$ Concentration of dead polymer of chain length r produced at j^{th} site, mol/cm^3

Re   Reynolds number

$R_p(j)$ Overall rate of polymerization at j^{th} catalyst active site, mol/cm^3/s

$R_A(j)$ Rate of cocatalyst at j^{th} catalyst active site, mol/cm^3/s

$R_{H2}(j)$ Rate of chain transfer agent at j^{th} catalyst active site, mol/cm^3/s

T Temperature, K

t Time, s

u Velocity, cm/s

u_{br} Bubble rise velocity, cm/s

V Reactor volume, cm^3

$w(r, j)$ Weight chain length distribution of chains of length r at "j' catalyst active site

$\overline{X_n}$ Number average degree of polymerization

$\dashv\square$ Empty orbital (Figure 2.2)

Greek letters

δ Volume fraction of bubbles

Δf_i First forward difference

Δh Step size, cm

ΔH Heat of polymerization, cal/g

ε Mean voidage

$\lambda(j)$ Live polymer moment for j^{th} site, mol/cm^3

$\mu(j)$ Bulk polymer moment for j^{th} site, mol/cm^3

μ_g Viscosity, g/cm/s

ρ Density, g/cm^3

φ Correction factor

ϕ A geometrical constant in Equation (3.5)

ϕ_s Particle sphericity

$\tau(j)$ Ratio of the total rate of transfer to the total rate of propagation at j^{th} site

Subscripts and superscripts

0	Entrance or superficial conditions
b	Bubble property
e	Emulsion property
g	Gas property
i	Number of grid points
j	Type of catalyst active site
mf	Minimum fluidization conditions
$polym$	Polymer property
T	Terminal property
s	Solid property

CHAPTER 1: INTRODUCTION

Polyethylene (PE) is one of the largest synthetic commodity and engineering polymers and is widely used throughout the world for its versatile physical and chemical properties. Characteristics of polyethylene include excellent toughness, good tear and burst strength, excellent chemical resistance, translucency, low heat resistance and low price because of simple production processes. The wide range of PE properties gives rise to a wide range of applications including coatings, packaging, fibres, films, plastic-ware and automotive parts.

Polyethylene was originally produced by high-pressure, high-temperature free radical polymerization on commercial scale for the production of flexible polymer referred to as low-density polyethylene (LDPE). The invention of Ziegler-Natta catalysts in early fifty's led to the production of other polyethylene types such as: High-density polyethylene (HDPE) and linear low-density polyethylene (LLDPE). High-density polyethylene is a highly crystalline polymer with no long or short chain branching. Because of its crystalline structure, it produces more rigid polymer products in comparison with other types of polyethylene (Figure 1.1). LLDPE is a copolymer of ethylene and α-olefins. For the incorporation of these two monomers, the LLDPE polymer product has short chain branching and consequently, is less dense and less crystalline than HDPE.

Modern polyethylene plants are continuous processes using Ziegler-Natta catalyst in bulk, solution, slurry or gas phase. In particular, the gas phase polymerization process is one of the most modern and versatile techniques. Due to its technological and economical advantages, the gas phase polymerization has been challenging other processes particularly for market share. It offers several distinguished characteristics making it a unique process (Xie et al., 1994):

- It is a dry process since it does not involve any liquid in the reaction zone. Thus, it is free of mass and heat transfer limitations inherent to viscous slurry and bulk systems.
- The catalyst/polymer system in the gas phase fluidized bed reactor has a good heat transfer.

1

- This process can also produce polymers with a wide range of densities and molecular weight distributions (MWDs).

- Production of high comonomer content polymers, such as high impact ethylene-propylene copolymers is another major advantage of the gas phase process.

- There are no solvent removal costs.

Figure 1. 1: Schematic molecular structure of high-density polyethylene (HDPE)

Figure 1. 2: Schematic molecular structure of low-density polyethylene (LDPE)

1.1 Literature Review

This investigation requires the study of the hydrodynamic behaviour, heat/mass transfer, reaction rates and flow patterns in a conventional fluidized bed reactor (FBR) for predicting its characteristics and behaviour. In a gas-solid fluidized bed reactor, the flow and contacting patterns are important factors to study and model. Early models of gas-solid fluidized bed reactors were generated on simple contacting models and flow patterns such as plug, mixed, and dispersion flows. After the development of a two-region model by Toomey and Johnstone (1952), several models have been derived to describe their performance.

2

Hydrodynamic models interpret the behaviour of fluidized beds in physical terms such as bubble performance and gas jets behaviour. They include three-phase models (Kunii and Levenspiel, 1968) and two-phase models (Davidson and Harrison, 1963; Kato and Wen, 1969; Fryer and Potter, 1976). Some of the two-region models consider the cloud as a part of the bubble or the emulsion; others assume bubble, cloud, and emulsion as three different phases with the wake being a part of the cloud or the bubble.

McAuley et al. (1990) developed a model for gas phase ethylene copolymerization in a fluidized bed reactor using Ziegler-Natta catalyst with multiple active sites. Applying Stockmayer's bivariate distribution function to each active site, they calculated average molecular weights and copolymer distributions for ethylene copolymers.

Choi and Ray (1985) proposed a FBR model, based on the concept of two-phase fluidization. The model incorporates temperature and concentration variations within the gas bubble phase throughout the bed and interaction of separate emulsion and bubble phases. McAuley et al. (1994) revised the model of Choi and Ray (1985), constant mean bubble size model, establishing a maximum stable bubble size. In the model of McAuley et al. (1994) it is assumed that there is unrestricted heat and mass transfer rate between the bubble and emulsion phase. However, this assumption is valid when small bubbles are presented in the bed also when the rate of heat and mass transfer between phases is relatively high. In both studies the emulsion phase was considered to behave as a fully mixed reactor.

Hatzantonis et al. (2000) extended previous work on gas phase olefin polymerization reactors to account for the effects of varying bubble size. In their study, a comprehensive kinetic model was proposed for ethylene copolymerization in the presence of multi-site Ziegler-Natta catalysts. The study compared the proposed bubble growth model with the previous well-mixed and constant bubble size models. The constant bubble size model over-predicted the emulsion phase temperature and monomer conversion; the well-mixed model underestimated them, whereas the proposed model showed an intermediate behaviour.

Fernandes et al. (2000) studied the influence of prepolymerization on the behaviour of fluidized bed reactors, related mainly to the temperature and concentration gradients throughout the bed. They demonstrated that the use of prepolymerized catalyst particles could reduce the reaction activity in the catalyst-feeding region, leading to lower temperature gradient in the bed.

3

Fernandes et al. (2001a) proposed a new steady-state model incorporating interactions between separate bubbles, emulsion gas phase and emulsion solid particles. The main difference of this model with previous ones is that the emulsion phase is considered to be in a counter-current plug flow regime. It differs from conventional well-mixed fluidized bed models by assuming particle segregation within the bed.

Moreover, Fernandes et al. (2001b) developed a heterogeneous dynamic model describing the behaviour of fluidized bed reactors in polymer production. The model focuses mainly on the influence of polymer yield and variations in operational condition on reactor behaviour and polymer properties. More recently, Fernandes et al. (2002) studied the effect of mass diffusion into polymer particles in a fluidized bed reactor. Polymer particle growth was considered for low and high reactor residence times. The study showed that the influence of intraparticle mass transfer is important for low residence time but also insignificant for high residence time.

Alizadeh et al. (2004) developed a pseudo-homogeneous model for predicting the behaviour of a LLDPE fluidized bed reactor. In particular, average concentrations of particles were predicted based on a dynamic two-phase structure.

Most of the previous models assumed well-mixed flow regimes in the emulsion phase. It should be emphasized that such assumption is reasonable only for laboratory scale and pilot-plant fluidized bed reactors which are violently fluidized with a height to diameter ratio close to one (Lynch and Wanke, 1991). However, for industrial large-scale fluidized bed reactors with a bed height to diameter ratio much greater than one, this assumption is not acceptable. Besides, based on the correlation of Wu and Baeyens (1998), the mixing index in a fluidized bed reactor ranges from 0.4 to 0.5, which can be interpreted as a poor mixing. Further, according to the study of Davidson (1992) on pilot-plant and industrial reactors, it is much more plausible to consider a plug flow regime in both emulsion and bubble phases.

In spite of several efforts on modeling fluidized bed reactors (FBRs) for simple first order catalytic reactions, only a limited number of studies tried to model the catalytic gas-phase olefin polymerization in fluidized bed reactors. The gas phase polymerization process involves a complex physicochemical transition from gaseous monomer to solid polymer. Therefore, a deep understanding of transport phenomena and chemical reactions is required to model gas-phase fluidized bed reactors. The main objective of the current dynamic model is

4

to achieve a comprehensive understanding of the effect of operational parameters on performance of industrial polyethylene reactors and polymer properties. The model gives insight as to which conditions would optimize reactor performance in order to increase monomer conversion. Specifically, the model can verify how changes in reactor key parameters, such as superficial gas velocity, mean particle size, bubble size and inlet temperature, will influence the dynamic and steady state behaviour of FBRs.

The thesis is organized into six chapters. In Chapter 2 a brief description is presented for the PE gas phase polymerization process and the Ziegler-Natta catalyst system. Chapter 3 describes the hydrodynamics of bubbling fluidized bed and important empirical and semi-empirical correlations for predicting hydrodynamics key parameters. The reaction mechanism and kinetic model for ethylene polymerization with Ziegler-Natta catalyst is introduced in detail in Chapter 4. Dynamic molar species and energy balances are derived to predict concentration of the reactants (monomer, catalyst, cocatalyst, chain transfer agent), the reaction temperature and the average molecular properties of polymer (number average, molecular weight average and molecular weight distribution) in the fluidized bed reactor. Furthermore, the numerical approach to solve the dynamic model is described in detail. The complementary results and discussion for the application of the model and the effect of important parameters on the behaviour of the FBR are discussed in Chapter 5. Finally a summary concludes the thesis.

CHAPTER 2: DESCRIPTION OF THE POLYMERIZATION PROCESS

2.1 Polymerization Fluidized Bed Reactor

Fluidized beds utilizing solid catalysts for olefin polymerization have been long recognized as important manufacturing processes. The first fluidized reactor for gas phase olefin polymerization was constructed by Union Carbide Company. The process commonly called UNIPOL has become the dominant option for producing HDPE and LLDPE. In such a process, small catalyst particles (e.g. 20-80 μm in diameter) are continuously fed into the reactor (Hatzantonis et al., 1998). The catalyst can be injected at about 5-30 % of the bed height above the distributor plate and react with the incoming fluidizing gas. Therefore, the polymerization is started in the bed by means of the ascending gas stream comprising the gaseous reaction monomer and the bed can be maintained in a fluidized state. An inert diluent gas such as argon and nitrogen or a gaseous chain transfer agent like hydrogen is preferably used to carry the catalyst in the bed. The fluidized bed reactor consists of a reaction zone and a disengagement zone. The latter is normally larger in diameter than the polymerization zone to reduce the gas flow and facilitate the settling of solid particles. To maintain a stable fluidized bed, superficial flow through the bed is about 3-6 times the minimum flow required for the fluidization (Wagner et al., 1981). The reactor usually operates at pressure between 20-35 atm and temperatures between 86-110 °C for HDPE and 30-85 °C for LLDPE productions.

In industrial fluidized bed reactors it is necessary to use a fluidization grid or distributor plate to allow the gas spreading out in the bed. The grid can also act as a support for the bed in case the gas supply is cut-off. The polymer product is continuously withdrawn from the reactor at a point just above the distributor plate.

Polymerization of olefins is an exothermic reaction; it is therefore necessary to remove the heat of reaction. The heat of reaction is removed by unreacted gases exiting the bed that are subsequently compressed, cooled up to above recycle gas dew point and recycled back into the reactor. The temperature of the recycled gas mixture can be adjusted in a heat exchanger to maintain the FBR temperature at a desired value.

During start-up, the reaction zone is usually charged with a base of polymer particles before introducing monomer gas into the reactor. This can prevent the formation of localized "hot

6

spots" and distribute evenly the powder᾽ ᾽ ᾽᾽dyst. During reactor operation, the polymer product is continuously withdrawn at a ᾽᾽ ᾽o that the fluidized bed is maintained at a constant level (Figure 2.1). The polymer proᴗuct is continuously withdrawn at a point close to the distributor plate through the sequential operation of a pair of timed valves. While the second valve (V2) is closed, the first valve is opened to emit a plug of gas and product to the segregation zone between it and valve V1, which is then closed. Afterwards, the second valve is opened to deliver the product to an external recovery system. This valve is then closed to await the next product recovery operation (Wagner et al. 1981).
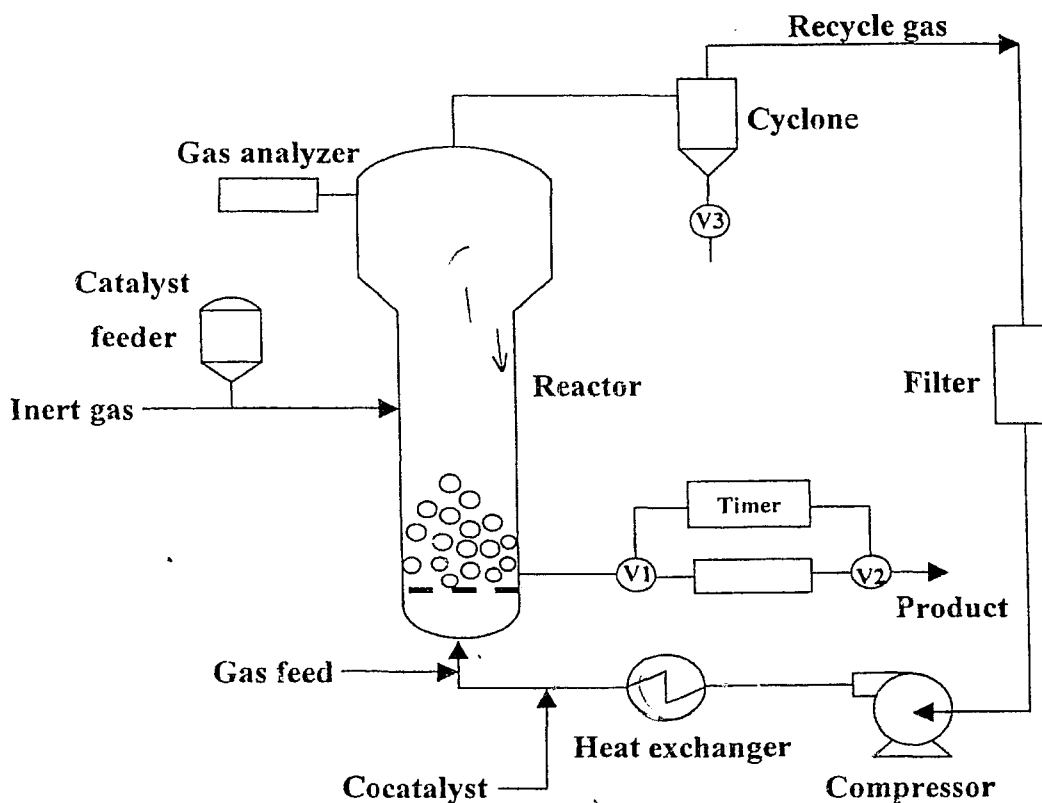
Figure 2.1: Schematic diagram of a fluidized bed reactor for olefin polymerization (Unipol process), Jorgensen et al., 1982.

7

2.2 Catalysts for Gas Phase Polymerization

Catalyst development plays an important role in polymerization of olefins especially in gas phase polymerization of ethylene. There are several requirements for industrial catalysts used in ethylene polymerization:

a) High productivity;

b) Proper kinetic behavior of polymerization;

c) Good catalyst morphology;

d) Good control of polymer morphology;

e) Easy feed to reactor;

f) Low cost and reproducible catalyst preparation;

g) Good comonomer incorporation.

Over the last decades, three major catalyst families have been used commercially in ethylene polymerization. These catalysts include titanium/vanadium-based catalyst (Ziegler-Natta catalyst), chromium oxide-based catalysts (Philips catalyst), and homogeneous catalysts (Metallocene catalyst). A typical industrial catalyst consists of active metal, modifiers and inert support (Xie et al., 1994). The Ti-based catalyst is usually prepared in three steps:

a) Preparation of a precursor containing Ti;

b) Incorporation of the precursor onto the support;

c) Activation of the catalyst.

These steps are usually accomplished by partial reaction of a catalyst and a cocatalyst. The main solid catalyst prepared using method 2 in Table 2.1, is then impregnated onto a porous support, such as silica or magnesium halide. The support is then impregnated with the precursor by dissolving the precursor in the electron donor compound. Afterwards, the solvent should be removed by drying at a temperature up to 80 °C (Jorgensen et al., 1982). When the size of catalyst is relatively small (method 3 in Table 2.1), the catalyst particles cannot be used directly in the bed. In this case, the precursor and cocatalyst are converted into prepolymer particles in a prepolymerization stage and then the prepolymer is fed to the bed.

8

Hence, the role of prepolymerization is to form a support for gas phase ethylene polymerization, instead of silica support.

Table 2.1 Operational methods to produce high activity catalyst (Karol, 1984)

1. Chemical anchoring to surface of support:

(a) $TiCl_4 / Mg(OH)Cl$

(b) CrO_3 / SiO_2

(c) $(C_5H_5)_2Cr / SiO_2$
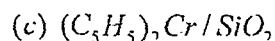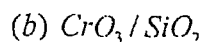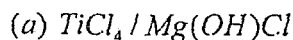
2. Formation of bimetallic complexes:

(a) $MgCl_2 + 2TiCl_4 + 8POCl_3 \rightarrow [TiCl_{10}]^{2-}[Mg(POCl_3)_6]^{2+} . 2POCl_3$

(b) $2MgCl_2 + TiCl_4 + 7THF \rightarrow [TiCl_5(THF)]^-[Mg_2Cl_3(THF)_6]^+$

(c) $MgCl_2 + TiCl_4 + 4CH_3CO_2C_2H_5 \rightarrow TiMgCl_6(CH_3CO_2C_2H_5)_4$
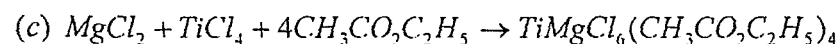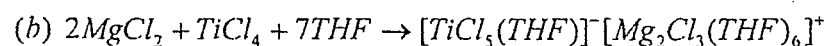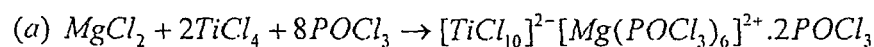
3. Insertion into defects of support

(a) $MgCl_2 + TiCl_4 + ethyl\ p-toluate \rightarrow ball - milling$

(b) $MgCl_2 + TiCl_4.dioxane \rightarrow ball - milling$
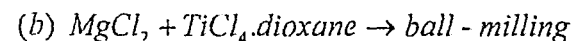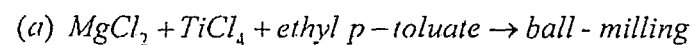
4. Formation of high surface area sponge:

(a) $TiCl_4 + Et_2AlCl \rightarrow \beta - TiCl_3.xEtAlCl_2 \xrightarrow{isoamyl\ ether} treated\ solid \xrightarrow{TiCl_4}$

$$[TiCl_3.(EtAlCl_2)_{0.03}(ether)_{0.01}]$$

(b) $Mg(OEt)_2 + TiCl_4 \rightarrow [MgCl_2.Mg(OEt)_2.(Mg(TiCl_6)]$

(c) $Mg(OEt)_2 + Ti(O-nC_4H_9)_4 + EtAlCl_2 \rightarrow trimetallic\ sponge$
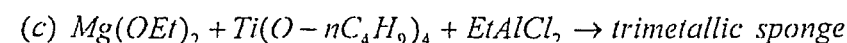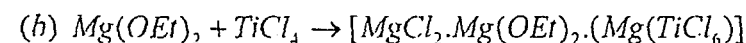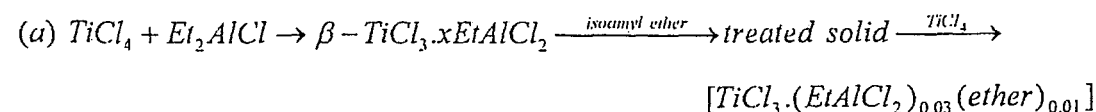
5. Formation of solid solution by cocrystallization (coprecipitation):

(a) $EtMgCl + TiCl_4 \rightarrow TiCl_3.MgCl_2 + Organic\ fragments$
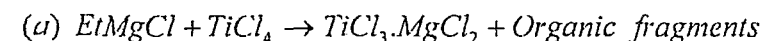
Cr-based catalysts are the first generation of catalysts that have been used for gas phase polymerization. The major difference between Cr-based and Ti-based catalysts is that the Chromium oxide based catalyst produce polymers with broader molecular weight distribution (MWD) than Ti-based catalysts (Method 1 in Table 2.1).

9

Ziegler-Natta catalysts are a remarkable group of catalysts. They are especially useful because they can make polymers that can't be made by any other ways such as linear unbranched polyethylene and isotactic polypropylene. Free radical vinyl polymerization can only produce branched polyethylene and polypropylene cannot be polymerized by free radical polymerization. There are different combinations of Ziegler-Natta catalysts but titanium-aluminium systems, more specifically $TiCl_3$ with $Al(C_2H_5)_2Cl$ and $TiCl_4$ with $Al(C_2H_5)_3$ are the most studied systems. The first generation of Ziegler-Natta catalysts had very low activity. However, for the new generation of Ziegler catalysts, increasing the effective surface area of the active component has remarkably increased the activity of these catalysts. This is accomplished by using a magnesium chloride (solid) support. Also by addition of electron-donor additives stereospecificity was kept high. Therefore, a typical recipe for a present day superactive catalyst system involves initial ball-milling (mechanical grinding or mixing) of magnesium chloride (or the alkoxide) and $TiCl_4$ followed by addition of $Al(C_2H_5)_3$ with an organic Lewis base solvent (Chien et al., 1982).

2.3 Reaction Mechanism of Ziegler-Natta Polymerization

Quite a few structures have been proposed for the active sites in Ziegler-Natta catalyst systems. However, due to the complexity of the components that can be produced by this catalyst, the proposed structures in the literature are commonly diverse. The proposed active centres fall into either of two general categories: monometallic mechanism and bimetallic mechanism (Odian 1991). For monometallic centres the active site occurs at the transition metal carbon bond, whereas bimetallic mechanisms maintain that the active site occurs as a complex between the transition metal and the cocatalyst metal. Figure 2.2 illustrates these two types of mechanism.
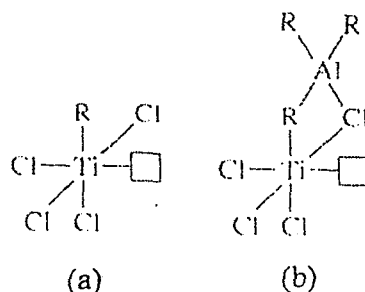
Figure 2.2: a) The monometallic active centre contrasted with b) the bimetallic active centre (taken from Odian, 1991)

2.3.1 Propagation Mechanism

A typical propagation mechanism based on monometallic active sites is depicted in Figure 2.3. The reaction mechanism is called Cossee mechanism, which is currently the most widely accepted mechanism explaining olefin insertion into a transition metal-carbon bond. At first, monomer coordinates at the vacant orbital of transition metal. Then a complex is formed involving the π-electrons of the alkene double bond and the empty orbitals of transition metal. After olefin coordination at the vacant site, a four-membered transition state is formed with the titanium and methylene of the Ti-C bond. Afterwards, the latter bond breaks and new Ti-C and C-C σ-bonds form between titanium, the last inserted monomer and the previously attached alkyl group. The polymer chain moves into the coordination site formerly occupied by the complexing monomer, and then a new vacant site for olefin coordination becomes available. Repetition of this process results in the propagation of the polymer chain (Figure 2.3).

The conventional cocatalyst usually used with Ziegler-Natta catalyst is aluminium alkyls such as triethylaluminium (AlEt$_3$). The main role of a cocatalyst is to activate a catalyst. In addition, AlEt$_3$ also acts as a scavenger of impurities in the polymerization system (McAuley et al., 1990). Other roles such as alkylating agent and reducing agent have been proposed by some researchers. According to Chien et al. (1987), AlEt$_3$ can also reduce MgCl$_2$ support particle size and increase surface area if AlEt$_3$ is used as an internal modifier during the

11

support preparation. The optimum molar ratio of Al/Ti is in the range of 10-30 (Dusseault and Hsu, 1993).
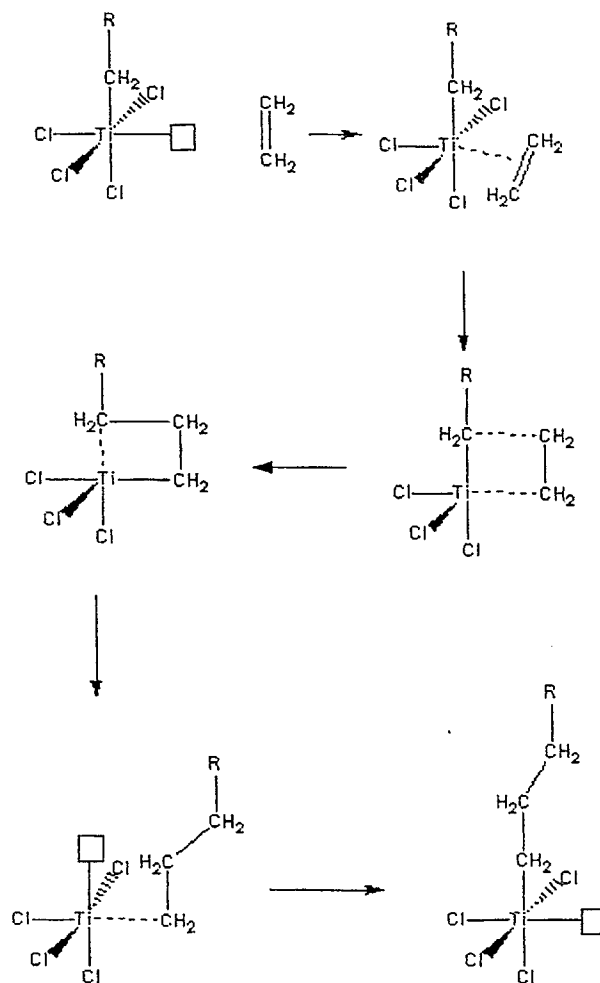
Figure 2.3: Propagation mechanism for monometallic active site (Odian, 1991)

Metallocene catalyst is another class of catalysts besides the chromium and Ziegler-Natta catalysts. Metallocenes are a relatively old class of organometallic complexes with Ferrocene being the first that was discovered in 1951. In contrast to Ziegler-Natta catalysts, which are heterogeneous and have multiple-active sites, metallocene catalysts are known as

12

homogeneous and single-sited catalysts. The manufacture of polyolefins by metallocene catalyst presents a revolution in modern polymer industry. Polymerization of olefins with single-site metallocene catalysts allows the production of polyolefins (e.g. polyethylene and polypropylene) with a highly ordered and superior structure. Moreover, the structure of metallocene catalysts can be varied in order to control the molecular structure of polymer and eventually, the properties of the polymer.

At first, metallocene was used to describe a complex with a metal sandwich between two eta-5-cyclopentadienyl (Cp) ligands. Later on, a large number of metallocene catalysts have been invented in a wide variety of organometallic structures such as those with substituted Cp rings, those with bent sandwich structures, and the half-sandwich or mono-Cp complexes (Figure 2.4).
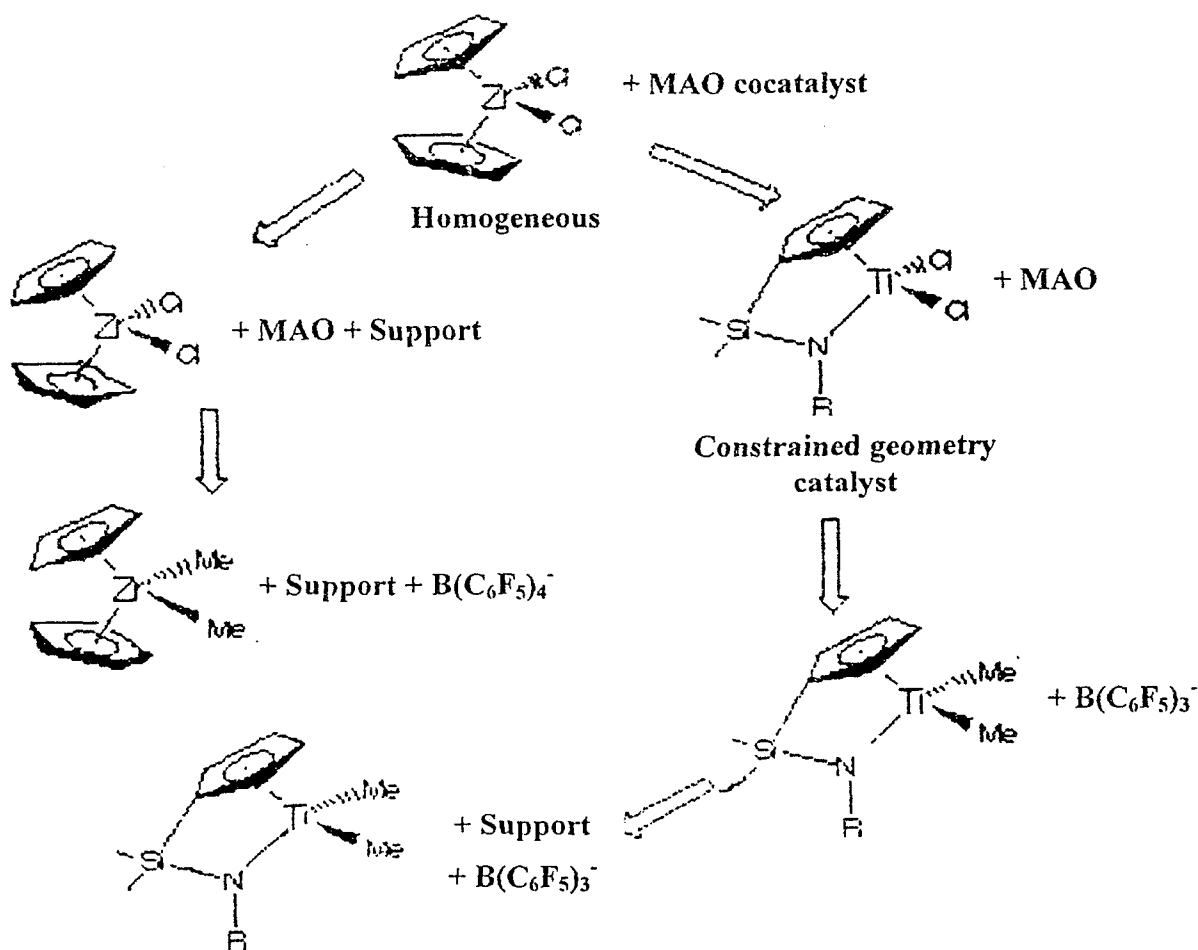
Figure 2.4: Evolution of metallocene catalysts

13

Methylaluminoxane (MAO) is a convenient cocatalyst for polymerization of olefins with metallocene catalysts. MAO is produced by hydrolysis of Trimethylaluminium $(Al(CH_3)_3)$. Up to now, experimental and theoretical evidence has revealed that a cationic alkyl-metallocene complex is an active species in olefin polymerization. Furthermore, it is believed that the role of MAO is to:

a) Alkylate the metallocene and form an active site;

b) Scavenge for impurities;

c) Stabilize the cationic centre in an ion pair interaction;

d) Prevent bimetallic deactivation from occurring.

Figure 2.5 depicts a schematic diagram of the formation of active site by metallocene catalysts. It is believed that the reaction mechanism follows the Cossee-Arlman mechanism.
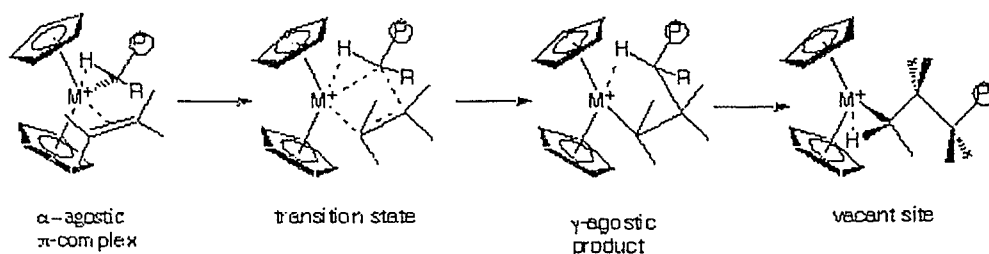
Figure 2.5: The Cossee-Arlman mechanism for formation of metallocene active sites

14

CHAPTER 3: HYDRODYNAMICS OF FLUIDIZED BEDS

Fixed bed reactors have several drawbacks for highly exothermic reactions. They favor the production of unwanted by-products and also produce localized hot or cold spots in the bed. However, in comparison with fixed beds, fluidized beds have several advantages. Once a solid is fluidized in the bed, it behaves like a liquid. This liquid-like behaviour enables a continuous feeding, handling and withdrawal of solids. These benefits of fluidized solids raised interests for flow modeling and contacting patterns inside the FBR.

Fluidized bed reactor models rely heavily on the use of empirical and semi-empirical correlations for predicting key model parameters, such as minimum fluidization velocity, bubble size and interphase mass and heat transfer coefficients. The traditional two-phase theory considers the existence of two phases only in a fluidized bed reactor, i.e. the solid free bubbles ($\varepsilon = 1$) and emulsion phase (dense phase) at minimum fluidization ($\varepsilon = \varepsilon_{mf}$). This approach postulates that the bubbles are solid free; hence reactions occur in the emulsion phase only. However, the actual flow structure in the fluidized beds is much more complicated than that at the minimum fluidization, and the bubbles may contain various amounts of particles as reported by Cui et al. (2000) and Li et al. (1996). Also the mean voidage in the bubble and emulsion phases and, that of the phase fractions vary with the superficial gas velocity. This phenomenon results in a dynamic gas-solid distribution of the phases with the voidage, which has a considerable effect on mass/heat transfer and apparent polymerization rate in fluidized bed reactors. The required hydrodynamic parameters and mass/heat transfer correlations are presented in the next sections.

3.1 Minimum Fluidization Velocity

In FBR calculations the first step is to determine the minimum fluidization velocity, i.e. the velocity at which the bed starts to fluidize. At the minimum fluidization velocity, all the particles are essentially supported by the gas stream. The pressure drop through the bed is defined as the weight divided by the cross-sectional area of the bed $\Delta P = W / A$. Below the minimum fluidization velocity, an increase in gas velocity usually causes an increase in pressure drop (Figure 3.1). However, at minimum fluidization velocity, further increase in the

15

velocity does not have any effect on pressure drop, which remains constant (provided $u_0 < u_T$).
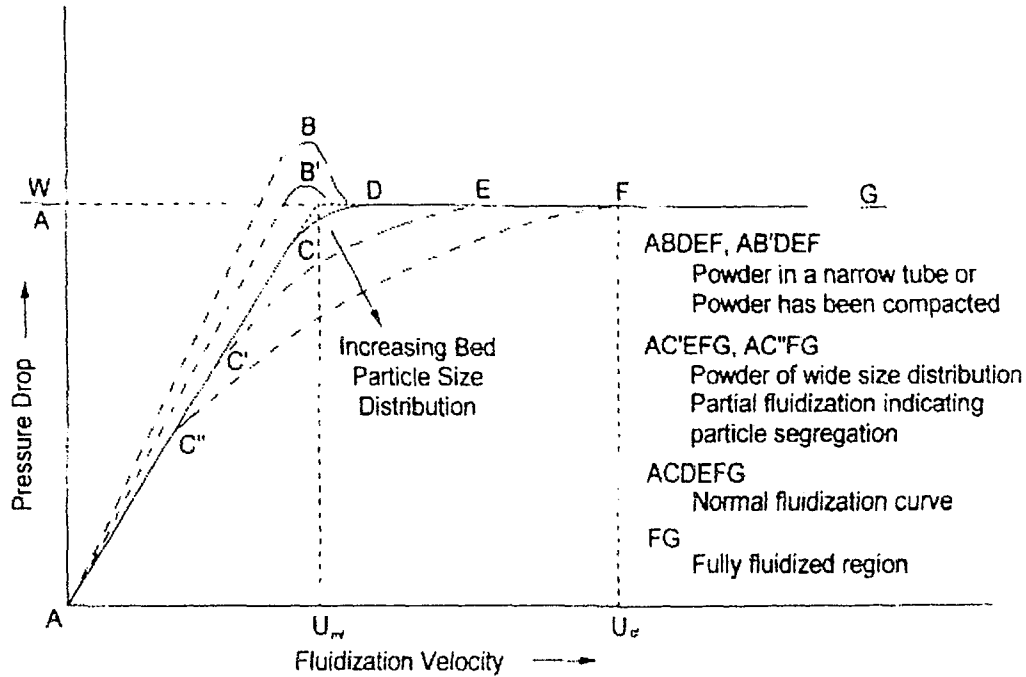
Figure 3.1: Profile of pressure drop versus fluidization velocity for determination of minimum fluidization velocity (Yang, 2003)

The minimum fluidization velocity can be calculated using Equation 3.1, which is a form of Ergun equation for Geldart particles of type B (Lucas et al., 1986):

$$\text{Re}_{mf} = \{(29.5)^2 + 0.0357 Ar\}^{1/2} - 29.5 \tag{3.1}$$

Re_{mf} and Ar are Reynolds and Archimedes numbers, respectively, defined as:

$$\text{Re}_{mf} = \frac{d_p u_{mf} \rho_g}{\mu_g} \tag{3.2}$$

$$Ar = \frac{d_p^3 \rho_g (\rho_{polym} - \rho_g) g}{\mu_g^2} \tag{3.3}$$

16

where ρ_g is the gas density, ρ_{polym} is the bulk polymer density, μ_g is the gas density, d_p is the particle diameter and g is the gravitational acceleration.

From (3.1) and (3.2), the minimum fluidization velocity is:

$$u_{mf} = \frac{\mathrm{Re}_{mf}\,\mu_g}{d_p \rho_g} \qquad (3.4)$$

3.2 Minimum Fluidization Porosity

The bed voidage at minimum fluidization can be estimated by the correlation of Broadhurst and Becker (1975):

$$\varepsilon_{mf} = 0.586\phi^{-0.72}\left(\frac{\mu_g^2}{\rho_g g(\rho_{polym} - \rho_g)d_p^3}\right)^{0.029}\left(\frac{\rho_g}{\rho_{polym}}\right)^{0.021} \qquad (3.5)$$

where ϕ is a geometrical constant ($\phi = 0.7$ in this study).

3.3 Bubble Size

Geldart (1973) classified different kinds of solid particles in a fluidized bed according to their size and behavior. He came up with a simple classification of solids known as Geldart classification: Geldart A, B, C and D (Figure 3.2).

The polymer particle for polymerization of ethylene is Geldart B with an average particle size of about 0.05 cm. The initial bubble size d_{b0} and the maximum stable bubble size d_{bm} are correlated by (Mori and Wen, 1975):

$$\frac{d_{bm} - d_b}{d_{bm} - d_{b0}} = \exp(-0.3\frac{h}{D}) \qquad (3.6)$$

For Geldart A particles, the bubble size correlation was established by Horio et al. (1987):

$$\left(\frac{\sqrt{d_b} - \sqrt{d_{be}}}{\sqrt{d_{b0}} - \sqrt{d_{be}}}\right)^{1-\zeta/\eta}\left(\frac{\sqrt{d_b} + \sqrt{\alpha}}{\sqrt{d_{b0}} + \sqrt{\alpha}}\right)^{1+\zeta/\eta} = \exp(0.3\frac{h}{D}) \qquad (3.7)$$

Where d_{be} is the equilibrium bubble size.

17
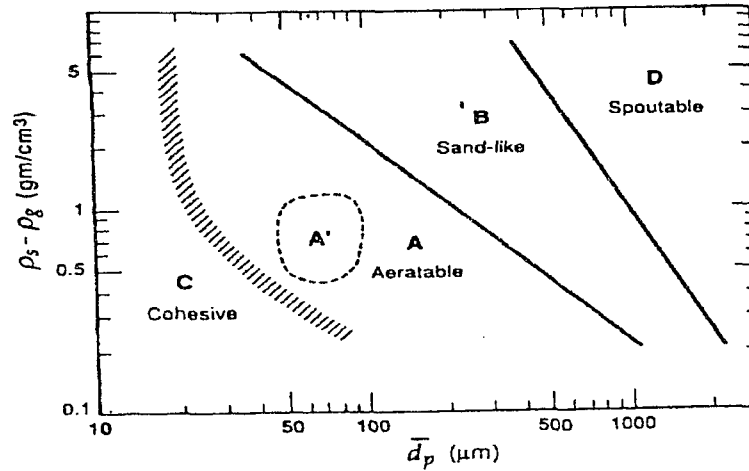
Figure 3.2: Geldart classification of solids in bubbling FBR (Geldart, 1973)

Maximum Stable Bubble Size:

In a FBR, bubbles grow continuously due to pressure drop and bubble coalescence, until a maximum stable size is reached (Hatzantonis et al., 2000). Bubbles, having exceeded the maximum, will break up and become smaller in size to maintain system stability. According to Davidson and Harrison (1963) bubbles may become unstable if their rising velocities become larger than the terminal velocity of particles in the bed. The expected limiting size of bubbles in a very deep bed is defined as:

$$d_{bm} = 2u_T^2 / g \tag{3.8}$$

where u_T is the terminal velocity of particles. Particles are blown out of the bed when the gas velocity exceeds the terminal velocity. The terminal velocity according to Haider and Levenspiel (1989) is given by:

$$u_T = u_T^* [\mu_g \rho_g^{-2} (\rho_{polym} - \rho_g) g]^{1/3} \tag{3.9}$$

And for irregularly shaped particles of sphericity ϕ_s:

$$u_T^* = [18(d_p^*)^{-2} + 2.335 - 1.744 \phi_s)(d_p^*)^{-0.5}]^{-1} \tag{3.10}$$

? extra bracket

where the particle sphericity ϕ_s is defined as:

18

$\phi_s = $ (Surface of a sphere/surface of a particle) with the same volume $\qquad$ (3.11)

· and for $0.5 < \phi_s \leq 1$,

$$d_p^* = d_p [\mu_g^{-2} \rho_g (\rho_{polym} - \rho_g) g]^{1/3} \qquad (3.12)$$

Since the above correlation usually gives conservative estimation of the maximum stable bubble size, Grace (1986) recommended the use of a correction factor of 2.7 for particle size ($d'_p = 2.7 d_p$). Consequently, higher values of maximum stable bubble size may be obtained.

Initial Bubble Size:

The initial bubble size formed near the bottom of the bed is defined as (Mori and Wen, 1975):

$$d_{b0} = 1.38 g^{-0.2} [(u_0 - u_{mf}) A / n_{ur}]^{0.4} \qquad \text{For perforated plate} \qquad (3.13)$$

where n_{ur} is the number of nuzzles on the distributor plate and A is the cross-sectional area of the bed.

Also for porous plate:

$$d_{b0} = 0.00376 [(u_0 - u_{mf})^2 \qquad \text{?} \qquad incomplete \qquad (3.14)$$

Equilibrium Bubble Size: $\qquad$ (Same as stable bubble size ?)

The equilibrium bubble size is expressed as:

$$d_{be} = D[-\zeta + \underbrace{(\zeta + 4 d_{bm} / D)^{0.5}}_{\eta}]^2 / 4 \quad \longleftarrow \quad \alpha, \eta \ \text{not used in formula !!} \qquad (3.15)$$

where D is the bed diameter and α and η were defined by Horio et al. (1987) as follows:

$$\alpha / D = (\zeta + \eta)^{0.2} / 4 \qquad (3.16)$$

$$\eta = (\zeta^2 + 4 d_{bm} / D)^{0.5} \qquad (3.17)$$

$$\zeta = 2.56 \times 10^{-2} (D / g)^{0.5} / u_{mf} \qquad (3.18)$$

19

3.4 Bubble Velocity

Werther (1983) proposed an equation for bubble rise velocity covering the whole range of Geldart A to D particle sizes and accounting for the vessel size:

$$u_b = u_0 - u_{mf} + \varphi \times u_{br} \qquad (3.19)$$

where u_{br} is the bubble rise velocity defined by Equation (3.20) and φ is a factor standing for the deviation of bed bubbles from single bubbles.

For type-A solids, φ is defined as:

$\varphi = 1$ For $D \leq 0.1\,\text{m}$

$\varphi = 0.25D^{0.4}$ For $0.1 \leq D \leq 1\,\text{m}$

$\varphi = 2.5$ For $D > 1\,\text{m}$

For type-B solids, φ is defined as:

$\varphi = 0.64$ For $D \leq 0.1\,\text{m}$

$\varphi = 1.6D^{0.4}$ For $0.1 \leq D \leq 1\,\text{m}$

$\varphi = 1.6$ For $D > 1\,\text{m}$

Bubble Rise Velocity:

On the basis of simple two-phase theory, Davidson and Harrison (1963) proposed the following rise velocity:

$$u_{br} = \sqrt{gd_b} \qquad (3.20)$$

Note that in the case of several heat exchange tubes as vertical internals in fluidized bed reactor, one should estimate the bubble size and bubble rise velocity by using the hydraulic diameter of bed D_h in place of D in the calculation.

20

3.5 Bubble Fraction

The actual flow pattern in fluidized beds show a highly complicated behavior due to gas-solid interactions. This phenomenon corresponds to dynamic gas-solid distribution as reported by (Cui et al., 2000). Based on the dynamic two-phase structure, the fraction of bed containing the bubbles is expressed as:

$$\delta = 0.534\left[1 - \exp\left(-\frac{u_0 - u_{mf}}{0.413}\right)\right] \tag{3.21}$$

Since the catalyst particles used in polyethylene production is Geldart B, the constants of Cui et al. (2000) were chosen accordingly.

3.6 Emulsion Velocity

Many recent studies show that the emulsion phase does not stay at minimum fluidization but it may contain more gas at higher gas velocities (Abrahamson et al. 1980, Chaouki et al. 1999, Cui et al. 2000). In this work, the emulsion phase velocity correlation of Hilligardt and Werther (1986) for Geldart B particles have been used.

$$\frac{u_e - u_{mf}}{u_0 - u_{mf}} = \frac{1}{3} \tag{3.22}$$

3.7 Bubble Phase and Emulsion Phase Voidage

The mean voidage of bubble and emulsion phases for Geldart B particles were defined by Cui et al. (2000):

$$\varepsilon_b = 1 - 0.146\exp\left(-\frac{u_0 - u_{mf}}{4.439}\right) \tag{3.23}$$

$$\varepsilon_e = \varepsilon_{mf} + 0.2 - 0.059\exp\left(-\frac{u_0 - u_{mf}}{0.429}\right) \tag{3.24}$$

3.8 Mass Transfer Coefficients

In bubbling fluidized beds, bubbles exchange mass with the emulsion phase. Kunii and Levenspiel (1969) considered that the mass is transferred from the bubble phase to the

21

surrounding clouds and then to the emulsion phase. The overall bubble to emulsion phase interchange coefficient can be expressed as:

$$K_{be} = (1/K_{bc} + 1/K_{ce})^{-1} \tag{3.25}$$

The interchange between the bubble and the cloud involves bulk flow across the boundary and diffusion of gas in between. These interchange coefficients were defined by Kunii and Levenspiel (1991):

$$K_{ce} = 6.77(\frac{D_g \varepsilon_c u_{br}}{d_b^3})^{\frac{1}{2}} \tag{3.26}$$

And:

$$K_{bc} = 4.5(\frac{u_c}{d_b}) + 5.85(\frac{D_g^{0.5} g^{0.25}}{d_b^{1.25}}) \tag{3.27}$$

3.9 Heat Transfer Coefficients

The heat interchange coefficient between bubble and emulsion phase in the FBR can be written as:

$$H_{be} = (1/H_{bc} + 1/H_{ce})^{-1} \tag{3.28}$$

Where:

$$H_{bc} = 4.5(\frac{u_c \rho_g Cp_g}{d_b}) + 5.85(\frac{g^{0.25} K_g^{0.5} \rho_g^{0.5} Cp_g^{0.5}}{d_b^{1.25}}) \tag{3.29}$$

$$H_{ce} = 6.77(\rho_g Cp_g K_g)^{0.5} (\frac{\varepsilon_c u_{br}}{d_b^3})^{0.5} \tag{3.30}$$

The subscripts *be*, *bc* and *ce* denotes the mass and heat interchange process between the bubble and emulsion, the bubble and the cloud and the cloud and emulsion phases, respectively.

CHAPTER 4: ETHYLENE POLYMERIZATION KINETICS AND MODELING

Polyolefins made with heterogeneous Ziegler-Natta catalysts have usually broad molecular weight distribution (MWD) and chemical composition distribution (CCD). The presence of multiple types of catalytic sites on the surface of heterogeneous Ziegler-Natta catalysts is generally considered to be responsible for broadness of MWDs and CCDs. Each site type has its own kinetic constants and produces polymer with often different MWD, CCDs and stereoregularities (de Carvalho et al., 1989; McAuley et al., 1990; Soares and Hamielec, 1995; Soares and Hamielec, 1996). The existence of multiple site types on heterogeneous Ziegler-Natta catalysts is supported by experimental data (Zucchini and Cecchin, 1983; Keii et al., 1984; Usami et al., 1986).

In this work, a dynamic model is developed for homopolymerization of ethylene using multiple-site heterogeneous Ziegler-Natta catalysts in a fluidized bed reactor.

4.1 Reaction Mechanism

The polymerization kinetics includes steps of site formation, initiation, propagation, transfer to monomer, transfer to cocatalyst, transfer to hydrogen, spontaneous transfer (β-hydride elimination) and deactivation. These elementary steps are employed to describe the majority of experimental polymerization data of olefins using Ziegler-Natta and metallocene catalysts (Soares and Hamielec, 1996).

In the kinetic equations below, C^* stands for a potential active site on the catalyst surface, R^* represents a live polymer chain which is chemically bonded to the active metal centre and P is a dead polymer chain. Monomer molecules are represented by M, cocatalyst by A and hydrogen by H_2. The indexes j and r represents the type of active sites and the length (in monomer units) of the polymer chain. In this study a Ziegler-Natta catalyst with two active sites is employed in kinetic model development (j=1, 2).

23

a) Site formation:

$$C^{\bullet}(j) + A \xrightarrow{\quad k_f(j) \quad} R^{\bullet}(0,j) \tag{4.1}$$

b) Initiation of active sites:

$$R^{\bullet}(0,j) + M \xrightarrow{\quad k_i(j) \quad} R^{\bullet}(1,j) \tag{4.2}$$

c) Propagation:

$$R^{\bullet}(r,j) + M \xrightarrow{\quad k_p(j) \quad} R^{\bullet}(r+1,j) \tag{4.3}$$
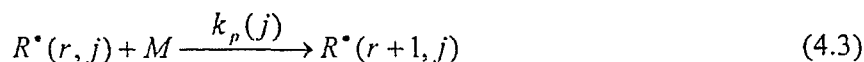
d) Chain transfer:

Transfer to monomer:
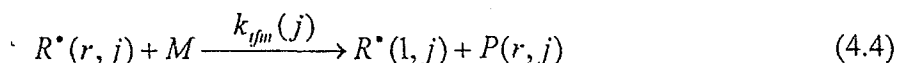
$$R^{\bullet}(r,j) + M \xrightarrow{\quad k_{tfm}(j) \quad} R^{\bullet}(1,j) + P(r,j) \tag{4.4}$$

Transfer to hydrogen:

$$R^{\bullet}(r,j) + H_2 \xrightarrow{\quad k_{tfH}(j) \quad} R_H^{\bullet}(0,j) + P(r,j) \tag{4.5}$$

Transfer to cocatalyst:

$$R^{\bullet}(r,j) + A \xrightarrow{\quad k_{tfA}(j) \quad} R_A^{\bullet}(1,j) + P(r,j) \tag{4.6}$$

Spontaneous transfer:

$$R^{\bullet}(r,j) \xrightarrow{\quad k_{tfs}(j) \quad} R_H^{\bullet}(0,j) + P(r,j) \tag{4.7}$$

e) Deactivation:

$$R^{\bullet}(r,j) \xrightarrow{\quad k_d(j) \quad} R_d(j) + P(r,j) \tag{4.8}$$

$$R^{\bullet}(0,j) \xrightarrow{\quad k_d(j) \quad} R_d(j) \tag{4.9}$$

$$R_H^{\bullet}(0,j) \xrightarrow{\quad k_d(j) \quad} R_d(j) \tag{4.10}$$

$$R_A^{\bullet}(0,j) \xrightarrow{\quad k_d(j) \quad} R_d(j) \tag{4.11}$$
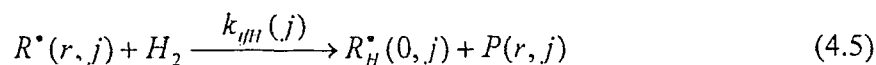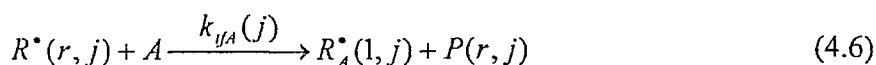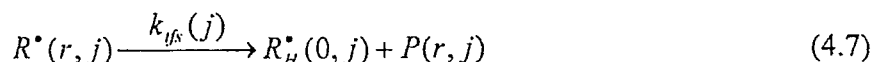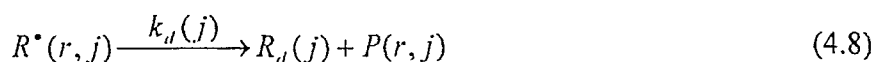
4.2 Kinetic Model Development

In this study, we develop a model for ethylene polymerization with Ziegler-Natta catalyst. We first assume that the reaction is isothermal and that it obeys the reactional mechanism

24

proposed in sub-section 4.1. The model is based on the molar balances of the appropriate species involved in reactions (4.1) to (4.11). The purpose of the model is to study the evolution of the consumed components, the formation of polymer species as well as the average weight distribution and molecular weight distribution of the polymer.

Model Assumptions

For the model development, few hypothesis were considered:

1. Polymerization reaction occurs both in the emulsion phase and the bubble phase.
2. Emulsion phase does not remain at its minimum fluidization velocity and travels up through the bed in a plug flow regime.
3. Bubbles grow only to a maximum stable size and travel up the reactor in a plug flow regime.
4. Particles are assumed to have a constant mean diameter.
5. Ethylene, hydrogen, nitrogen and cocatalyst are assumed to be present in the gas phase. Homopolymerization of ethylene is assumed.
6. Radical concentrations and temperature gradients within the bed, resistance to material transfer between gas and solids and elutriation are assumed to be negligible.

In the mole balance relations, the rate equations can be written for each species (e.g. hydrogen, cocatalyst...) in each phase (bubble phase and emulsion phase) based on the corresponding monomer, active sites, cocatalyst and hydrogen concentrations.

$$\lambda_i(j) = \sum_{i=1}^{\infty} r^i R^*(r, j) \quad \text{and} \quad \mu_i = \sum_{i=1}^{\infty} r^i P(r, j) \tag{4.12}$$

4.2.1 Reaction Rate for Catalyst and Active Sites

The reaction rate of potential active sites $C^*(j)$ is given by:

$$R_{C^*(j)} = \frac{dC^*(j)}{dt} = -k_f(j)C^*(j)[A] \qquad j=1, 2 \tag{4.13}$$

The reaction rates of initiated sites $R^*(0, j)$ and $R_H^*(0, j)$:

$$R_{R^*(0,j)} = \frac{dR^*(0,j)}{dt} = k_f(j)C^*(j)[A] - R^*(0,j)\{k_i(j)[M] + k_d(j)\} \qquad j=1, 2 \tag{4.14}$$

25

$$R_{R_{H}^{\bullet}(0,j)} = \frac{dR_H^{\bullet}(0,j)}{dt} = \lambda_0(j)\{k_{tH}(j)[H_2] + k_{tfs}(j)\} - R_H^{\bullet}(0,j)k_d(j) \qquad j=1,2 \qquad (4.15)$$

Where $k_f(j)$, $k_i(j)$, $k_d(j)$ are the rate constants for site formation, site initiation and site deactivation and $k_{tH}(j)$ and $k_{tfs}(j)$ are the rate constants for transfer to hydrogen and spontaneous transfer, respectively. Also λ_0 is the zeroth moment of live polymer defined in (4.12).

4.2.2 Reaction Rate for Cocatalyst

As the reaction proceeds, ethylene and catalysts are continuously consumed. A molar balance on each species gives their rate of consumption. The cocatalyst consumption rate can be written as:

$$R_A = \frac{d[A]}{dt} = \sum_{j=1}^{Ns}\{-k_f(j)[C^{\bullet}(j)][A] - k_{tfA}(j)[A]\lambda_0(j)\} \qquad (4.16)$$

Where Ns denotes the total number of active sites (Ns=2 in this study) and $k_{tfA}(j)$ is the rate constant for transfer to cocatalyst at j^{th} catalyst active site.

4.2.3 Reaction Rate for Gaseous Components

a) Molar balance on hydrogen:

Hydrogen is consumed in both sites by live polymer radicals $R^{\bullet}(r,j)$:

$$R_{H2} = \frac{d[H_2]}{dt} = \sum_{j=1}^{Ns}\{-k_{tH}(j)[H_2]\lambda_0(j)\} \qquad (4.17)$$

Where $[H_2]$ is concentration of hydrogen and $\lambda_0(j)$ is the zeroth moment of live polymer chains at j^{th} catalyst active site.

b) Molar balance on monomer:

Ethylene is consumed in three reactions: Initiation, propagation and transfer to monomer. So the reaction rate of ethylene is given by:

26

$$R_p = \frac{d[M]}{dt} = \sum_{j=1}^{N_s} \{ -k_p(j)[M]\lambda_0(j) - k_{tfm}(j)[M]\lambda_0(j) - k_i(j)[M]R^*(0,j) \} \qquad (4.18)$$

4.2.4 Molar Balances on Living Polymer Chains

a) Zeroth moment (Assuming V=Constant):

Writing up molar balances and then applying steady state hypothesis for the molar balance of the growing live polymer chains, $R^*(r,j)$, we get:

$$k_i(j)[M]R^*(0,j) = \{ k_{tfH}(j)[H_2] + k_{tfA}(j)[A] + k_{tfs}(j) + k_d(j) \}\lambda_0(j) \qquad (4.19)$$

Which is finally written as, for both active sites:

$$\lambda_0(j) = \frac{k_i(j)[M]R^*(0,j)}{k_{tfH}(j)[H_2] + k_{tfA}(j)[A] + k_{tfs}(j) + k_d(j)} \qquad j=1,2 \qquad (4.20)$$

Details in the development of moments have been previously reported in Felorzabihi (2003c). $\lambda_0(1)$ and $\lambda_0(2)$ represent the total molar concentration of live polymers, which have been growing on each active site 1 and 2, respectively. It is important to note that higher moments, especially first and second are required in the polymer model and also in the calculation of molecular weight averages. Hence first and second moments are developed next.

b) First moment (Assuming V=Constant):

Again writing up molar balances and assuming steady state hypothesis for the first moment of the growing live polymer chains, it was shown that:

$$k_i(j)[M]R^*(0,j) + k_p(j)[M]\lambda_0(j) + k_{tfm}(j)[M]\lambda_0(j) = \{ k_{tfm}(j)[M] + k_{tfH}(j)[H_2]$$
$$+ k_{tfA}(j)[A] + k_{tfs}(j) + k_d(j) \}\lambda_1(j) \qquad (4.21)$$

Which is arranged to give first moment $\lambda_1(j)$ for site j:

$$\lambda_1(j) = \frac{k_p(j)[M]\lambda_0(j) + k_i(j)[M]R^*(0,j) + k_{tfm}(j)[M]\lambda_0(j)}{k_{tfm}(j)[M] + k_{tfH}(j)[H_2] + k_{tfA}(j)[A] + k_{tfs}(j) + k_d(j)} \qquad (4.22)$$

Since in this study have two active sites for $j=1$:

27

$$\lambda_1(1) = \frac{k_p(1)[M]\lambda_0(1) + k_i(1)[M]R^*(0,1) + k_{tfm}(1)[M]\lambda_0(1)}{k_{tfm}(1)[M] + k_{tfH}(1)[H_2] + k_{tfA}(1)[A] + k_{tfs}(1) + k_d(1)}$$

And for $j=2$:

$$\lambda_1(2) = \frac{k_p(2)[M]\lambda_0(2) + k_i(2)[M]R^*(0,2) + k_{tfm}(2)[M]\lambda_0(2)}{k_{tfm}(2)[M] + k_{tfH}(2)[H_2] + k_{tfA}(2)[A] + k_{tfs}(2) + k_d(2)}$$

c) Second moment (Assuming V=Constant):

Similarly, the steady-state molar balance equation for the second moment $\lambda_2(j)$ was shown to be:

$$k_i[M]R^*(0,j) + k_p(j)[M]\{2\lambda_1(j) + \lambda_0(j)\} + k_{tfm}(j)[M]\lambda_0(j) = \{k_{tfm}(j)[M]$$
$$+ k_{tfH}(j)[H_2] + k_{tfA}(j)[A] + k_{tfs}(j) + k_d(j)\}\lambda_2(j) \tag{4.23}$$

Which is finally arranged as, for each active site j:

$$\lambda_2(j) = \frac{k_p(j)[M]\{2\lambda_1(j) + \lambda_0(j)\} + k_i(j)[M]R^*(0,j) + k_{tfm}(j)[M]\lambda_0(j)}{k_{tfm}(j)[M] + k_{tfH}(j)[H_2] + k_{tfA}(j)[A] + k_{tfs}(j) + k_d(j)} \tag{4.24}$$

For a catalyst with two active sites, for $j=1$:

$$\lambda_2(1) = \frac{k_p(1)[M]\{2\lambda_1(1) + \lambda_0(1)\} + k_i(1)[M]R^*(0,1) + k_{tfm}(1)[M]\lambda_0(1)}{k_{tfm}(1)[M] + k_{tfH}(1)[H_2] + k_{tfA}(1)[A] + k_{tfs}(1) + k_d(1)}$$

And for $j=2$:

$$\lambda_2(2) = \frac{k_p(2)[M]\{2\lambda_1(2) + \lambda_0(2)\} + k_i(2)[M]R^*(0,2) + k_{tfm}(2)[M]\lambda_0(2)}{k_{tfm}(2)[M] + k_{tfH}(2)[H_2] + k_{tfA}(2)[A] + k_{tfs}(2) + k_d(2)}$$

4.2.5 Molar Balances on Dead Polymer Chains

Writing up molar balances for the dead polymer $P(r,j)$ a set of dynamic equations was developed. Again, equations of three moments for the dead polymer $P(r,j)$ are given next:

28

a) Zeroth moment (Assuming V=Constant):

The change in the total dead polymer concentrations, known as zeroth moment, is written for active site j:

$$R_{\mu_0(j)} = \frac{d\mu_0(j)}{dt} = k_{tfm}(j)[M]\lambda_0(j) + k_{tfH}(j)[H_2]\lambda_0(j) + k_{tfA}(j)[A]\lambda_0(j) + k_{tfs}(j)\lambda_0(j) + k_d(j)\lambda_0(j)$$

(4.25)

Since we have two active sites, for $j=1$:

$$R_{\mu_0(1)} = \frac{d\mu_0(1)}{dt} = k_{tfm}(1)[M]\lambda_0(1) + k_{tfH}(1)[H_2]\lambda_0(1) + k_{tfA}(1)[A]\lambda_0(1) + k_{tfs}(1)\lambda_0(1) + k_d(1)\lambda_0(1)$$

And for $j=2$:

$$R_{\mu_0(2)} = \frac{d\mu_0(2)}{dt} = k_{tfm}(2)[M]\lambda_0(2) + k_{tfH}(2)[H_2]\lambda_0(2) + k_{tfA}(2)[A]\lambda_0(2) + k_{tfs}(2)\lambda_0(2) + k_d(2)\lambda_0(2)$$

b) First moment (Assuming V=Constant):

High moments are required to complete the polymer model, so the first moment for P in each active site j:

$$R_{\mu_1(j)} = \frac{d\mu_1(j)}{dt} = k_{tfm}(j)[M]\lambda_1(j) + k_{tfH}(j)[H_2]\lambda_1(j) + k_{tfA}(j)[A]\lambda_1(j) + k_{tfs}(j)\lambda_1(j) + k_d(j)\lambda_1(j)$$

(4.26)

For $j=1$:

$$R_{\mu_1(1)} = \frac{d\mu_1(1)}{dt} = k_{tfm}(1)[M]\lambda_1(1) + k_{tfH}(1)[H_2]\lambda_1(1) + k_{tfA}(1)[A]\lambda_1(1) + k_{tfs}(1)\lambda_1(1) + k_d(1)\lambda_1(1)$$

and for $j=2$:

$$R_{\mu_1(2)} = \frac{d\mu_1(2)}{dt} = k_{tfm}(2)[M]\lambda_1(2) + k_{tfH}(2)[H_2]\lambda_1(2) + k_{tfA}(2)[A]\lambda_1(2) + k_{tfs}(2)\lambda_1(2) + k_d(2)\lambda_1(2)$$

c) Second moment (Assuming V=Constant):

Similarly, the second moments for the dead polymer which has grown at site j is given as:

$$R_{\mu_2(j)} = \frac{d\mu_2(j)}{dt} = k_{tfm}(j)[M]\lambda_2(j) + k_{tfH}(j)[H_2]\lambda_2(j) + k_{tfA}(j)[A]\lambda_2(j) + k_{tfs}(j)\lambda_2(j) + k_d(j)\lambda_2(j)$$

(4.27)

Since we have two active sites for $j=1$:

29

$$R_{\mu_2(1)} = \frac{d\mu_2(1)}{dt} = k_{tfm}(1)[M]\lambda_2(1) + k_{tfH}(1)[H_2]\lambda_2(1) + k_{tfA}(1)[A]\lambda_2(1) + k_{tfs}(1)\lambda_2(1) + k_d(1)\lambda_2(1)$$

And for $j=2$:

$$R_{\mu_2(2)} = \frac{d\mu_2(2)}{dt} = k_{tfm}(2)[M]\lambda_2(2) + k_{tfH}(2)[H_2]\lambda_2(2) + k_{tfA}(2)[A]\lambda_2(2) + k_{tfs}(2)\lambda_2(2) + k_d(2)\lambda_2(2)$$

4.3 Reactor Model

The fluidized bed reactor considered in this study for polyethylene production consists of two different phases: bubble phase and emulsion phase. Also each phase contains a solid polymer phase. The catalyst is fed to the reactor and the polymer product is continuously withdrawn from it at a rate such that the bed height is held constant. Monomer, hydrogen, and inert gas are admitted to the bottom of the reactor. The schematic diagram of the different phases in the fluidized bed reactor is conceptualized below in Figure 4.1.
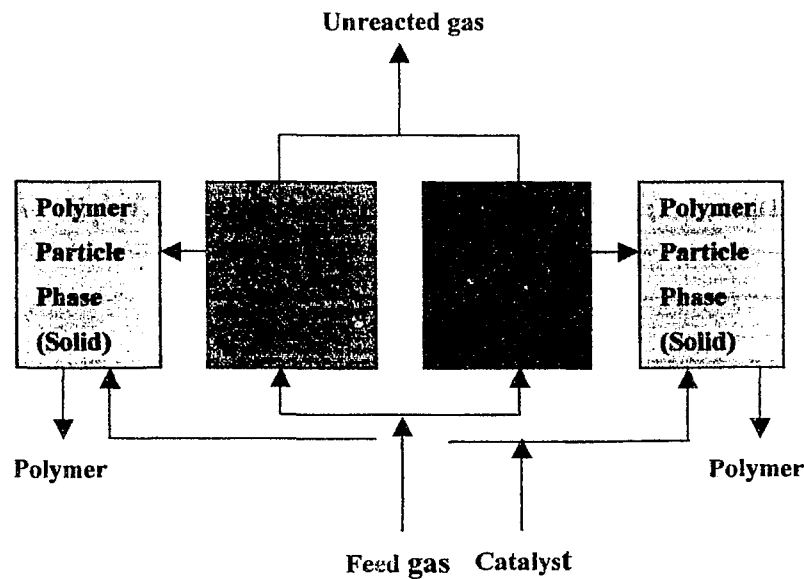
Figure 4.1: Phase diagram and assumptions used for modeling a fluidized bed reactor

30

Figure 4.2 shows the flow pattern and interactions between the phases defined in Figure 4.1.
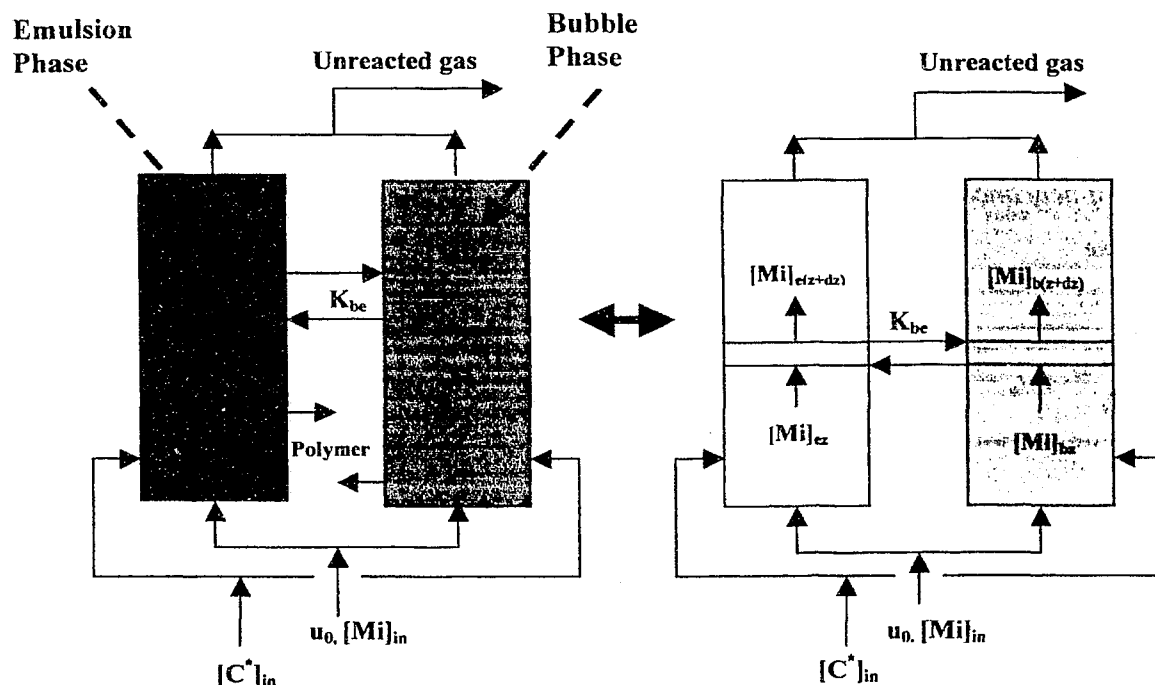
Figure 4.2: Schematic diagram of the FBR model

4.3.1 Bubble Phase Molar Balance

A FBR behaves as a tubular reactor and the model should take into account the rate of accumulation and the rate of advection along with the rate of transfer of material or energy. Hence, the material and energy balance equations in the emulsion and bubble phases were developed for each reactant concentration (monomer, chain transfer agent, cocatalyst, active sites) and for the reactor temperature throughout the bed.

Therefore, the change in the monomer molar balance in the bubble phase is represented by:

Disappearance in the bubble phase = Transfer to emulsion phase + Reaction in the bubble phase

31

$$\frac{\partial [M]_b}{\partial t} + u_b \frac{\partial [M]_b}{\partial z} = \frac{K_{be}([M]_e - [M]_b)}{\varepsilon_b} + \frac{(1-\varepsilon_b)R_{p,b}}{\varepsilon_b} \tag{4.28}$$

4.3.2 Emulsion Phase Molar Balance

Similarly, the molar balance for monomer in the emulsion phase can be written as:

Disappearance in the emulsion phase= Transfer to bubble phase + Reaction in the emulsion phase

$$\frac{\partial [M]_e}{\partial t} + u_e \frac{\partial [M]_e}{\partial z} = \frac{\delta K_{be}([M]_b - [M]_e)}{(1-\delta)\varepsilon_e} + \frac{(1-\varepsilon_e)R_{p,e}}{\varepsilon_e} \tag{4.29}$$

Where, δ is the volume fraction of bubbles in the bed, ε_e and ε_b are the porosity of emulsion phase and bubble phase, respectively; K_{be} is the mass transfer coefficient defined by Equation (3.25); $R_{p,e}$ and $R_{p,b}$ are the polymerization rate in the bubble phase and emulsion phase, respectively.

The overall concentration of each species in the bed can be written as:

$$[C_i] = (1-\delta)[C_i]_e + \delta[C_i]_b \tag{4.30}$$

Where C_i corresponds to the concentrations of monomer M, potential active site C^*, cocatalyst A and hydrogen H_2.

4.3.3 Bubble Phase Energy Balance

The energy balance in both phases consists of the convective and conductive heat transfer between the bubble and emulsion phases, the heat generated by exothermic polymerization reactions and the enthalpy associated with the mass transfer of gas from the bubble phase to the emulsion phase. The bubble phase energy balance can be written as:

$$\frac{\partial T_b}{\partial t} + u_b \frac{\partial T_b}{\partial z} = \frac{H_{be}(T_e - T_b)}{Cp_g^* \varepsilon_b [M]_b + (1-\varepsilon_b)\rho_{polym}Cp_{polym}} + \frac{R_{p,b}(1-\varepsilon_b)(-\Delta H_b)Mw}{Cp_g^* \varepsilon_b [M]_b + (1-\varepsilon_b)\rho_{polym}Cp_{polym}}$$

32

$$+ \frac{Cp_g^* K_{be}([M]_e - [M]_b)(T_e - T_b)}{Cp_g^* \varepsilon_b [M]_b + (1 - \varepsilon_b)\rho_{polym}Cp_{polym}} \qquad (4.31)$$

4.3.4 Emulsion Phase Energy Balance

Similar to bubble phase, the emulsion phase energy balance can be written as:

$$\frac{\partial T_e}{\partial t} + u_e \frac{\partial T_e}{\partial z} = \frac{\delta H_{be}(T_b - T_e)}{(1 - \delta)\{Cp_g^* \varepsilon_e [M]_e + (1 - \varepsilon_e)\rho_{polym}Cp_{polym}\}} + \frac{R_{p,e}(1 - \varepsilon_e)(-\Delta H_e)Mw}{Cp_g^* \varepsilon_e [M]_e + (1 - \varepsilon_e)\rho_{polym}Cp_{polym}}$$

$$+ \frac{\delta Cp_g^* K_{be}([M]_b - [M]_e)(T_e - T_b)}{(1 - \delta)\{\varepsilon_e [M]_e Cp_g^* + (1 - \varepsilon_e)\rho_{polym}Cp_{polym}\}} \qquad (4.32)$$

Where Mw is the molecular weight of monomer, ΔH is the heat of reaction (which is assumed to be equal in both phases), Cp_g^* is the molar specific heat of gas, Cp_{polym} is the specific heat of polymer and $[M]$ is the concentration of monomer. Details in the development of model energy balances have been previously reported in Felorzabihi (2003c).

4.3.5 Dynamic Model

The complete dynamic model for ethylene polymerization in the FBR is given below:

For monomer:

$$\frac{\partial [M]_b}{\partial t} + u_b \frac{\partial [M]_b}{\partial z} = \frac{K_{be}([M]_e - [M]_b)}{\varepsilon_b} + \frac{(1 - \varepsilon_b)R_{p,b}}{\varepsilon_b} \qquad (4.33)$$

$$\frac{\partial [M]_e}{\partial t} + u_e \frac{\partial [M]_e}{\partial z} = \frac{\delta K_{be}}{(1 - \delta)\varepsilon_e}([M]_b - [M]_e) + \frac{(1 - \varepsilon_e)R_{p,e}}{\varepsilon_e} \qquad (4.34)$$

For hydrogen:

$$\frac{\partial [H_2]_b}{\partial t} + u_b \frac{\partial [H_2]_b}{\partial z} = \frac{K_{be,H2}([H_2]_e - [H_2]_b)}{\varepsilon_b} + \frac{(1 - \varepsilon_b)R_{H2,b}}{\varepsilon_b} \qquad (4.35)$$

$$\frac{\partial [H_2]_e}{\partial t} + u_e \frac{\partial [H_2]_e}{\partial z} = \frac{\delta K_{be,H2}}{(1 - \delta)\varepsilon_e}([H_2]_b - [H_2]_e) + \frac{(1 - \varepsilon_e)R_{H2,e}}{\varepsilon_e} \qquad (4.36)$$

33

For potential catalyst active sites:

$$\frac{\partial [C^{\bullet}(j)]_h}{\partial t} + u_h \frac{\partial [C^{\bullet}(j)]_h}{\partial z} = \frac{(1-\varepsilon_h) R_{C^{\bullet}(j),h}}{\varepsilon_h} \qquad j = 1, 2 \qquad (4.37)$$

$$\frac{\partial [C^{\bullet}(j)]_e}{\partial t} + u_e \frac{\partial [C^{\bullet}(j)]_e}{\partial z} = \frac{(1-\varepsilon_e) R_{C^{\bullet}(j),e}}{\varepsilon_e} \qquad j = 1, 2 \qquad (4.38)$$

For uninitiated sites produced by formation reactions:

$$\frac{\partial [R^{\bullet}(0,j)]_h}{\partial t} + u_h \frac{\partial [R^{\bullet}(0,j)]_h}{\partial z} = \frac{(1-\varepsilon_h) R_{R^{\bullet}(0,j),h}}{\varepsilon_h} \qquad j = 1, 2 \qquad (4.39)$$

$$\frac{\partial [R^{\bullet}(0,j)]_e}{\partial t} + u_e \frac{\partial [R^{\bullet}(0,j)]_e}{\partial z} = \frac{(1-\varepsilon_e) R_{R^{\bullet}(0,j),e}}{\varepsilon_e} \qquad j = 1, 2 \qquad (4.40)$$

For cocatalyst:

$$\frac{\partial [A]_h}{\partial t} + u_h \frac{\partial [A]_h}{\partial z} = \frac{(1-\varepsilon_h) R_{A,h}}{\varepsilon_h} \qquad (4.41)$$

$$\frac{\partial [A]_e}{\partial t} + u_e \frac{\partial [A]_e}{\partial z} = \frac{(1-\varepsilon_e) R_{A,e}}{\varepsilon_e} \qquad (4.42)$$

For moments of dead polymer:

$$\frac{\partial [\mu_k(j)]_h}{\partial t} + u_h \frac{\partial [\mu_k(j)]_h}{\partial z} = \frac{(1-\varepsilon_h) R_{\mu_k(j),h}}{\varepsilon_h} \qquad j = 1, 2 \text{ and } k = 0, 1, 2 \qquad (4.43)$$

$$\frac{\partial [\mu_k(j)]_e}{\partial t} + u_e \frac{\partial [\mu_k(j)]_e}{\partial z} = \frac{(1-\varepsilon_e) R_{\mu_k(j),e}}{\varepsilon_e} \qquad j = 1, 2 \text{ and } k = 0, 1, 2 \qquad (4.44)$$

For temperature:

$$\frac{\partial T_h}{\partial t} + u_h \frac{\partial T_h}{\partial z} = \frac{H_{he}(T_e - T_h)}{Cp_g^{\bullet} \varepsilon_h [M]_h + (1-\varepsilon_h)\rho_{polym} Cp_{polym}} + \frac{R_{p,h}(1-\varepsilon_h)(-\Delta H_h) MW}{Cp_g^{\bullet} \varepsilon_h [M]_h + (1-\varepsilon_h)\rho_{polym} Cp_{polym}}$$

$$+ \frac{Cp_g^{\bullet} K_{he}([M]_e - [M]_h)(T_e - T_h)}{Cp_g^{\bullet} \varepsilon_h [M]_h + (1-\varepsilon_h)\rho_{polym} Cp_{polym}} \qquad (4.45)$$

$$\frac{\partial T_e}{\partial t} + u_e \frac{\partial T_e}{\partial z} = \frac{\delta H_{he}(T_h - T_e)}{(1-\delta)\{Cp_g^{\bullet} \varepsilon_e [M]_e + (1-\varepsilon_e)\rho_{polym} Cp_{polym}\}} + \frac{R_{p,e}(1-\varepsilon_e)(-\Delta H_e) MW}{Cp_g^{\bullet} \varepsilon_e [M]_e + (1-\varepsilon_e)\rho_{polym} Cp_{polym}}$$

$\rightarrow (1-\delta)$ here ??

34

$$+ \frac{\delta Cp_g^* K_{be}([M]_b - [M]_e)(T_b - T_e)}{(1-\delta)\{\varepsilon_e [M]_e Cp_g^* + (1-\varepsilon_e)\rho_{polym} Cp_{polym}\}} \qquad (4.46)$$

The subscripts b and e denote bubble phase and emulsion phase, respectively.

4.3.6 Initial and Boundary Conditions

The initial conditions for the FBR can be written as:

$$At \quad t = 0 \begin{cases} [M]_b = [M]_e = [M]_{in} \\ [H_2]_b = [H_2]_e = [H_2]_{in} \\ [C^*(j)]_b = [C^*(j)]_e = [C^*(j)]_{in} \\ [A]_b = [A]_e = [A]_{in} \\ [R^*(0,j)]_b = [R^*(0,j)]_e = 0 \\ [\mu_0(j)]_b = [\mu_0(j)]_e = [\mu_1(j)]_b = [\mu_1(j)]_e = [\mu_2(j)]_b = [\mu_2(j)]_e = 0 \\ [\lambda_0(j)]_b = [\lambda_0(j)]_e = [\lambda_1(j)]_b = [\lambda_1(j)]_e = [\lambda_2(j)]_b = [\lambda_2(j)]_e = 0 \\ T_b = T_e = T_{in} \end{cases} \qquad (4.47)$$

Where $j = 1, 2$.

And the boundary condition is:

$$At \quad z = 0 \begin{cases} [M]_b = [M]_e = [M]_{in} \\ [H_2]_b = [H_2]_e = [H_2]_{in} \\ [C^*(j)]_b = [C^*(j)]_e = [C^*(j)]_{in} \\ [A]_b = [A]_e = [A]_{in} \\ [R^*(0,j)]_b = [R^*(0,j)]_e = 0 \\ [\mu_0(j)]_b = [\mu_0(j)]_e = [\mu_1(j)]_b = [\mu_1(j)]_e = [\mu_2(j)]_b = [\mu_2(j)]_e = 0 \\ [\lambda_0(j)]_b = [\lambda_0(j)]_e = [\lambda_1(j)]_b = [\lambda_1(j)]_e = [\lambda_2(j)]_b = [\lambda_2(j)]_e = 0 \\ T_b = T_e = T_{in} \end{cases} \qquad (4.48)$$

where $j = 1, 2$.

35

4.3.7 Reactor Operating at Steady-State

For non-isothermal steady state operation the reactor model becomes a set of ordinary differential equations:

For monomer:

$$\frac{d[M]_h}{dz} = \frac{K_{he}}{\varepsilon_h u_h}([M]_e - [M]_h) + \frac{R_{p,h}(1-\varepsilon_h)}{\varepsilon_h u_h} \tag{4.49}$$

$$\frac{d[M]_e}{dz} = \frac{\delta K_{he}}{(1-\delta)\varepsilon_e u_e}([M]_h - [M]_e) + \frac{(1-\varepsilon_e)}{\varepsilon_e u_e} R_{p,e} \tag{4.50}$$

For hydrogen:

$$\frac{d[H_2]_h}{dz} = \frac{K_{he,H2}([H_2]_e - [H_2]_h)}{\varepsilon_h u_h} + \frac{(1-\varepsilon_h)R_{H2,h}}{\varepsilon_h u_h} \tag{4.51}$$

$$\frac{d[H_2]_e}{dz} = \frac{\delta K_{he,H2}}{(1-\delta)\varepsilon_e u_e}([H_2]_h - [H_2]_e) + \frac{(1-\varepsilon_e)R_{H2,e}}{\varepsilon_e u_e} \tag{4.52}$$

The reaction is fast so live polymers do not live enough to diffuse so for potential catalyst active sites, uninitiated sites, cocatalyst and dead polymers:

For potential catalyst active sites:

$$\frac{d[C^*(j)]_h}{dz} = \frac{(1-\varepsilon_h)R_{C^*(j),h}}{\varepsilon_h u_h} \qquad j = 1, 2 \tag{4.53}$$

$$\frac{d[C^*(j)]_e}{dz} = \frac{(1-\varepsilon_e)R_{C^*(j),e}}{\varepsilon_e u_e} \qquad j = 1, 2 \tag{4.54}$$

For uninitiated sites produced by formation reactions:

$$\frac{d[R^*(0,j)]_h}{dz} = \frac{(1-\varepsilon_h)R_{R^*(0,j),h}}{\varepsilon_h u_h} \qquad j = 1, 2 \tag{4.55}$$

$$\frac{d[R^*(0,j)]_e}{dz} = \frac{(1-\varepsilon_e)R_{R^*(0,j),e}}{\varepsilon_e u_e} \qquad j = 1, 2 \tag{4.56}$$

36

For cocatalyst:

$$\frac{d[A]_h}{dz} = \frac{(1-\varepsilon_h)R_{A,h}}{\varepsilon_h u_h} \tag{4.57}$$

$$\frac{d[A]_e}{dz} = \frac{(1-\varepsilon_e)R_{A,e}}{\varepsilon_e u_e} \tag{4.58}$$

For moments of dead polymers:

$$\frac{d[\mu_k(j)]_h}{dz} = \frac{(1-\varepsilon_h)R_{\mu_k(j),h}}{\varepsilon_h u_h} \qquad j = 1, 2 \text{ and } k = 0, 1, 2 \tag{4.59}$$

$$\frac{d[\mu_k(j)]_e}{dz} = \frac{(1-\varepsilon_e)R_{\mu_k(j),e}}{\varepsilon_e u_e} \qquad j = 1, 2 \text{ and } k = 0, 1, 2 \tag{4.60}$$

For reactor temperature:

$$\frac{dT_h}{dz} = \frac{H_{be}(T_e - T_h)}{u_h\{Cp_g^*\varepsilon_h[M]_h + (1-\varepsilon_h)\rho_{polym}Cp_{polym}\}} + \frac{R_{p,h}(1-\varepsilon_h)(-\Delta H_h)Mw}{u_h\{Cp_g^*\varepsilon_h[M]_h + (1-\varepsilon_h)\rho_{polym}Cp_{polym}\}}$$

$$+ \frac{Cp_g^* K_{be}([M]_e - [M]_h)(T_e - T_h)}{u_h\{Cp_g^*\varepsilon_h[M]_h + (1-\delta)\rho_{polym}Cp_{polym}\}} \;\to\; (1 - \varepsilon_b) \; ? \tag{4.61}$$

$$\frac{dT_e}{dz} = \frac{\delta H_{be}(T_h - T_e)}{u_e(1-\delta)\{Cp_g^*\varepsilon_e[M]_e + (1-\varepsilon_e)\rho_{polym}Cp_{polym}\}} + \frac{R_{p,e}(1-\varepsilon_e)(-\Delta H_e)Mw}{u_e\{Cp_g^*\varepsilon_e[M]_e + (1-\varepsilon_e)\rho_{polym}Cp_{polym}\}}$$

$$+ \frac{\delta Cp_g^* K_{be}([M]_h - [M]_e)(T_e - T_h)}{u_e(1-\delta)\{\varepsilon_e[M]_e Cp_g^* + (1-\varepsilon_e)\rho_{polym}Cp_{polym}\}} \;\to\; + \; (1-\delta) \; ? \tag{4.62}$$

In the above equations for reactants concentration and temperature profile along the bed height $R_{p,h}$, $R_{p,e}$, $R_{H_2,h}$, $R_{H_2,e}$, $R_{c^*(j),h}$, $R_{c^*(j),e}$, $R_{R^*(0,j),h}$, $R_{R^*(0,j),e}$, $R_{A,h}$, $R_{A,e}$, $R_{\mu_k(j),h}$ and $R_{\mu_k(j),e}$ are polymerization rates in the bubble and emulsion phases, hydrogen reaction rates in the bubble and emulsion phases, potential active site reaction rates in the bubble and emulsion phases, uninitiated sites reaction rates in the bubble and emulsion phases, cocatalyst reaction rates in the bubble and emulsion phases and moments of dead polymer in the bubble and emulsion phases, respectively.

37

4.4 Polymer Properties

Based on the moment's balance, polymer properties such as number and weight average molecular weight, polydispersity index and molecular weight distribution of polymer can be determined.

4.4.1 Number Average and Molecular Weight Average

The number and weight average molecular weight of growing polymer can be defined as:

$$\overline{M_n} = Mw \cdot \frac{\sum\limits_{j=1}^{Ns} \mu_1(j) + \lambda_1(j)}{\sum\limits_{j=1}^{Ns} \mu_0(j) + \lambda_0(j)} \tag{4.63}$$

$$\overline{M_w} = Mw \cdot \frac{\sum\limits_{j=1}^{Ns} \mu_2(j) + \lambda_2(j)}{\sum\limits_{j=1}^{Ns} \mu_1(j) + \lambda_1(j)} \tag{4.64}$$

Where Mw is the molecular weight of the monomer and λ_i and μ_i, the moments of live and dead polymers, are defined in Equation (4.12):

4.4.2 Polydispersity Index

The polydispersity index (*PDI*) of polymer chain can be defined by the ratio of the weight average to number average molecular weight and can be written as:

$$PDI = \frac{\overline{M_w}}{\overline{M_n}} \tag{4.65}$$

4.4.3 Molecular Weight Distribution

Molecular weight distribution (MWD) is an important polymer property because it reflects the kinetics and mechanistic history of the polymer synthesis. Also it is an important tool to assess the quality of a polymer product for a specific application. Two polymers being similar by standard methods of chemical analysis may be different in MWD; consequently, their physical, mechanical and reological properties are different as well.

38

Flory's most probable distribution (Flory, 1953) can be used to describe the instantaneous MWD of polyolefins with linear chains made with single-site type catalysts:

$$w(r) = \tau^2 r \exp(-\tau r) \tag{4.66}$$

where $w(r)$ is the weight chain length distribution of chains of length r and τ is the ratio of transfer rates to propagation rate.

The ratio of rate of transfer reactions to propagation rate τ can be written as:

$$\tau = \frac{R_{tfs}}{R_{pr}} + \frac{R_{tfm}}{R_{pr}} + \frac{R_{tfH}}{R_{pr}} + \frac{R_{tfA}}{R_{pr}} = \frac{k_{tfs}}{k_p[M]} + \frac{k_{tfm}}{k_p} + \frac{k_{tfH}[H_2]}{k_p[M]} + \frac{k_{tfA}[A]}{k_p[M]} \tag{4.67}$$

where R_{pr}, R_{tfs}, R_{tfm}, R_{tfH} and R_{tfA} are the rates of propagation, spontaneous transfer, transfer to monomer, transfer to transfer agent (hydrogen in this study) and transfer to cocatalyst respectively.

Many Ziegler-Natta and metallocene catalysts produce polyolefins with MWD that can be closely predicted by Flory's most probable distribution. It turns out that for polymers obeying Flory's distribution, the polydispersity index is equal 2 and the number average chain length, r_n, of polymer is equal to $1/\tau$.

For multiple site catalysts, some researchers have demonstrated that each site type produces polymer chains that instantaneously follow Flory's distribution. In this case, the instantaneous MWD for the whole polymer will be a weighted sum of individual Flory's distribution (Soares and Hamielec, 1995).

$$\overline{w(r)} = \sum_{j}^{Ns} m_j w_j(r) = \sum_{j}^{Ns} m_j \tau_j^2 r \exp(-\tau_j r) \tag{4.68}$$

where j indicates active site type and m_j is the mass fraction of polymer produces with each site type.

4.5 Numerical Solutions

In this section the numerical solution of the reactor model is discussed.

39

4.5.1 Steady-State Model

The steady-state model describes the variations of concentrations for monomer, catalyst, cocatalyst, hydrogen, bulk polymer and reactor temperature along the bed. The final system of ordinary differential equations consists of twenty-eight ordinary differential equations and can be solved using several numerical methods for solving ordinary differential equation. In this work we employed MATLAB software using multi-step Gear's method for stiff equations. The software is capable of finding the best initial step size for each set of ordinary differential equations in each run. The boundary conditions that were considered for this model are presented in section 4.3.6.

4.5.2 Dynamic Model

The dynamic model describes the variations of the monomer, catalyst, cocatalyst, hydrogen and polymer component with axial position in the reactor and time, for non-isothermal conditions. The model can be solved by the method of Finite Differences. With this method the set of partial differential equations can be converted to a set of ordinary differential equations by using proper grid points along the reactor height. Therefore, this set of equations can be solved by multi-step Gear's method for stiff equations. The boundary and initial conditions are presented in section 4.3.6.

Finite Difference Method

Finite difference method is a simple and efficient method for solving ordinary differential equations (ODEs) and partial differential equations (PDEs) in problem regions with simple boundaries. The method requires the construction of a mesh defining local coordinate surfaces. For each node of this mesh, the unknown function values are found, replacing the differential equations by difference equations. Employing Taylor series expansion we can derive the finite-divided-difference approximations of derivatives. Forward, backward and centered difference approximations are three main approximations derived from Taylor series expansions. The Finite Difference approximations can be represented generally as:

40

$$f'(x_i) = \frac{f(x_{i+1}) - f(x_i)}{x_{i+1} - x_i} + O(x_{i+1} - x_i)$$ (4.69)

or

$$f'(x_i) = \frac{\Delta f_i}{\Delta h} + O(\Delta h)$$ (4.70)

Where Δf_i is refered to as the first forward difference and Δh is the step size, that is the length of interval over which the approximation is made.

In order to have high-accuracy divided-difference formulas $\frac{\Delta f_i}{\Delta h}$, one has to include more additional terms from the Taylor series expansion. Hence, Taylor series expansion can be written as:

$$f'(x_{i+1}) = f(x_i) + f'(x_i)\Delta h + \frac{f''(x_i)}{2}\Delta h^2 + ...$$ (4.71)

Which can be solved for $f'(x_i)$ as:

$$f'(x_i) = \frac{f(x_{i+1}) - f(x_i)}{\Delta h} - \frac{f''(x_i)}{2}\Delta h + O(\Delta h^2)$$ (4.72)

By substituting the following approximation of the second derivative:

$$f''(x_i) = \frac{f(x_{i+2}) - 2f(x_{i+1}) + f(x_i)}{\Delta h^2} + O(\Delta h^2)$$ (4.73)

Into Equation (4.72) to yield:

$$f'(x_i) = \frac{-f(x_{i+2}) + 4f(x_{i+1}) - 3f(x_i)}{2\Delta h} + O(\Delta h^2)$$ (4.74)

Notice that inclusion of second derivative term has improved the accuracy to $O(\Delta h^2)$. Similar improved relations can be developed for central and backward difference as well as for the approximation of higher derivatives. In this work, the improved first order forward difference for the first grid point, improved first order backward difference for the last grid

41

point and central difference approximation for other grid points have been used. The formulas are summarized in Table 4.1.

Table 4.1: Finite difference approximations for different grid points (Chapra and Canale 1988)

a) Forward Finite - Divided - Difference formula (for the first grid point):

$$f'(x_i) = \frac{-f(x_{i+2}) + 4f(x_{i+1}) - 3f(x_i)}{2\Delta h}$$

b) Backward Finite - Divided - Difference formula (for the last grid point):

$$f'(x_i) = \frac{3f(x_i) - 4f(x_{i-1}) + f(x_{i-2})}{2\Delta h}$$

c) Centered Finite - Divided - Difference formula (for all other grid points):

$$f'(x_i) = \frac{f(x_{i+1}) - f(x_{i-1})}{2\Delta h}$$

Based on the Finite Difference method the set of partial differential equations (Equations 4.49-4.62) are converted to ordinary differential equations as follows:

For monomer concentration in the bubble phase:

For case i=1:

$$\frac{d[M]_{b,i}}{dt} = -u_b \frac{-[M]_{b,i+2} + 4[M]_{b,i+1} - 3[M]_{b,i}}{2dz} + \frac{K_{bc}}{\varepsilon_b}([M]_{c,i} - [M]_{b,i}) + \frac{(1-\varepsilon_b)}{\varepsilon_b} R_{p,b,i} \quad (4.75)$$

For case $i = \frac{n}{m}$ (n: $N_{gridpt} \times m$ and m: Number of equations):

$$\frac{d[M]_{b,i}}{dt} = -u_b \frac{3[M]_{b,i} - 4[M]_{b,i-1} + [M]_{b,i-2}}{2dz} + \frac{K_{bc}}{\varepsilon_b}([M]_{c,i} - [M]_{b,i}) + \frac{(1-\varepsilon_b)}{\varepsilon_b} R_{p,b,i} \quad (4.76)$$

For other values of i $(1 < i < \frac{n}{m})$:

$$\frac{d[M]_{b,i}}{dt} = -u_b \frac{[M]_{b,i+1} - [M]_{b,i-1}}{2dz} + \frac{K_{bc}}{\varepsilon_b}([M]_{c,i} - [M]_{b,i}) + \frac{(1-\varepsilon_b)}{\varepsilon_b} R_{p,b,i} \quad (4.77)$$

For monomer concentration in the emulsion phase:

For case $i = \dfrac{n}{m}+1$ (n: $N_{gridpt} \times m$ and m: Number of equations): (4.78)

$$\frac{d[M]_{e,i}}{dt} = -u_e \frac{-[M]_{e,i+2}+4[M]_{e,i+1}-3[M]_{e,i}}{2dz} + \frac{\delta K_{be}}{\varepsilon_e(1-\delta)}([M]_{b,i}-[M]_{e,i}) + \frac{(1-\varepsilon_e)}{\varepsilon_e}R_{p,e,i}$$

For case $i = \dfrac{2n}{m}$: (4.79)

$$\frac{d[M]_{e,i}}{dt} = -u_e \frac{3[M]_{e,i}-4[M]_{e,i-1}+[M]_{e,i-2}}{2dz} + \frac{\delta K_{be}}{\varepsilon_e(1-\delta)}([M]_{b,i}-[M]_{e,i}) + \frac{(1-\varepsilon_e)}{\varepsilon_e}R_{p,e,i}$$

For other values of i $(\dfrac{n}{m}+1 < i < \dfrac{2n}{m})$:

$$\frac{d[M]_{e,i}}{dt} = -u_e \frac{[M]_{e,i+1}-[M]_{e,i-1}}{2dz} + \frac{\delta K_{be}}{\varepsilon_e(1-\delta)}([M]_{b,i}-[M]_{e,i}) + \frac{(1-\varepsilon_e)}{\varepsilon_e}R_{p,e,i} \qquad (4.80)$$

For hydrogen concentration in the bubble phase:

For case $i = \dfrac{2n}{m}+1$ (n: $N_{gridpt} \times m$ and m: Number of equations): (4.81)

$$\frac{d[H_2]_{b,i}}{dt} = -u_b \frac{-[H_2]_{b,i+2}+4[H_2]_{b,i+1}-3[H_2]_{b,i}}{2dz} + \frac{K_{be,H2}}{\varepsilon_b}([H_2]_{e,i}-[H_2]_{b,i}) + \frac{(1-\varepsilon_b)}{\varepsilon_b}R_{H2,b,i}$$

For case $i = \dfrac{3n}{m}$: (4.82)

$$\frac{d[H_2]_{b,i}}{dt} = -u_b \frac{3[H_2]_{b,i}-4[H_2]_{b,i-1}+[H_2]_{b,i-2}}{2dz} + \frac{K_{be,H2}}{\varepsilon_b}([H_2]_{e,i}-[H_2]_{b,i}) + \frac{(1-\varepsilon_b)}{\varepsilon_b}R_{H2,b,i}$$

For other values of i $(\dfrac{2n}{m}+1 < i < \dfrac{3n}{m})$:

$$\frac{d[H_2]_{b,i}}{dt} = -u_b \frac{[H_2]_{b,i+1}-[H_2]_{b,i-1}}{2dz} + \frac{K_{be,H2}}{\varepsilon_b}([H_2]_{e,i}-[H_2]_{b,i}) + \frac{(1-\varepsilon_b)}{\varepsilon_b}R_{H2,b,i} \qquad (4.83)$$

For hydrogen concentration in the emulsion phase:

For case $i = \dfrac{3n}{m}+1$ (n: $N_{gridpt} \times m$ and m: Number of equations): (4.84)

43

$$\frac{d[H_2]_{e,i}}{dt} = -u_e \frac{-[H_2]_{e,i+2} + 4[H_2]_{e,i+1} - 3[H_2]_{e,i}}{2dz} + \frac{\delta K_{be,H2}}{\varepsilon_e(1-\delta)}([H_2]_{b,i} - [H_2]_{e,i}) + \frac{(1-\varepsilon_e)}{\varepsilon_e}R_{H2,e,i}$$

For case $i = \frac{4n}{m}$: (4.85)

$$\frac{d[H_2]_{e,i}}{dt} = -u_e \frac{3[H_2]_{e,i} - 4[H_2]_{e,i-1} + [H_2]_{e,i-2}}{2dz} + \frac{\delta K_{be,H2}}{\varepsilon_e(1-\delta)}([H_2]_{b,i} - [H_2]_{e,i}) + \frac{(1-\varepsilon_e)}{\varepsilon_e}R_{H2,e,i}$$

For other values of i $(\frac{3n}{m}+1 < i < \frac{4n}{m})$

$$\frac{d[H_2]_{e,i}}{dt} = -u_e \frac{[H_2]_{e,i+1} - [H_2]_{e,i-1}}{2dz} + \frac{\delta K_{be,H2}}{\varepsilon_e(1-\delta)}([H_2]_{e,i} - [H_2]_{b,i}) + \frac{(1-\varepsilon_e)}{\varepsilon_e}R_{H2,e,i}$$ (4.86)

For cocatalyst concentration in the bubble phase:

For case $i = \frac{4n}{m}+1$ (n: $N_{gridpt} \times m$ and m: Number of equations):

$$\frac{d[A]_{b,i}}{dt} = -u_b \frac{-[A]_{b,i+2} + 4[A]_{b,i+1} - 3[A]_{b,i}}{2dz} + \frac{(1-\varepsilon_b)}{\varepsilon_b}R_{A,b,i}$$ (4.87)

For case $i = \frac{5n}{m}$:

$$\frac{d[A]_{b,i}}{dt} = -u_b \frac{3[A]_{b,i} - 4[A]_{b,i-1} + [A]_{b,i-2}}{2dz} + \frac{(1-\varepsilon_b)}{\varepsilon_b}R_{A,b,i}$$ (4.88)

For other values of i $(\frac{4n}{m}+1 < i < \frac{5n}{m})$

$$\frac{d[A]_{b,i}}{dt} = -u_b \frac{[A]_{b,i+1} - [A]_{b,i-1}}{2dz} + \frac{(1-\varepsilon_b)}{\varepsilon_b}R_{A,b,i}$$ (4.89)

For cocatalyst concentration in the emulsion phase:

For case $i = \frac{5n}{m}+1$ (n: $N_{gridpt} \times m$ and m: Number of equations):

$$\frac{d[A]_{e,i}}{dt} = -u_e \frac{-[A]_{e,i+2} + 4[A]_{e,i+1} - 3[A]_{e,i}}{2dz} + \frac{(1-\varepsilon_e)}{\varepsilon_e}R_{A,e,i}$$ (4.90)

For case $i = \frac{6n}{m}$:

44

$$\frac{d[A]_{e,i}}{dt} = -u_e \frac{3[A]_{e,i} - 4[A]_{e,i-1} + [A]_{e,i-2}}{2dz} + \frac{(1-\varepsilon_e)}{\varepsilon_e} R_{A,e,i} \qquad (4.91)$$

For other values of i $(\frac{5n}{m}+1 < i < \frac{6n}{m})$ *:*

$$\frac{d[A]_{e,i}}{dt} = -u_e \frac{[A]_{e,i+1} - [A]_{e,i-1}}{2dz} + \frac{(1-\varepsilon_e)}{\varepsilon_e} R_{A,e,i} \qquad (4.92)$$

where dz = Reactor height / Number of grid steps

and

Number of grid steps=Number of grid points-1

Using the Finite Difference discretization method one can solve other molar balance equations for potential active sites, uninitiated active sites, reactor temperature and moments of dead polymers in both phases. The method used above allows transforming any number of partial differential equations with any number of grid points. These sets of discretized equations and the numerical algorithm schematic diagram are presented in Appendix A.

45

CHAPTER 5: SIMULATION RESULTS AND DISCUSSION

5.1 Steady-State Model

The reactor model is comprised of a hydrodynamic model and a kinetic model for ethylene polymerization. The hydrodynamic model representing physical phenomena describes the properties of bubble and emulsion phases. The kinetic model representing the chemical phenomena describes the chemical changes occurring in each phase. The reactor model is superior to a traditional two-phase concept in that it considers the progress of reaction with the existence of solid particles in both phases. Also, it shows a more realistic understanding of the phenomena encountered in a FBR. A comprehensive kinetic model has been developed for polymerization of ethylene. Characterization of polymer properties is simulated using the method of moments (Felorzabihi, 2004b). Application of the method of moments enables prediction of useful information (polymer production rate, monomer conversion, active site information) and the physicochemical characteristics of the polymer (average molecular weights, density, polydispersity, melt index, branching frequency). The hydrodynamic model and the kinetic model were coupled and solved simultaneously to show a complete simulation of the fluidized bed reactor.

The model ability to predict the behaviour of the reactor is assessed through several runs for ethylene polymerization in the presence of Ziegler-Natta catalyst under different reactor operating conditions. The physical properties of the inlet gas to the reactor were calculated using Hysis simulation package.

The model output shows interesting results for the reactants concentrations in the bed. The basic parameters used in this study are shown in Table 5.1. The effects of model main parameters and reactor operating conditions are investigated for the highest ethylene conversion along the bed.

46

Table 5.1: Operational conditions and reactor data used in the simulation

Reactor parameter:	References
H (cm)=1100	Fernandes et al. (2002)
D (cm)=396	McAuley et al. (1994)
Feeding temperature (K)=380	Wagner et al. (1981)
Pressure (atm)=20	Fernandes et al. (2002)
Ethylene (mol/L)=0.85 (90 %)	McAuley et al. (1994)
Hydrogen= 5 %	Wagner et al. (1981)
Nitrogen=5 %	Wagner et al. (1981)
Cocatalyst (mol/L)=0. 7	Wagner et al. (1981)
Gas parameter:	
u_0 (cm/s)=18 (3 u_{mf})	Wagner et al. (1981)
μ_g (g/cm s)=1.3965×10^{-4}	Hysis
K_g (Cal/cm/s/K)=8.448×10^{-5}	Hysis
ρ_g (g/cm3)=0.01792	Hysis
Cp_g (Cal/g/K)=0.45485	Hysis
D_g (cm^2/s)=0.004	Hatzantonis et al. (2000)
D_{H2} (cm^2/s)=0.03884	Treybal (1980)
Polymer properties:	
ρ_{polym} (g/cm^3)=0.96	Xie et al. (1994)
ΔH (Cal/g)= -916	Choi and Ray (1985)
Cp_{polym}(Cal/g/K)=0.456	Choi and Ray (1985)
Catalyst data:	
C* (mol/cm^{3}cat.)=10e-5	Wagner et al. (1981)
$\rho_{catalyst}$ (g/cm^3)=2.37	McAuley et al. (1994)
$d_p(cm)$=0.05	McAuley et al. (1994)
A_{sf}^1 =0.5	Yiagopoulos et al. (2001)
A_{sf}^2 =0.5	Yiagopoulos et al. (2001)

47

Table 5.2: Numerical values of the kinetic rate constants

Rate constant	Site 1	Site 2	References
Site formation:			
k_f (cm^3/mol/s)	$1 \times 10^{4'}$	1×10^4	Hatzantonis et al. (2000)
E_f (cal/mol)	8000	8000	Hatzantonis et al. (2000)
Site activation:			
k_i (cm^3/mol/s)	4.2×10^5	4.2×10^5	Hatzantonis et al. (2000)
E_i (cal/mol)	9000	9000	Hatzantonis et al. (2000)
Propagation:			
k_p (cm^3/mol/s)	8.5×10^4	8.5×10^4	McAuley et al. (1994)
E_p (cal/mol)	9000	9000	McAuley et al. (1994)
Transfer to monomer:			
k_{tfm} (cm^3/mol/s)	2.1	2.1	McAuley et al. (1994)
E_{tfm} (cal/mol)	9000	9000	McAuley et al. (1994)
Transfer to cocatalyst:			
k_{tfA} (cm^3/mol/s)	24	120	McAuley et al. (1994)
E_{tfA} (cal/mol)	9000	9000	McAuley et al. (1994)
Transfer to hydrogen:			
k_{tfH} (cm^3/mol/s)	88	370	McAuley et al. (1994)
E_{tfH} (cal/mol)	9000	9000	McAuley et al. (1994)
Spontaneous transfer:			
k_{tfs} (1/s)	0.0012	0.0012	Hatzantonis et al. (2000)
E_{tfs} (cal/mol)	8000	8000	Hatzantonis et al. (2000)
Deactivation:			
k_d (1/s)	1.8×10^{-4}	1.8×10^{-4}	Hatzantonis et al. (2000)
E_d (cal/mol)	10000	10000	Hatzantonis et al. (2000)

5.1.1 Steady-State and Isothermal

In contrast to most conventional fluidized bed reactors, the solid phase (polymer) is of prime importance in gas phase olefin polymerization (Choi and Ray, 1985). The conversion of monomer per one pass in a fluidized bed reactor is relatively low and it is about 1% to 5% per one pass (McAuley et al., 1994). A typical result for monomer conversion and molecular properties of polymer under isothermal condition is shown in Figures 5.1-5.5. Other relevant plots are arranged in Appendix B.

As shown in Figures 5.1.a and 5.1.b, monomer conversion is much higher in emulsion phase than in bubble phase because of higher reaction rate (Figure B.4). This is due to the existence of more solid catalyst particles in the emulsion phase and also because of higher residence time for polymerization reaction and diffusion of monomer in the emulsion phase. The profile of overall monomer conversion in the bed according to Equation (4.29) is shown in Figure 5.1.c. The overall monomer conversion is about 1% per pass in the fluidized bed reactor under isothermal condition.

Figure 5.1: Profile of monomer conversion versus reactor axial position (isothermal)

49
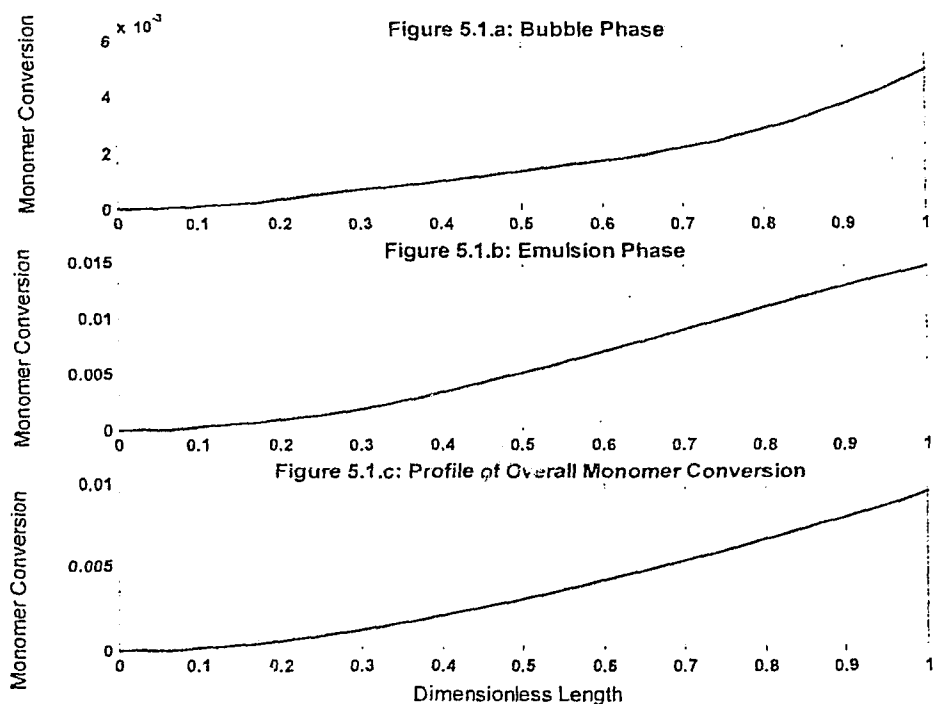
The cumulative number average and weight average molecular weight of polymer per pass versus conversion are plotted in Figures 5.2 and 5.3, respectively. They decrease with monomer conversion. This is due to a high reduction in concentration of reactants in comparison with formation of living polymer chains. Besides, $\overline{M_n}$ and $\overline{M_w}$ decrease more rapidly in the emulsion phase than in the bubble phase because of higher reaction rate. $\overline{M_n}$ is in the range of 60600 in the bed, whereas $\overline{M_w}$ is in the range of 135600, giving a polydispersity index of 2.24. These values are in good agreement with actual data reported for number and weight average molecular weights of HDPE polymer produced with Ziegler-Natta catalysts (Odian, 1991). However the *PDI* in this study is lower than the actual polydispersity index for HDPE since the rate constants are selected in the way that *PDI* in each site be equal to 2 (McAuley 1990).

Figure 5.2: Profile of number average molecular weight of polymer versus conversion (isothermal)

Mnb: Number average molecular weight (Bubble phase)
Mne: Number average molecular weight (Emulsion phase)
Mn: Overall number average molecular weight in the bed

50
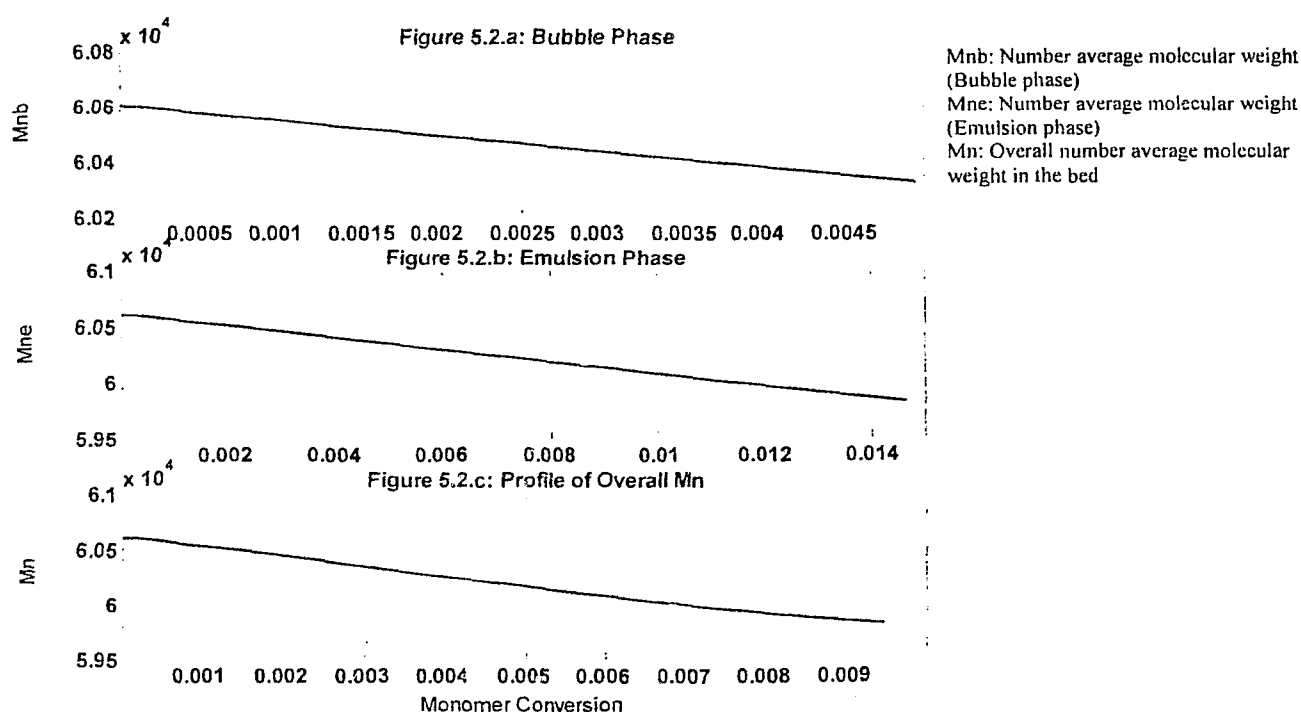
Figure 5.3: Profile of weight average molecular weight of polymer versus conversion (isothermal)

Figure 5.3.a: Bubble Phase

Figure 5.3.b: Emulsion Phase

Figure 5.3.c: Profile of Overall Mw

Monomer Conversion

Mwb: Weight average molecular weight (Bubble phase)
Mwe: Weight average molecular weight (Emulsion phase)
Mw: Overall weight average molecular weight in the bed
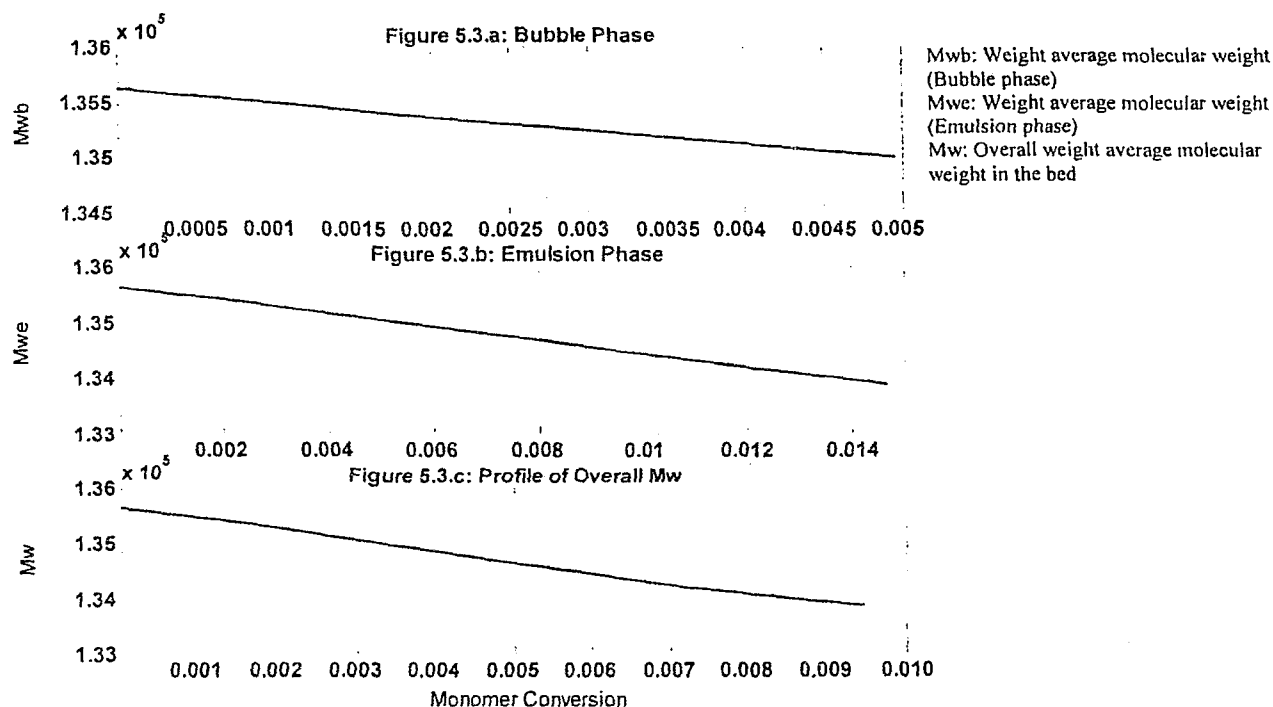
Profiles of polydispersity index are shown in Figure 5.4. Polydispersity index increases slightly in the bubble phase, whereas in the emulsion phase it decreases from 2.24 to about 2.22. The overall polydispersity index in the bed obeys the same trends as bubble phase does. These values are basically dependent on the numerical values of kinetic rate constants and operating conditions and can also be above these values.

Figures 5.5.a, 5.5.b and 5.5.c show profiles of molecular weight distribution MWD of the polymer for bubble phase, emulsion phase and overall MWD in the bed, respectively. The model considers the existence of two active sites on Ziegler-Natta catalyst and simulations showed that about 94 % (by weight) of solid polymer is produced by site one and 6% by site two (for both bubble and emulsion phases). The simulation predicts that site one produces polymer with broader molecular weight distribution than site two.

51

Figure 5.4: Profile of polydispersity index versus conversion (isothermal)

Figure 5.4.a: Polydispersity Index (Bubble Phase)

PDIb: Polydispersity index (Bubble phase)
PDIe: Polydispersity index (Emulsion phase)
PDI: Overall polydispersity index in the bed

Figure 5.4.b: Polydispersity Index (Emulsion Phase)

Figure 5.4.c: Profile of Overall Polydispersity Index

Conversion
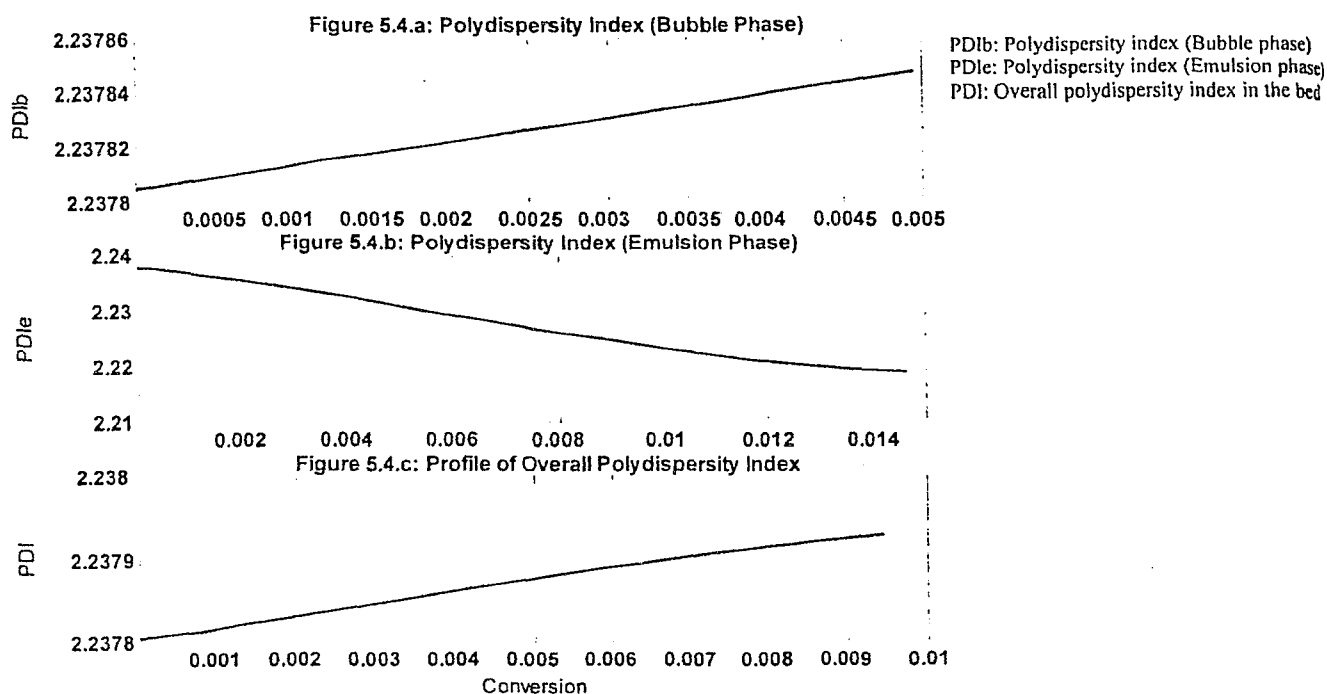
Figure 5.5: Profile of molecular weight distribution of polymer at the exit of bed (isothermal)

Figure 5.5.a: Profile of MWD (Bubble Phase)

Site 1
Site 2
Total

Figure 5.5.b: Profile of MWD (Emulsion Phase)

Site 1
Site 2
Total

Figure 5.5.c: Profile of Overall MWD in the Bed

Site 1
Site 2
Total

r

52
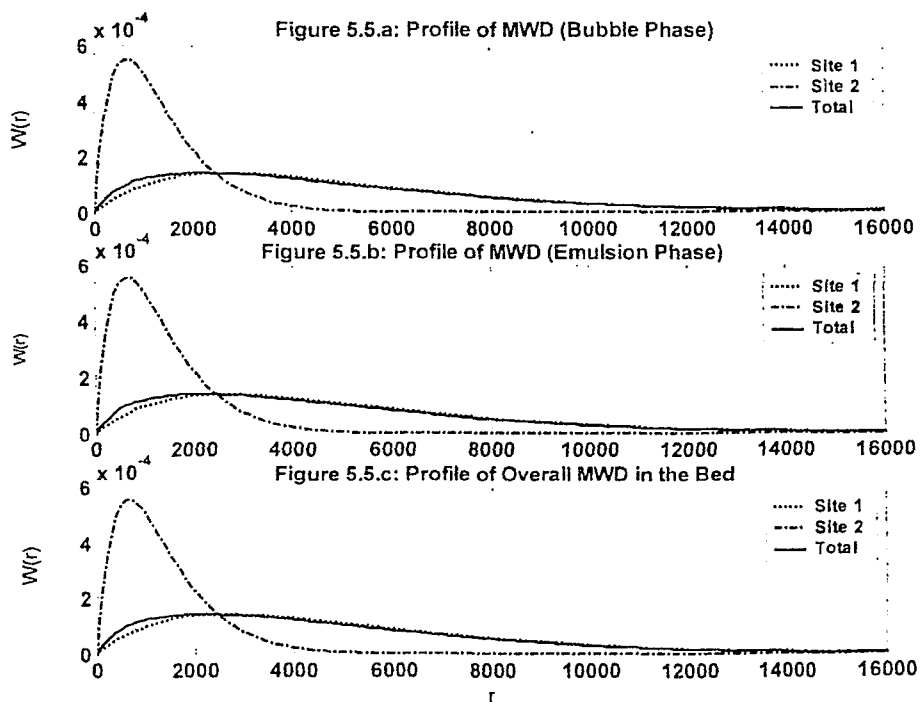
The cocatalyst reacts with the catalyst and it is constantly consumed to prepare active sites for polymerization. However, more cocatalyst is consumed in the emulsion phase than the bubble phase because of higher polymerization rate. Figures B.1 and B.2 in Appendix B show catalyst and cocatalyst consumption in both phases and their overall concentration in the bed. In the bubble phase catalyst consumption remains relatively low, but in emulsion phase catalyst concentration decreases slightly from 0.05 mol/L to about 0.0496 mol/L per pass in the bed. Hydrogen is used as a chain transfer agent in ethylene polymerization to control the molecular weight of the polymer. It also can be used for transferring solid catalyst particles into the bed. Figure B.3 shows a relatively small consumption rate of hydrogen in both phases.

In FBR the bubble size, which depends on the distributor character, is an important and influential hydrodynamic parameter, which affects bubble velocity and heat/mass transfer coefficients. The bubble size increases along the bed height until it reaches to its maximum allowable size. Figure B.5 shows the profile of bubble growth along the bed.

5.1.2 Steady-State and Non-Isothermal

Figures 5.6-5.11 show profiles of monomer conversion, number average and weight average molecular weight ($\overline{M_n}$ and $\overline{M_w}$), polydispersity index (PDI), molecular weight distribution (MWD) and reactor temperature for a non-isothermal fluidized bed reactor. All these plots demonstrate a high monomer conversion in the non-isothermal case in comparison with the isothermal one (about %1.5).

The simulations show that, for the non-isothermal process, both $\overline{M_n}$ and $\overline{M_w}$ are slightly higher at the beginning of polymerization reaction in comparison with the isothermal process (Figures 5.7.c and 5.8.c). But, as the reaction proceeds they decrease to a slightly lower level. Besides, as it is illustrated in Figure 5.9.c, PDI increases slightly with conversion and is lower for the non-isothermal process.

53

Figure 5.6: Profile of monomer conversion versus reactor axial position (non-isothermal)

Figure 5.6.a: Bubble Phase

Figure 5.6.b: Emulsion Phase

Figure 5.6.c: Profile of Overall Monomer Conversion
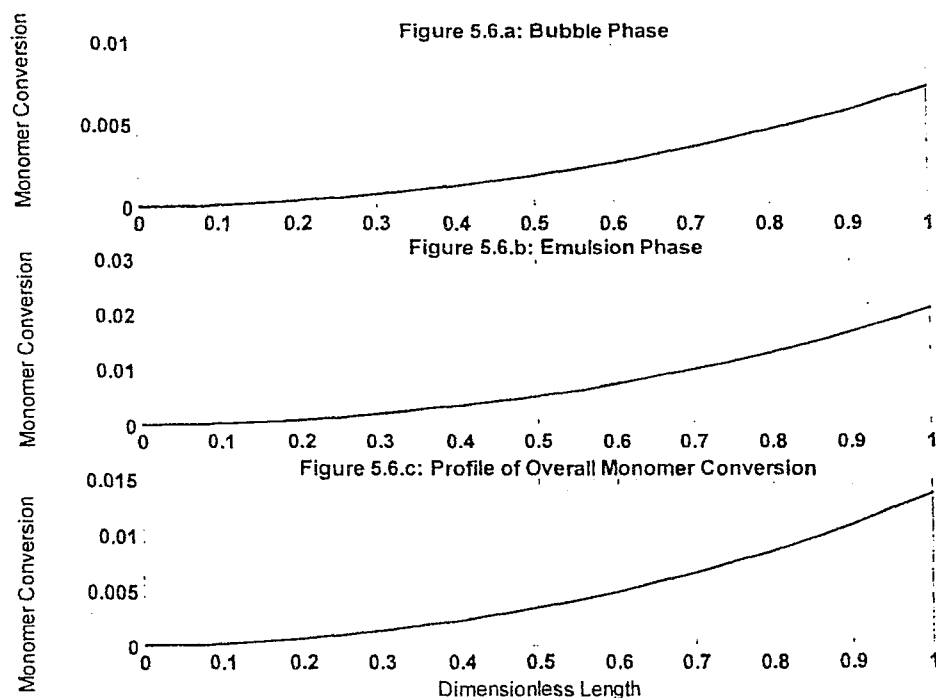
Figure 5.7: Profile of number average molecular weight of polymer versus conversion (non-isothermal)

Figure 5.7.a: Bubble Phase

Figure 5.7.b: Emulsion Phase

Figure 5.7.c: Profile of Overall Mn

Mnb: Number average molecular weight (Bubble phase)
Mne: Number average molecular weight (Emulsion phase)
Mn: Overall number average molecular weight in the bed

54
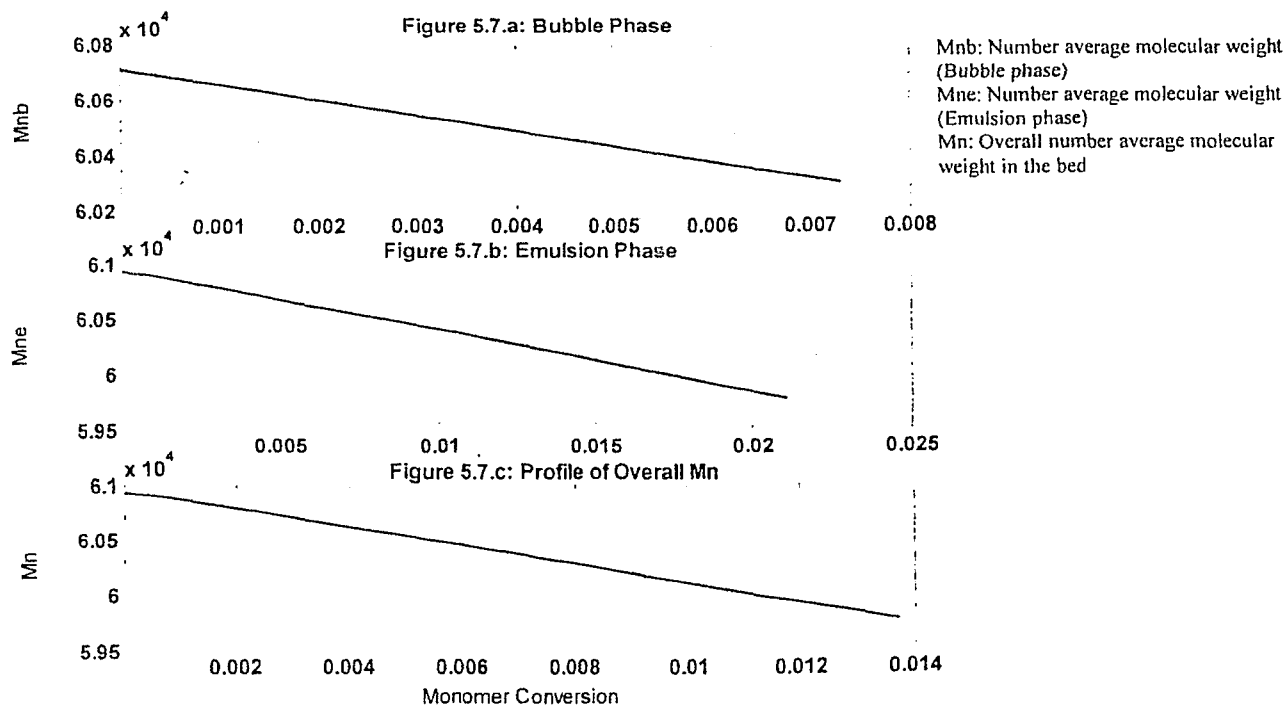
Figure 5.8: Profile of weight average molecular weight of polymer versus conversion (non-isothermal)

Figure 5.8.a: Bubble Phase

Figure 5.8.b: Emulsion Phase

Figure 5.8.c: Profile of Overall Mw

Monomer Conversion

Mwb: Weight average molecular weight (Bubble phase)
Mwe: Weight average molecular weight (Emulsion phase)
Mw: Overall weight average molecular weight in the bed
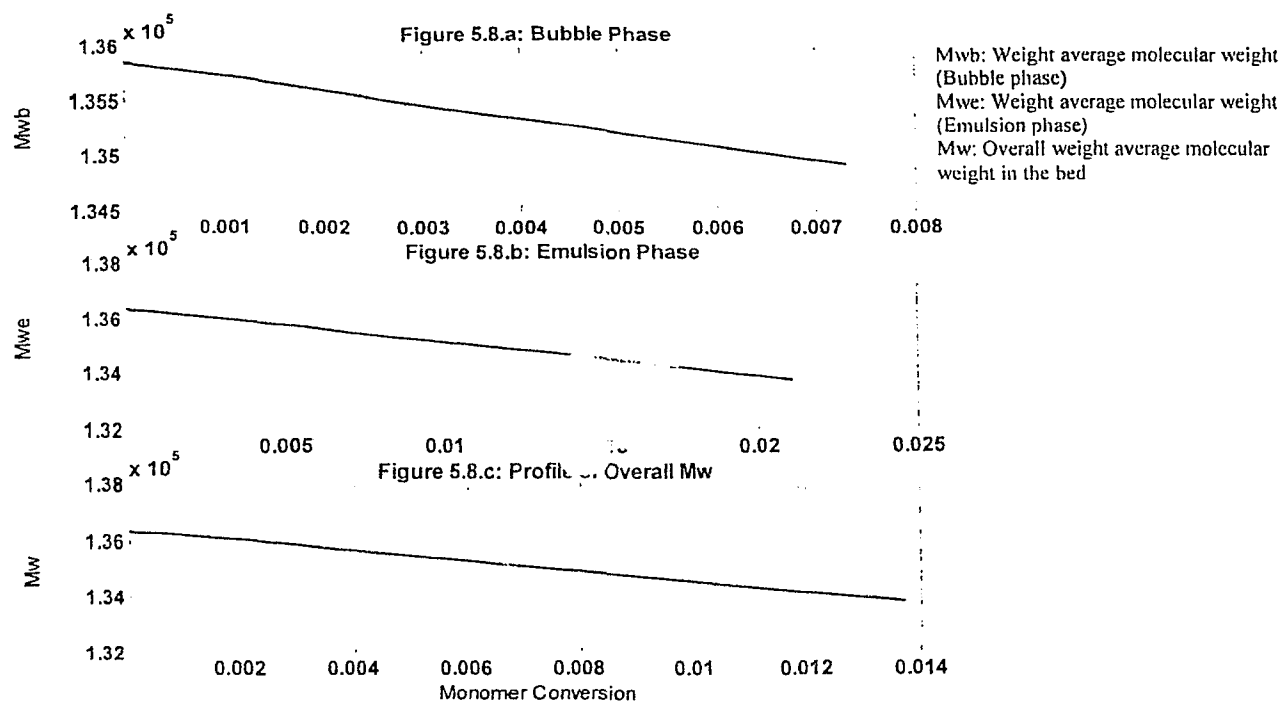
Figure 5.9: Profile of polydispersity index versus conversion (non-isothermal)

Figure 5.9.a: Polydispersity Index (Bubble Phase)

Figure 5.9.b: Polydispersity Index (Emulsion Phase)

Figure 5.9.c: Profile of Overall Polydispersity Index

Conversion

PDIb: Polydispersity index (Bubble phase)
PDIe: Polydispersity index (Emulsion phase)
PDI: Overall polydispersity index in the bed
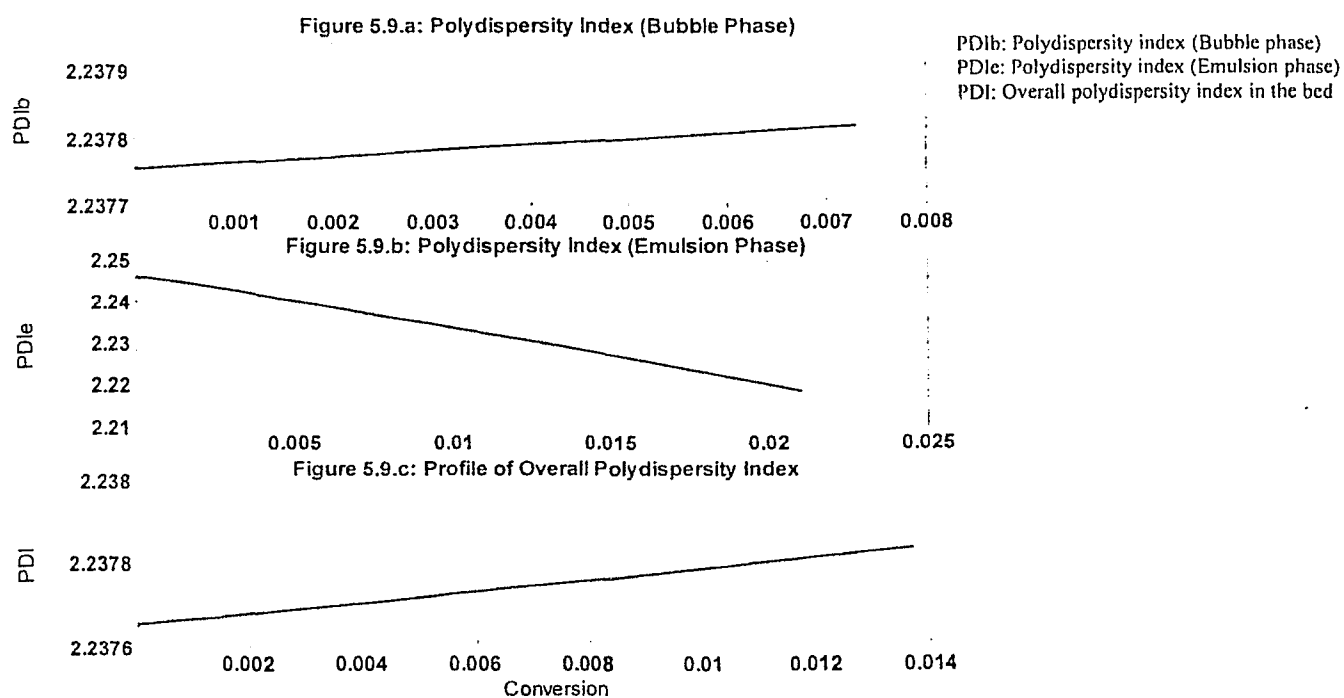
Figure 5.10: Profile of molecular weight distribution of polymer at the exit of bed (non-isothermal)

Figure 5.10.a: Profile of MWD (Bubble Phase)

Figure 5.10.b: Profile of MWD (Emulsion Phase)
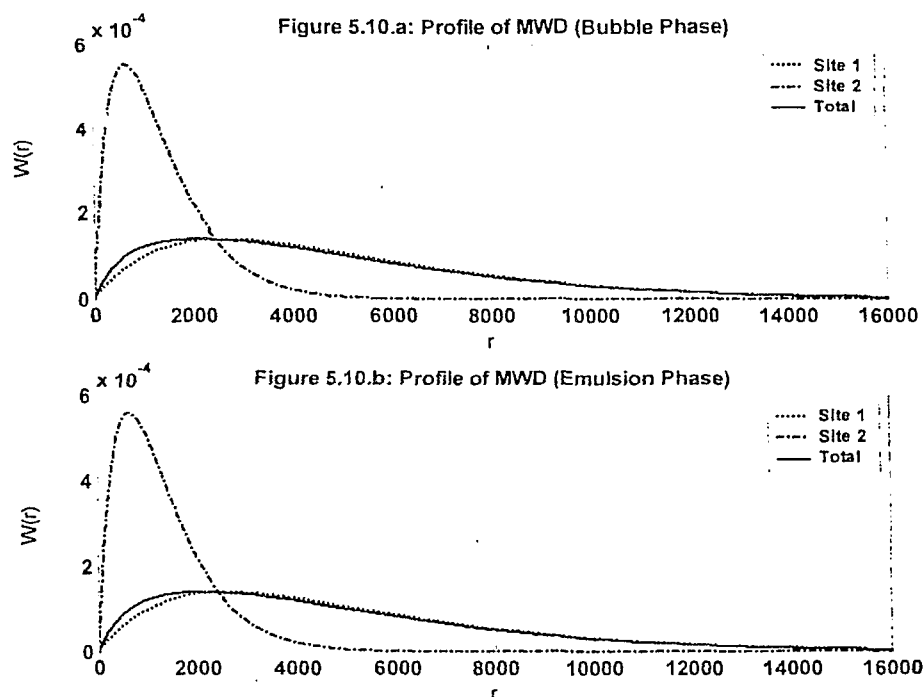
The profile of reactor temperature is shown in Figure 5.11. The reactor temperature increases gradually along the bed from 380 K to about 383 K in the bubble phase and to about 389 K in emulsion phase. The top portion of reactor is much warmer than the lower portion. The temperature increase is attributed to a higher activity of catalyst in the propagation of young polymer particles (as fluidizing gas moves upward in the bed and react with the catalyst, more active sites undergo initiation process). Also, reactor temperature increases more rapidly in emulsion phase than in the bubble phase because of higher polymerization rate in emulsion phase (Figure B.9).

Catalyst consumption in the bubble phase is not significantly influenced in a non-isothermal process. Cocatalyst consumption in the bubble phase and emulsion phase is not altered significantly in the non-isothermal process (Figure B.7).

56

Figure 5.11: Profile of reactor temperature versus reactor axial position (non-isothermal)

Figure 5.11.a: Bubble phase

Figure 5.11.b: Emulsion phase
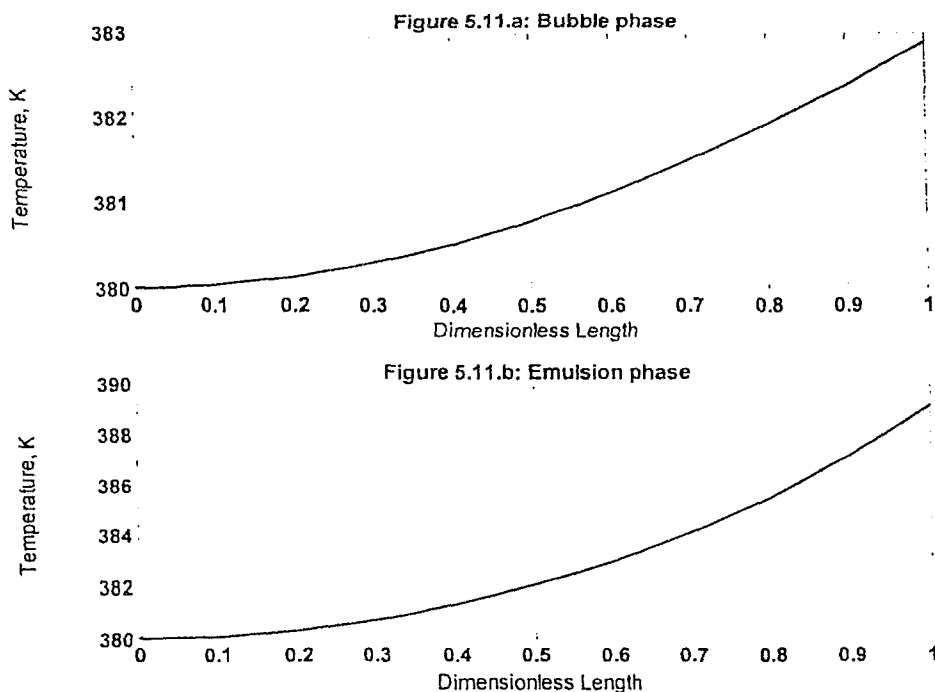
5.2 Effects of Other Operational Parameters (Steady-State)

The effect of important reactor parameters (e.g. superficial gas velocity, mean particle size, bubble size, gas feed temperature, chain transfer agent and recycle stream), on the steady-state behavior of the FBR is thoroughly investigated.

5.2.1 Superficial Gas Velocity

The superficial velocity is an important parameter. It must remain sufficiently high to entrain large solid particles moving upward in the bed and at the same time permit good heat removal (Choi and Ray, 1985). Therefore, as reported by Wagner et al. (1981), industrial polyethylene fluidized bed reactors operate at superficial gas velocities ranging from 3 to 6 times the minimum fluidization velocity.

Increasing superficial gas velocity allows bubble growth size to expand (Figure C.5 in Appendix C) and reduces interfacial area between phases, which ultimately reduces mass/heat interchange between phases. On the other hand, a decrease in the superficial gas velocity results in an increase of reactants mean residence time in the bed. As a result, concentrations

57

of monomer, hydrogen and cocatalyst in both phases decrease more rapidly. However, this effect is more significant in bubble phase than in emulsion phase. The effect of superficial gas velocity on monomer conversion is illustrated in Figure 5.12.

Figure 5.12: The effect of superficial gas velocity on profile of monomer conversion versus reactor axial position per pass
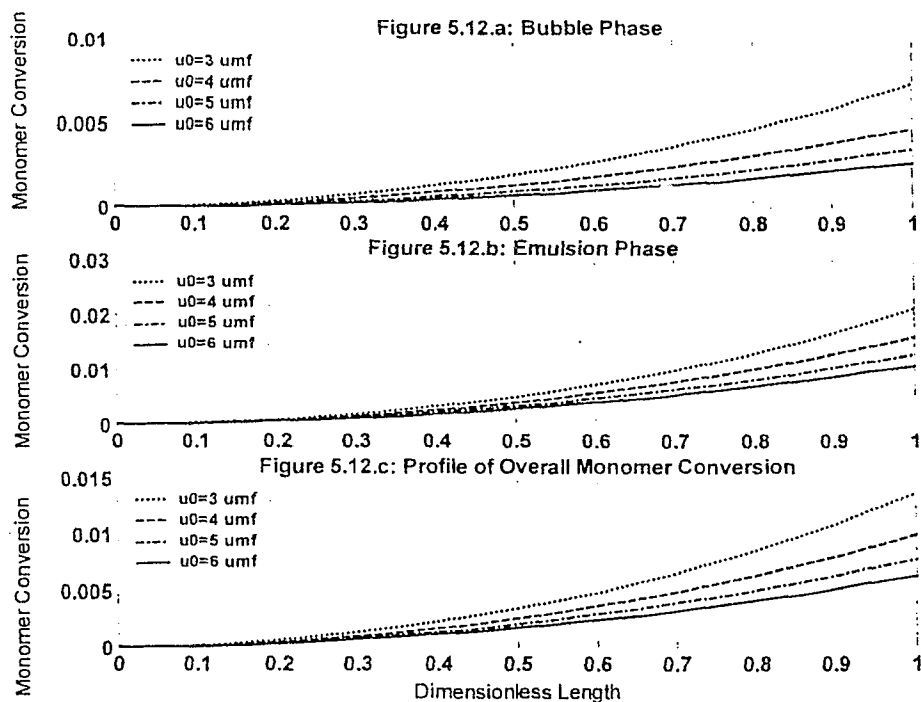
It can be seen that reducing superficial gas velocity by half will almost double the conversion of monomer in the emulsion phase and triple the conversion in the bubble phase. Also, the temperature increases more rapidly along the bed with lower superficial gas velocities for both phases (Figure 5.13).

Figure 5.13: The effect of superficial gas velocity on profile of reactor temperature versus reactor axial position

Figure 5.13.a: Bubble phase

Figure 5.13.b: Emulsion phase
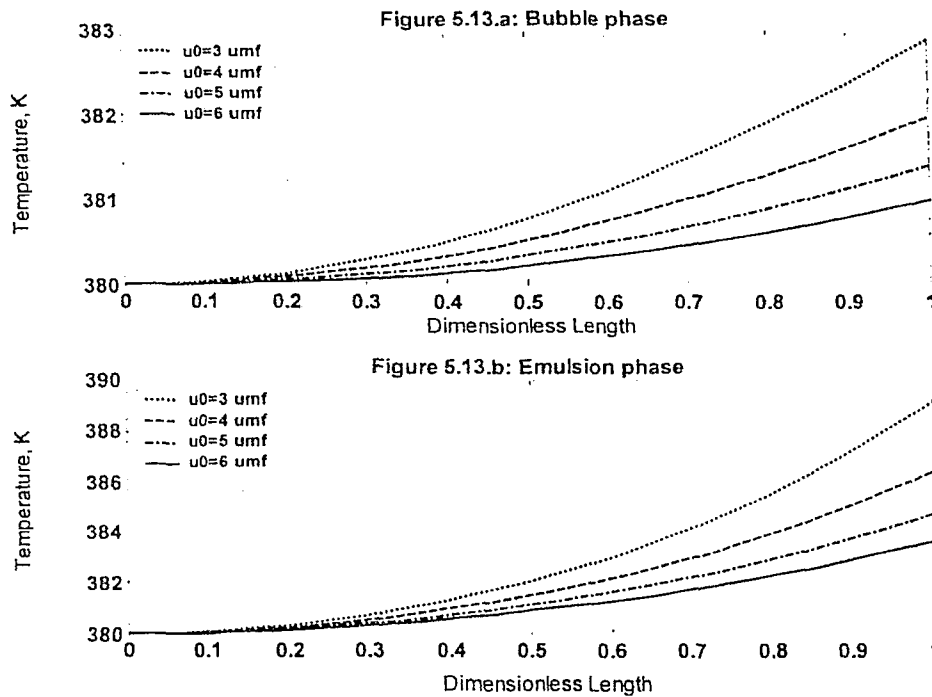
Figures 5.14 and 5.15 show the effect of superficial gas velocity on the profiles of number and weight average molecular weight of polymer in the bed. The figures demonstrate that processes with lower superficial gas velocities has higher $\overline{M_n}$ and $\overline{M_w}$ at low conversions but at high conversions $\overline{M_n}$ and $\overline{M_w}$ are lower with lower superficial gas velocities. As superficial gas velocity decreases, the rate of heat and mass transfer between the phases increase, therefore, the production of active sites and moments of polymer increases. As a result $\overline{M_n}$ and $\overline{M_w}$ increases. But as the reaction proceeds, more active sites undergo deactivation process therefore moments of polymer and $\overline{M_n}$ and $\overline{M_w}$ become lower at higher conversions.

The effect of superficial gas velocity on the polydispersity index is shown in Figure 5.16. The *PDI* in the bubble phase is lowered as superficial gas velocity decreases. However in emulsion phase, this trend is opposite. The *PDI* profile in the bed is illustrated in Figure 5.16.c. This plot shows that the superficial gas velocity affects significantly the profile of overall polydispersity index in the bed.

59

Figure 5.14: The effect of superficial gas velocity on profile of number average molecular weight of polymer versus conversion

Figure 5.14.a: Bubble Phase

Mnb: Number average molecular weight (Bubble phase)
Mne: Number average molecular weight (Emulsion phase)
Mn: Overall number average molecular weight in the bed

Figure 5.14.b: Emulsion Phase

Figure 5.14.c: Profile of Overall Mn

Monomer Conversion
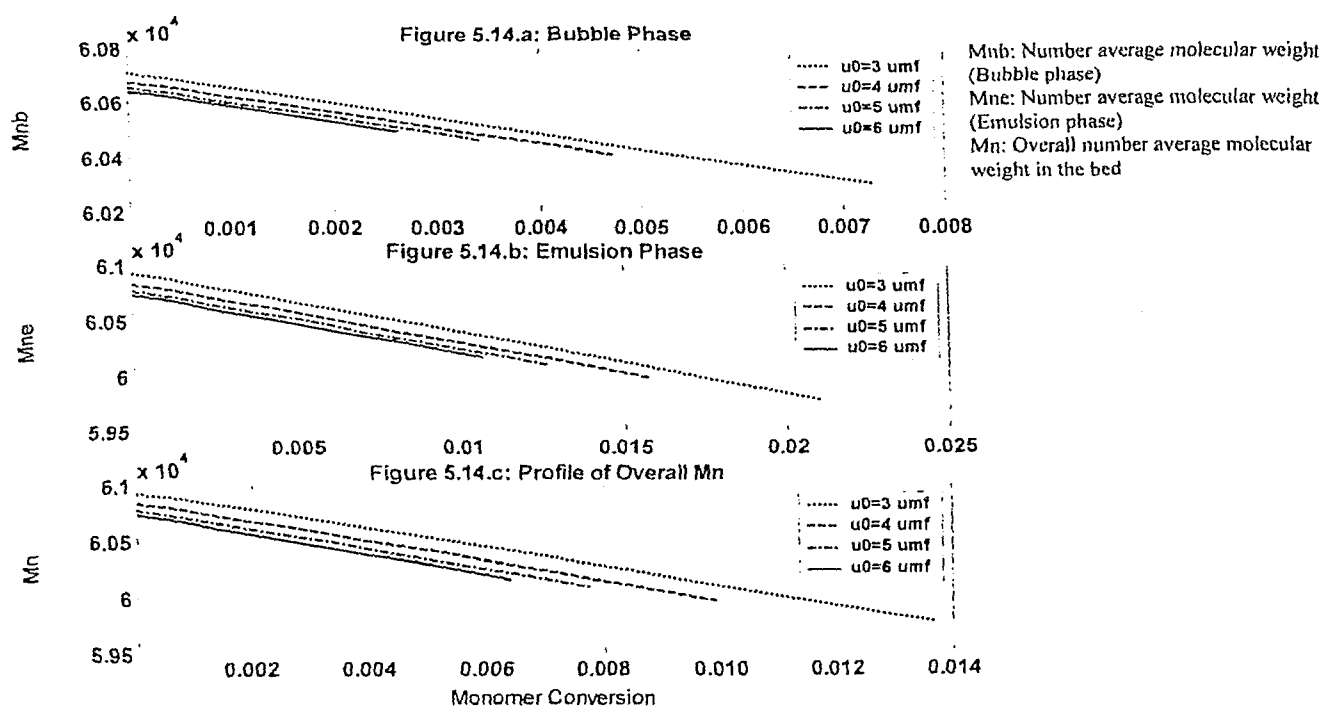
Figure 5.15: The effect of superficial gas velocity on profile of weight average molecular weight of polymer versus conversion

Figure 5.15.a: Bubble Phase

Mwb: Weight average molecular weight (Bubble phase)
Mwe: Weight average molecular weight (Emulsion phase)
Mw: Overall weight average molecular weight in the bed

Figure 5.15.b: Emulsion Phase

Figure 5.15.c: Profile of Overall Mw

Monomer Conversion

60
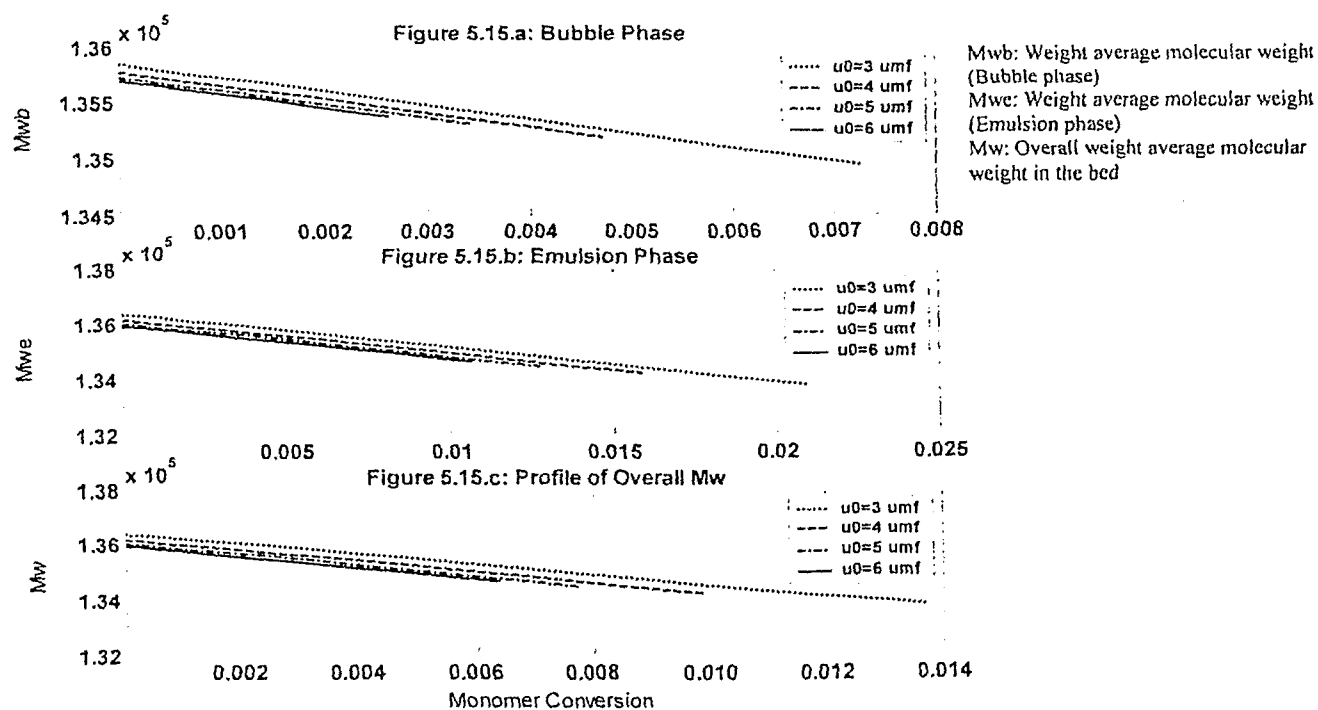
Figure 5.16: The effect of superficial gas velocity on profile of polydispersity index versus conversion

Figure 5.16.a: Polydispersity Index (Bubble Phase)
Figure 5.16.b: Polydispersity Index (Emulsion Phase)
Figure 5.16.c: Profile of Overall Polydispersity Index

PDIb: Polydispersity index (Bubble phase)
PDIe: Polydispersity index (Emulsion phase)
PDI: Overall polydispersity index the bed
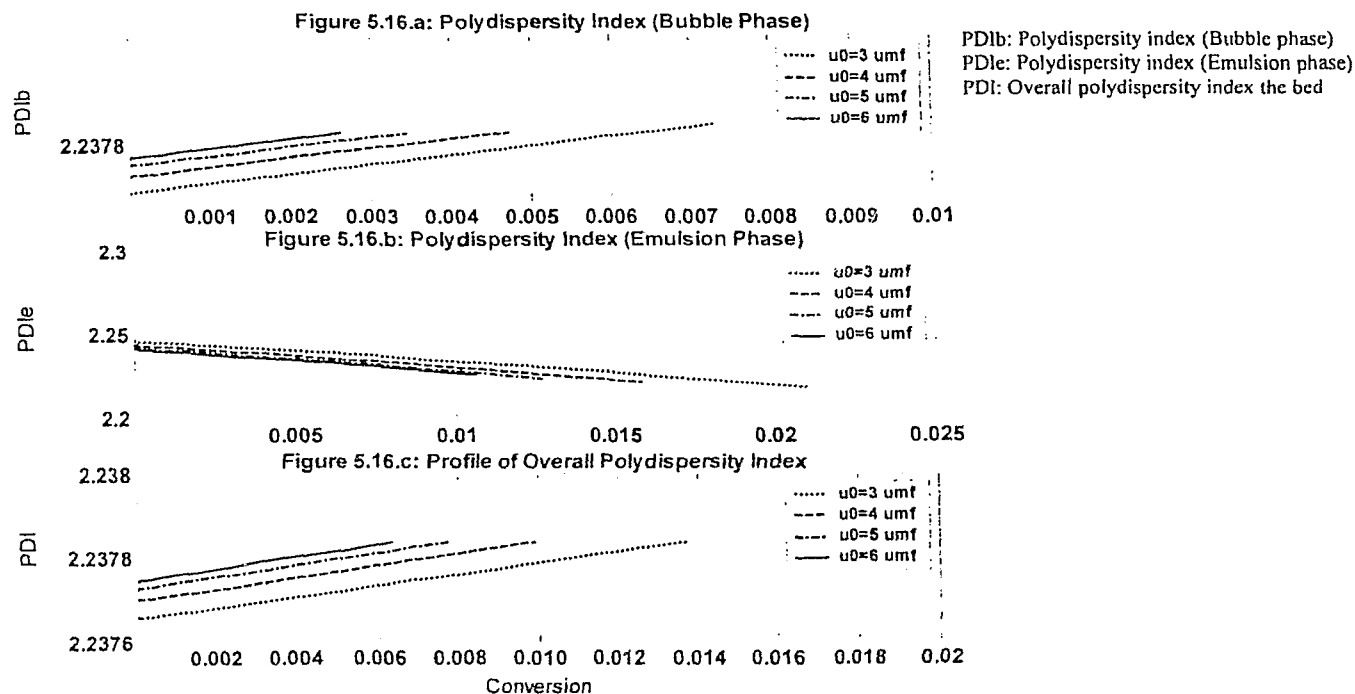
Figure C.2 in Appendix C illustrates the effect of superficial gas velocity on cocatalyst consumption in the bed. But at higher superficial gas velocities there is no significant difference in cocatalyst consumption rate in bubble phase. However, at lower superficial gas velocities (u0=3 cm/s), there is a steep decrease in cocatalyst concentration. Similar trend is predicted for catalyst in the bubble phase (Figure C.1.a). In emulsion phase, catalyst and cocatalyst concentrations decrease with reducing superficial gas velocity, which is primarily attributed to an increase in the polymerization rate.

The effect of superficial gas velocity on polymerization rate in both phases is illustrated in Figure C.4. This variable has a very significant effect on improving the reaction rate in the bubble phase. Reducing superficial gas velocity by half will almost double the polymerization rate in the emulsion phase and increase it in the bubble phase by more than ten times.

61

5.2.2 Mean Particle Size

In practice, the continuous addition of catalyst and removal of product leads to a distribution of particle size in the bed ranging from 0.005 to 0.2 cm (McAuley, et al. 1994). If all particles in the FBR have the same size, then an increase in the particle size implicitly affects all main fluidization parameters including minimum fluidization velocity, terminal velocity, maximum stable bubble size and heat and mass transfer coefficient between the bubble phase and emulsion phase. Figure 5.17 and 5.20 illustrate the effect of mean particle size on the steady state monomer conversion and temperature, respectively. Monomer conversion and temperature vary significantly with the average particle size in the bubble phase. It is important to note that an increase in the mean particle size results in an increase in the minimum fluidization velocity. A secondary effect is to increase the terminal velocity and maximum stable bubble size (Figure C.10). In the bubble phase, an increase in the bubble growth reduces interfacial area between the phases. As a result, the heat and mass transfer rate between the phases reduces significantly. On the other hand, using larger particle size in the bed increases minimum fluidization velocity. Hence, emulsion velocity increases and its residence time decreases accordingly. Therefore, polymerization rate is lowered by increasing particle size in the emulsion phase (Figure C.9.b)

Profiles of number average molecular weight and *PDI* are shown in Figures 5.18 and 5.19, respectively. According to these figures, processes with smaller particle size may produce polymers with higher number and weight average molecular weights and lower *PDI*.

Figure 5.17: The effect of mean particle size on profile of monomer conversion versus reactor axial position

Figure 5.17.a: Bubble Phase

Figure 5.17.b: Emulsion Phase

Figure 5.17.c: Profile of Overall Monomer Conversion

Figure 5.18: The effect of mean particle size on profile of number average molecular weight of polymer versus conversion

Figure 5.18.a: Bubble Phase

Mnb: Number average molecular weight (Bubble phase)
Mne: Number average molecular weight (Emulsion phase)
Mn: Overall number average molecular weight in the bed

Figure 5.18.b: Emulsion Phase

Figure 5.18.c: Profile of Overall Mn

63

Figure 5.19: The effect of mean particle size on profile of polydispersity index versus conversion

Figure 5.19.a: Polydispersity Index (Bubble Phase)

PDIb: Polydispersity index (Bubble phase)
PDIe: Polydispersity index (Emulsion phase)
PDI: Overall polydispersity index the bed

Figure 5.19.b: Polydispersity Index (Emulsion Phase)

Figure 5.19.c: Profile of Overall Polydispersity Index

Figure 5.20: The effect of mean particle size on profile of reactor temperature versus reactor axial position .

Figure 5.20.a: Bubble phase

Figure 5.20.b: Emulsion phase

64
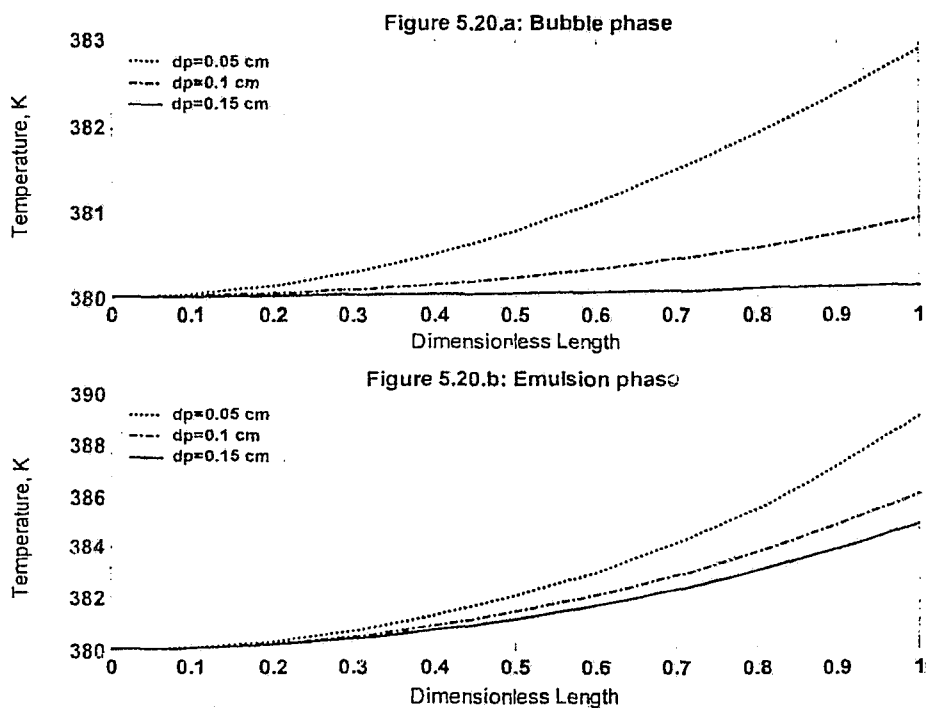
5.2.3 Gas Feed Temperature

Figure 5.21 illustrates profiles of the monomer concentration in a FBR for bubble and emulsion phases and for three different gas-feed temperatures. As the inlet gas temperature rises, the concentration of reactants falls because of the higher reaction rate. In the first 25% of the reactor, there is no significant difference between monomer conversion profiles at the three different temperatures. However, in the upper reactor portion, ethylene concentration decreases faster with higher gas feed temperatures due to higher reaction rate. For a 10 K increase in the inlet gas temperature, the monomer conversion almost doubles in the bed. Similar trend is obtained for catalyst and cocatalyst in the first 10 % of the reactor height and for hydrogen in the first 25% of the height (Figures C.11, C.12 and C.13).

Figure 5.21: The effect of gas feed temperature on profile of monomer conversion versus reactor axial position
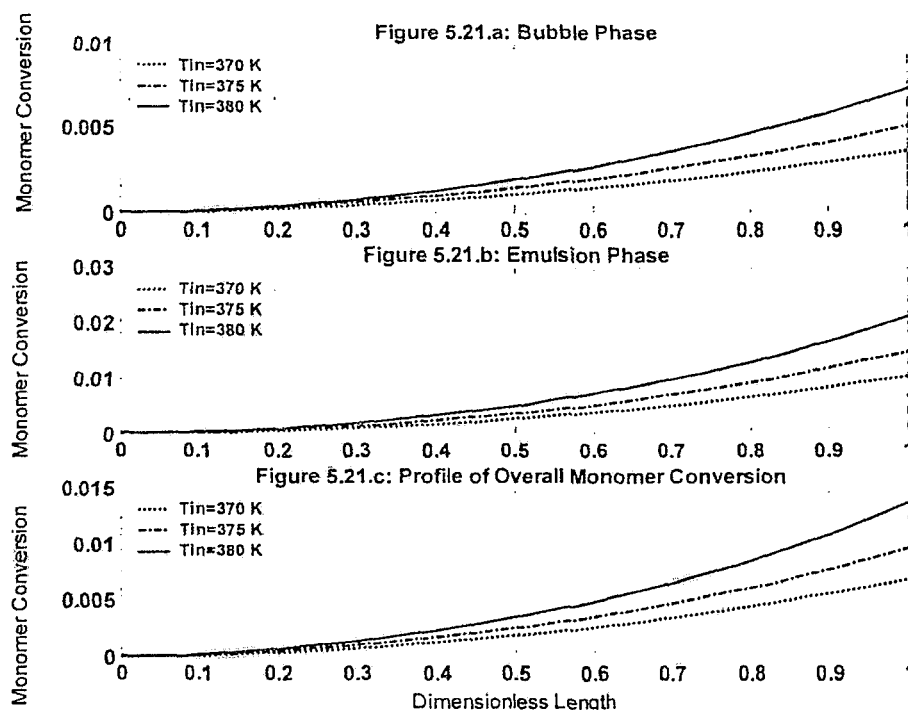
Furthermore, in the case of gas feed temperature above 116 ° C, the reactor temperature can go up to the polymer melting point and causes production of unwanted sticky material deteriorating polyethylene production rate. Therefore, although the inlet gas feed temperature

65

is one of the most influential parameters in ethylene polymerization, it should be carefully selected in order to prevent formation of hot spots and unwanted materials. Further, similar trend is obtained for weight average molecular weights of the polymer along the bed. At low conversions, higher inlet temperatures produce polymers with elevated $\overline{M_n}$ and $\overline{M_w}$. But at higher conversions (at the exit of the bed) $\overline{M_n}$ and $\overline{M_w}$ are lower in higher inlet gas temperatures.

Increasing inlet gas temperature reduces *PDI* in the bubble phase (Figure 5.24), but it has hardly any effect on *PDI* in the emulsion phase. Furthermore, no effect is registered for *MWD* of polymer in this range of temperatures, even though it is expected that MWD becomes narrower as temperature increases.

Figure 5.22: The effect of gas feed temperature on profile of reactor temperature versus reactor axial position
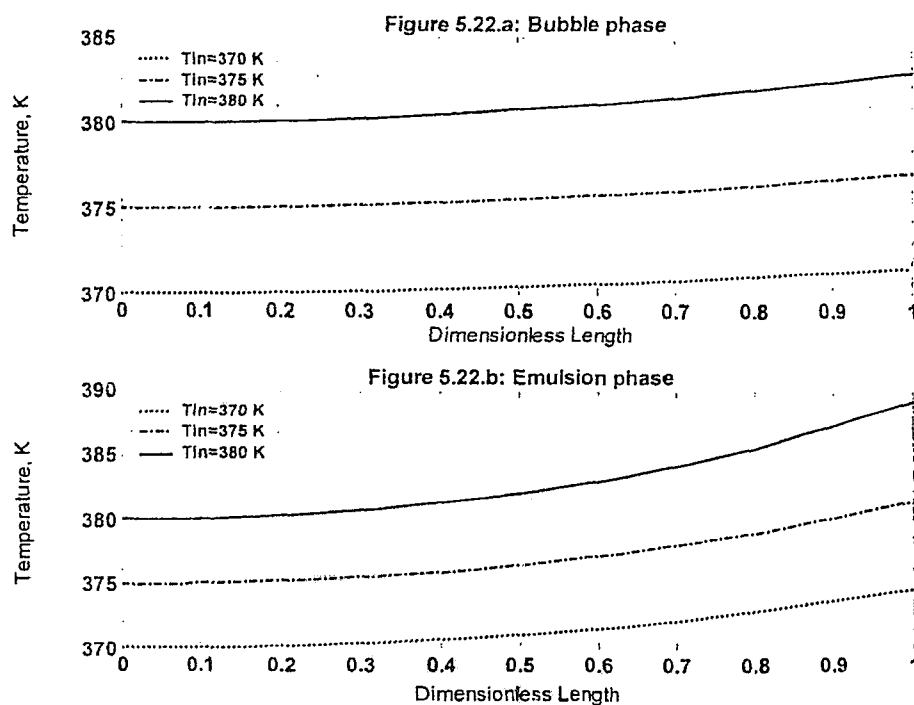
Figure 5.23: The effect of gas feed temperature on profile of number average molecular weight of polymer versus conversion

Figure 5.23.a: Bubble Phase

Figure 5.23.b: Emulsion Phase

Figure 5.23.c: Profile of Overall Mn

Mnb: Number average molecular weight (Bubble phase)
Mne: Number average molecular weight (Emulsion phase)
Mn: Overall number average molecular weight in the bed
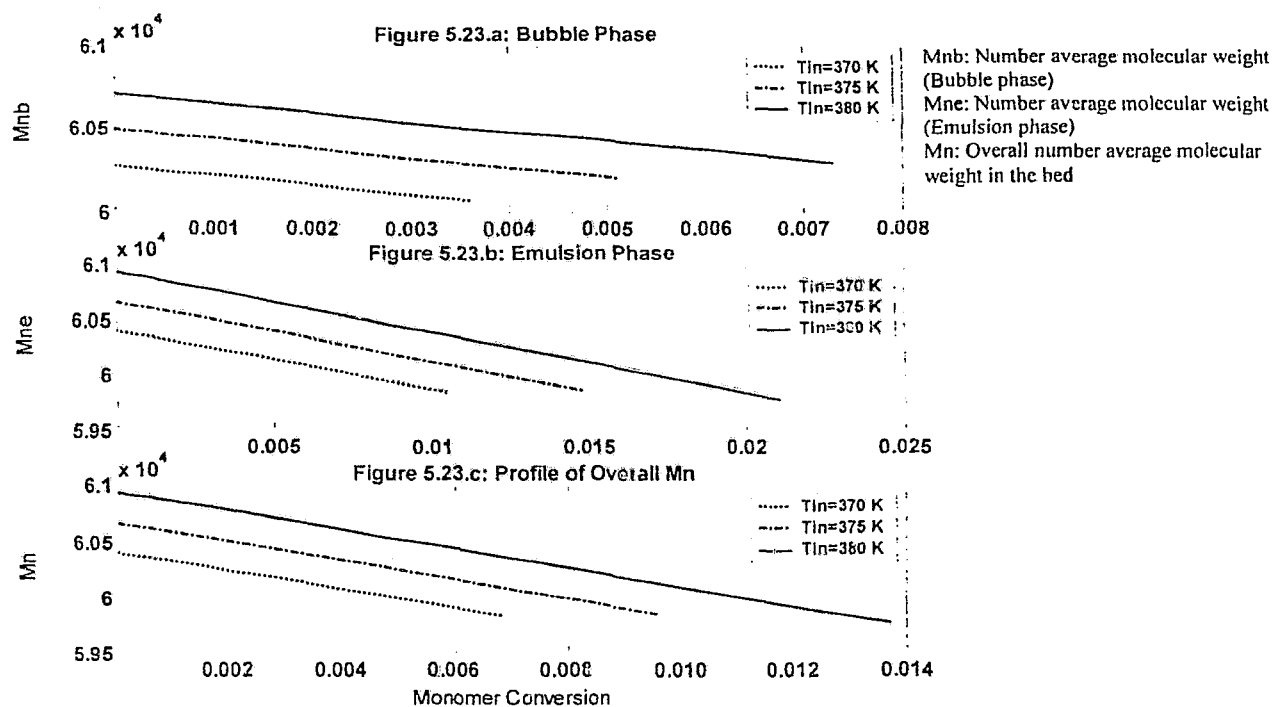
Figure 5.24: The effect of gas feed temperature on profile of polydispersity index versus conversion

Figure 5.24.a: Polydispersity Index (Bubble Phase)

Figure 5.24.b: Polydispersity Index (Emulsion Phase)

Figure 5.24.c: Profile of Overall Polydispersity Index

PDlb: Polydispersity index (Bubble phase)
PDle: Polydispersity index (Emulsion phase)
PDI: Overall polydispersity index the bed

5.2.4 Bubble Size

To investigate the importance of using an accurate bubble growth size, simulations were performed to determine the effect of the bubble growth size on model prediction. The bubble diameter has been varied by changing the maximum stable bubble diameter in the bed. Since this parameter directly affects the profile of bubble growth in the bed (Figure C.18). For the operating conditions of Table 5.1, the Davidson-Harrison correlation predicts a maximum bubble size of approximately 23.46 cm. However, Grace (1986) recommended that this parameter should be taken with caution since the maximum bubble diameter depends strongly on the type of solid particles in the FBR and the fluidization mode. Figure 5.25 shows the effect of maximum bubble diameter on steady-state model predictions of monomer conversion in the bed.

Figure 5.25: The effect of bubble size on profile of monomer conversion versus reactor axial position
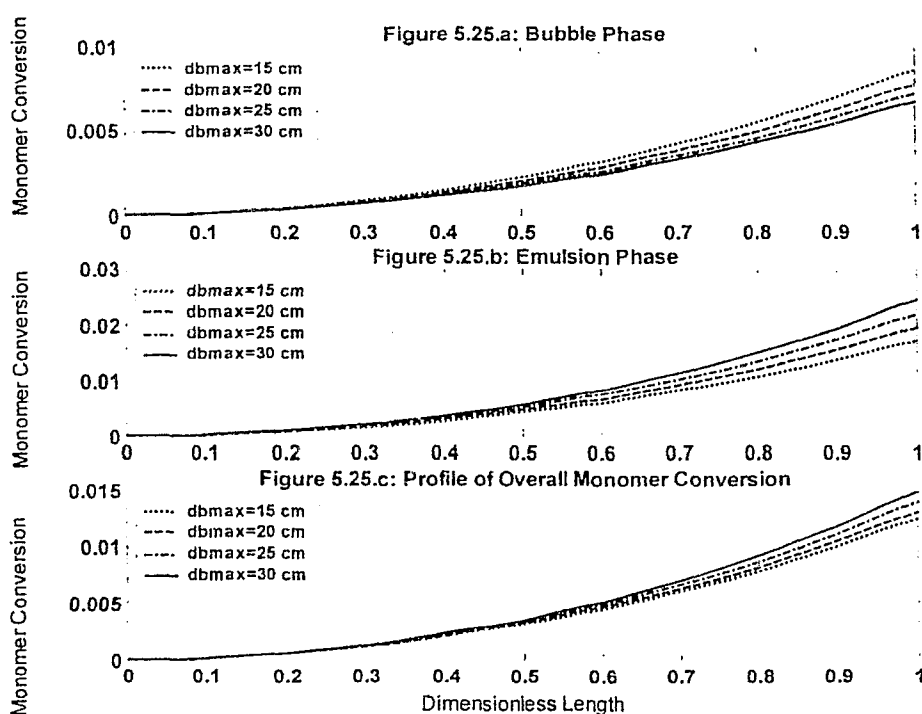
The interfacial area between the phases decreases with larger bubble diameters, which consequently lowers the heat/mass interchange rate between them. As a result, larger bubble

68

size in a fluidized bed causes low monomer conversion and also low temperature rise in the bubble phase (Figures 5.25 and 5.28). In the first half of the bed, monomer conversion in the emulsion phase is not appreciably influenced by bubble growth rate. In the second half it increases with larger bubble size due to increase in diffusion of gases from emulsion phase to the bubble phase. In contradiction with the finding of McAuley et al. (1994), the simulation has shown that the maximum bubble size is not a critical system parameter. This result is in good agreement with the findings of Hatzantonis et al. (2000).

The number and weight average molecular weights of polymer increase with reducing maximum bubble size in the bubble. But, $\overline{M_n}$, $\overline{M_w}$ and PDI are not altered significantly for all the ranges of maximum bubble size in the emulsion phase.
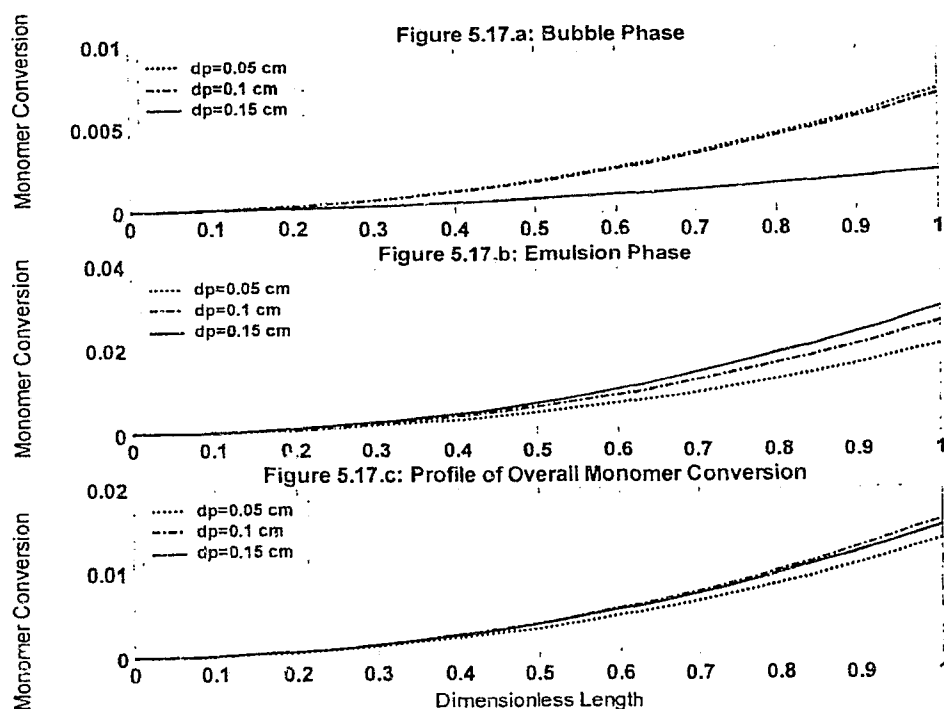
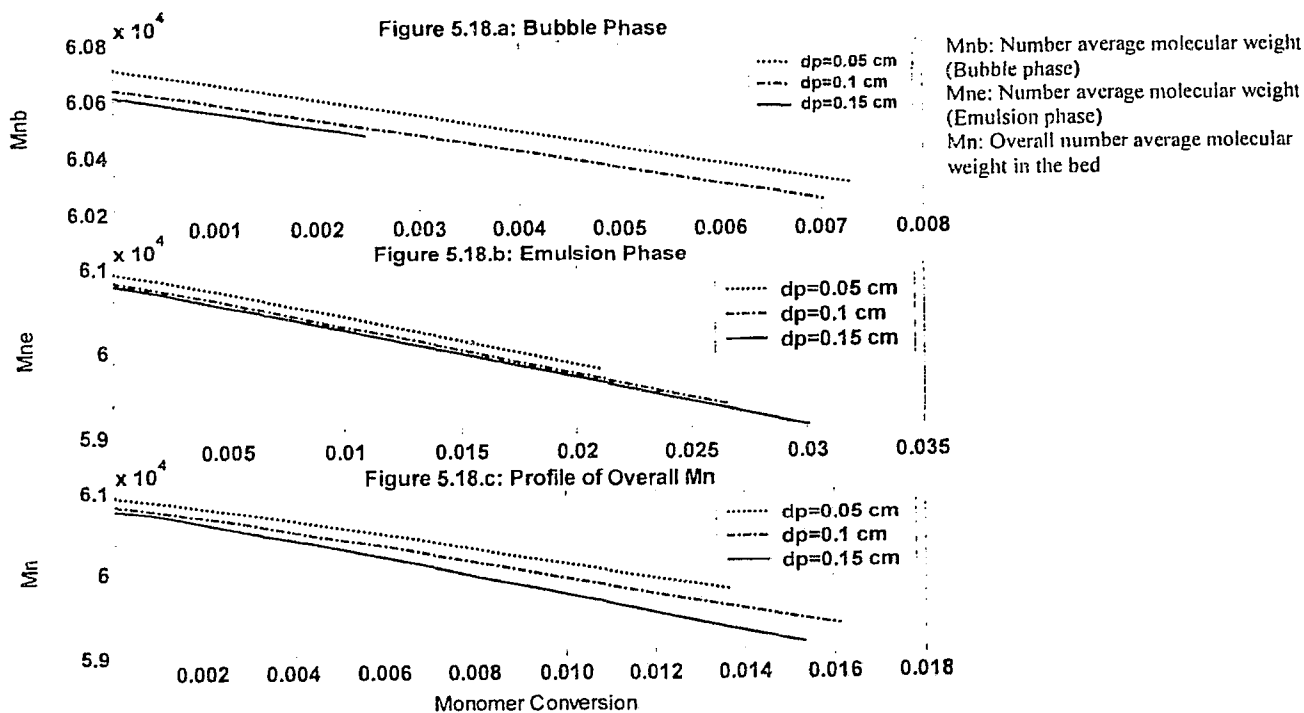Figure 5.26: The effect of bubble size on profile of weight average molecular weight of polymer versus conversion
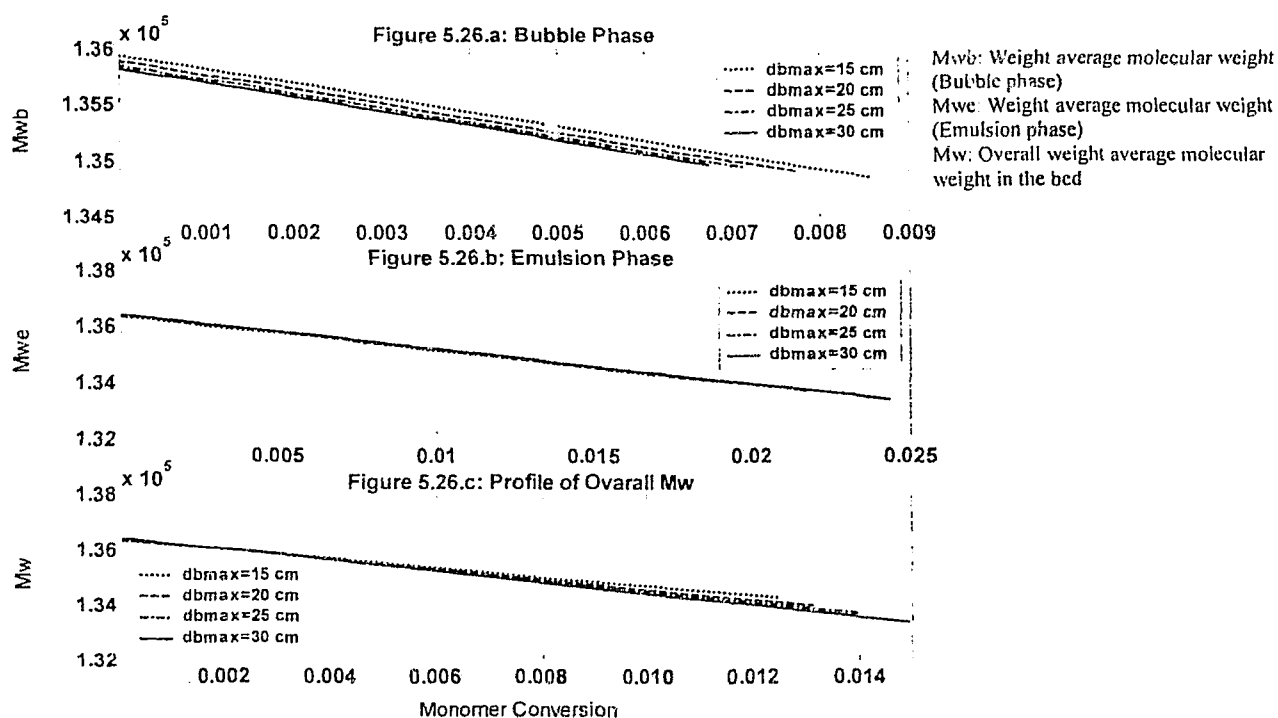
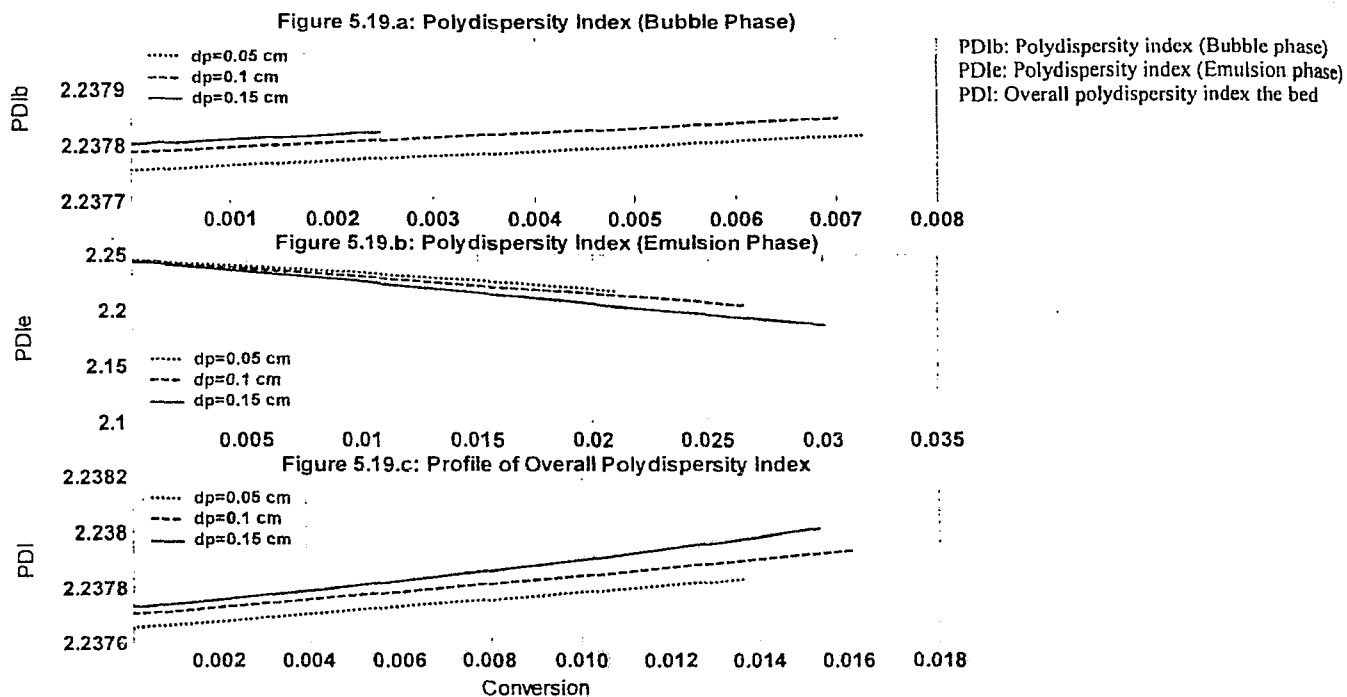Figure 5.27: The effect of bubble size on profile of polydispersity index versus conversion

Figure 5.27.a: Polydispersity Index (Bubble Phase)

Figure 5.27.b: Polydispersity Index (Emulsion Phase)

Figure 5.27.c: Profile of Overall Polydispersity Index

PDIb: Polydispersity index (Bubble phase)
PDIe: Polydispersity index (Emulsion phase)
PDI: Overall polydispersity index the bed
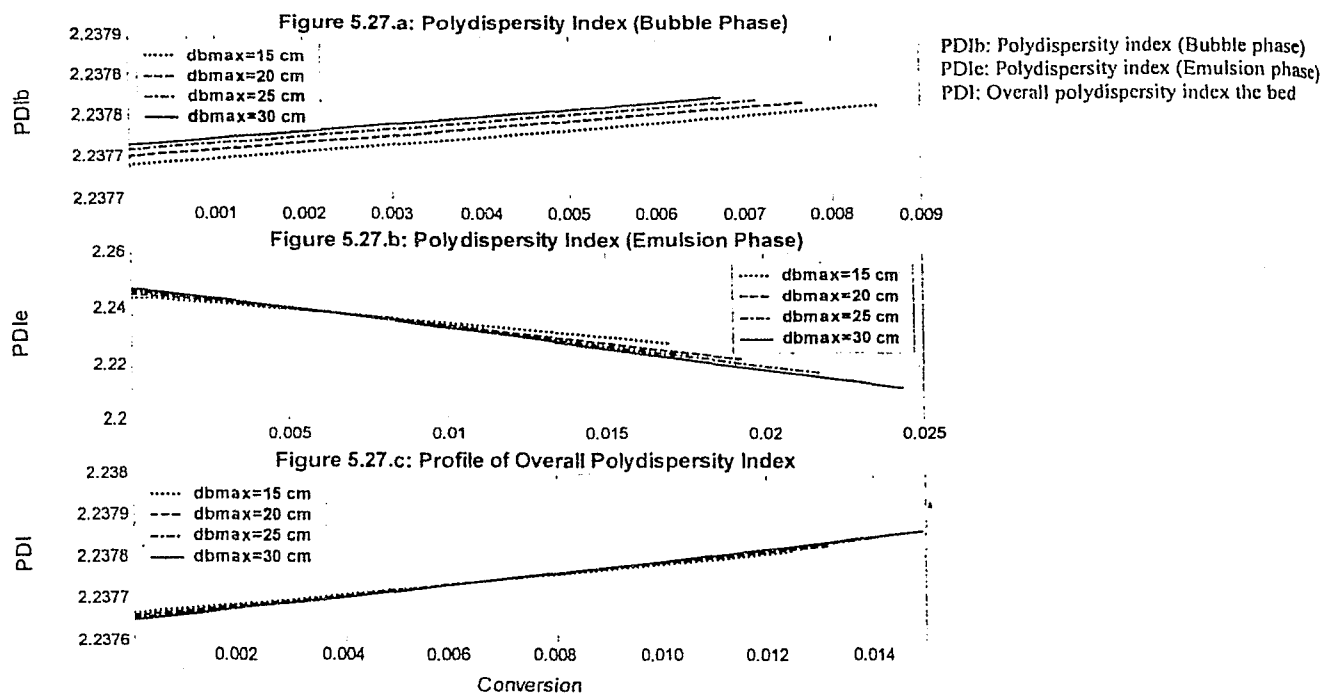
Figure 5.28: The effect of bubble size on profile of reactor temperature versus reactor axial position

Figure 5.28.a: Bubble phase

Figure 5.28.b: Emulsion phase

70
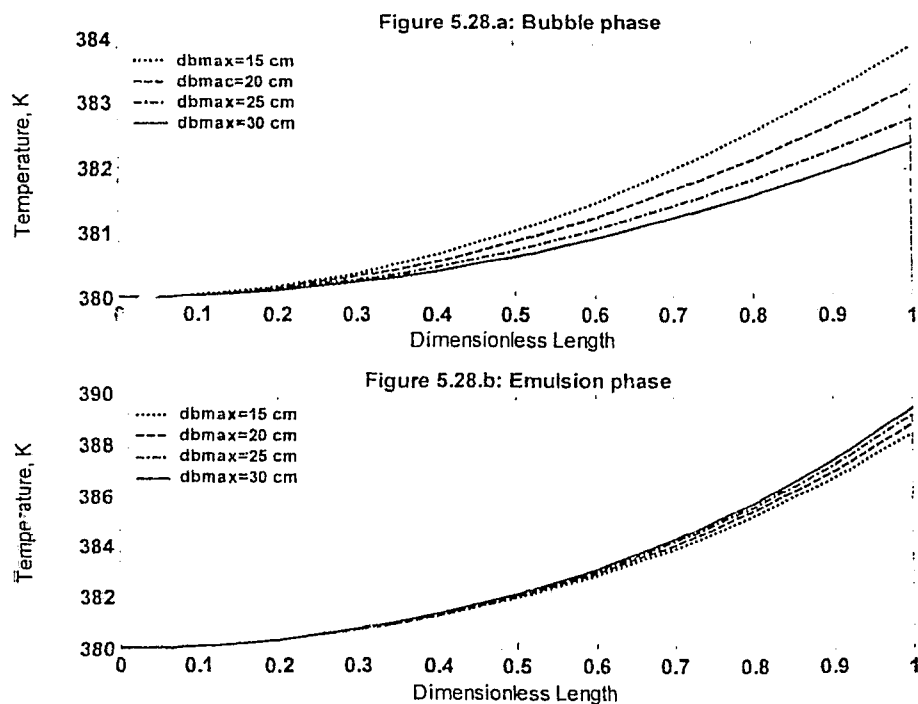
As in Figure 5.28, the temperature increases more rapidly in bubble phase with smaller bubble size due to higher heat and mass transfer rates. In emulsion phase it has opposite trend. But this effect is more significant in the bubble phase.

Furthermore, profiles of cocatalyst and hydrogen concentration are shown in Figures C.16 and C.17, respectively, and it is shown that the maximum bubble size does not have any effect on the average concentrations of cocatalyst and hydrogen in the bed.

5.2.5 Recycle Stream

The conversion of monomer per one pass in a fluidized bed reactor is relatively low and it is about 1% to 5% per one pass (McAuley et al., 1994). Furthermore, olefin polymerization is a highly exothermic reaction and a recycle stream equipped with a cooling system should remove the excess heat of reaction as it is described in detail in Chapter 2. In order to assess the performance of the system with a recycle stream, the previous model has been modified to accommodate the effect of a recycle. It is assumed that the cooling system (heat exchanger and compressor) reduces the temperature of the recycled gas to the inlet temperature of the main stream, which remains unchanged in terms of composition. Monomer conversion is plotted in Figure 5.29. After 20, 30 and 40 passes monomer conversion reaches about 84%, 89% and 92%, respectively, in the bed in steady-state mode. Furthermore, increasing the number of passes results in decreasing number average molecular weight of polymer from 11000 to about 5000 and weight average molecular weight of polymer from 22500 to about 12000. Also, $\overline{M_n}$ and $\overline{M_w}$ in the bubble phase have narrower distribution in comparison to emulsion phase.

Figure 5.32 shows that polydispersity index decreases when adding number of cycles due to decrease in number and weight average molecular weights in the bubble phase. In the emulsion phase, there is an overshoot in the PDI as conversion increases per each pass in the bed. Also higher number of cycles favors PDI in the emulsion phase, leading to an increase in polydispersity index of the polymer in the bed.

71

Figure 5.29: The effect of recycle stream on profile of monomer conversion versus reactor axial position

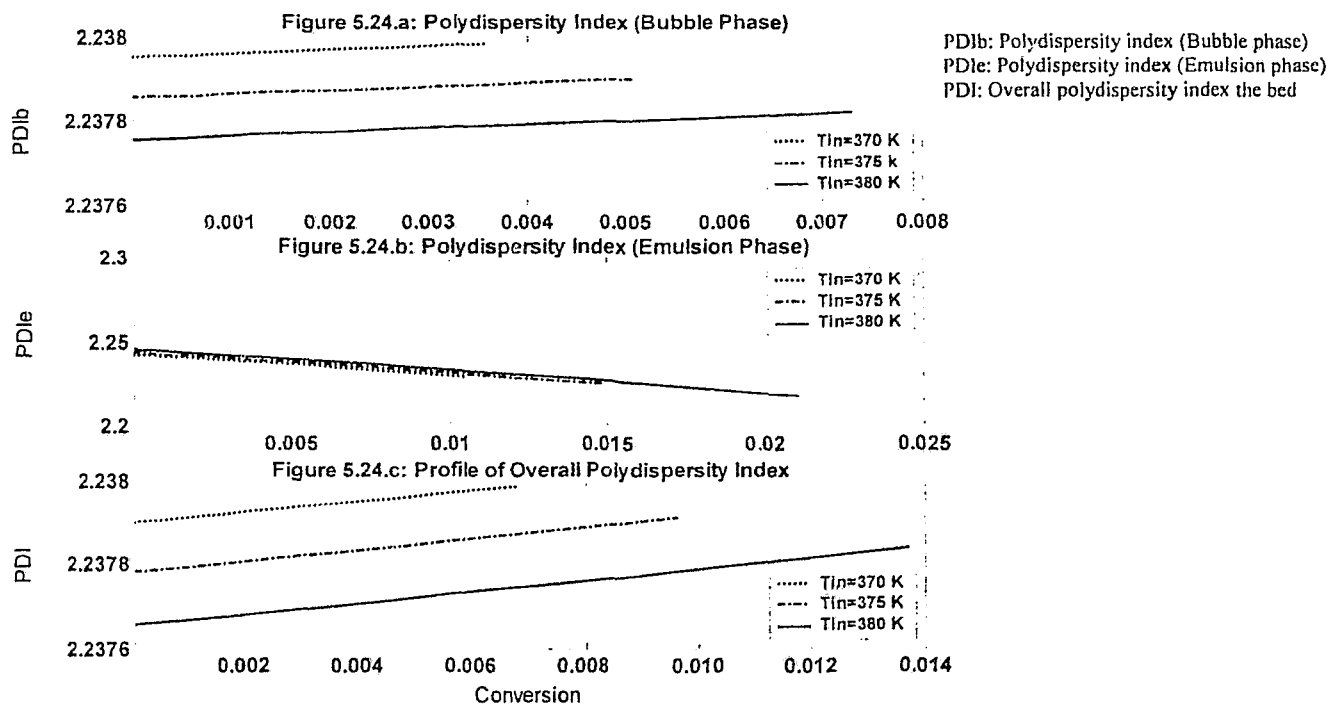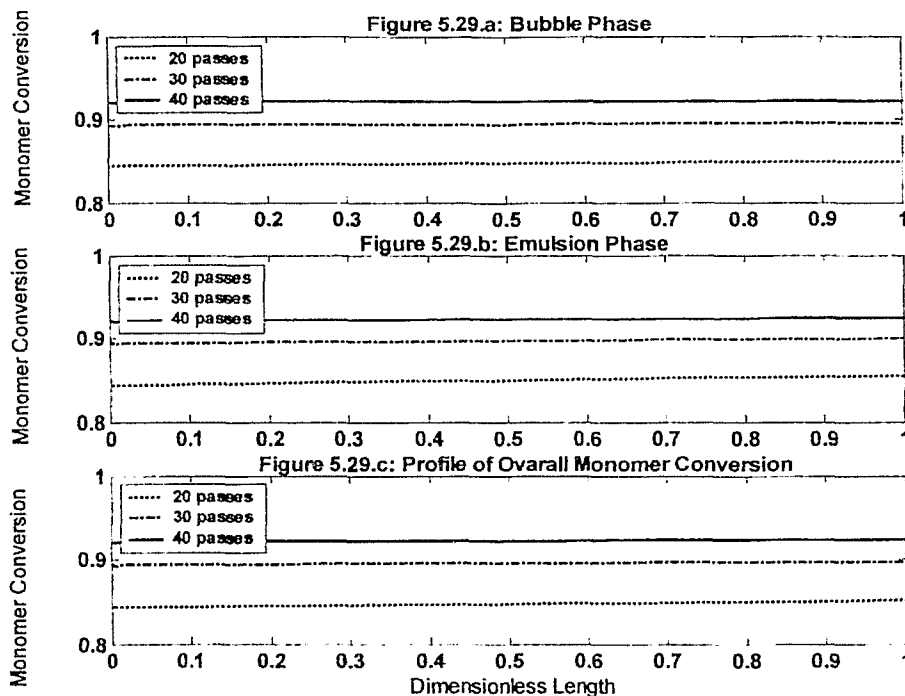Figure 5.30: The effect of recycle stream on profile of number average molecular weight of polymer versus conversion

Mnb: Number average molecular weight (Bubble phase)
Mne: Number average molecular weight (Emulsion phase)
Mn: Overall number average molecular weight in the bed

72
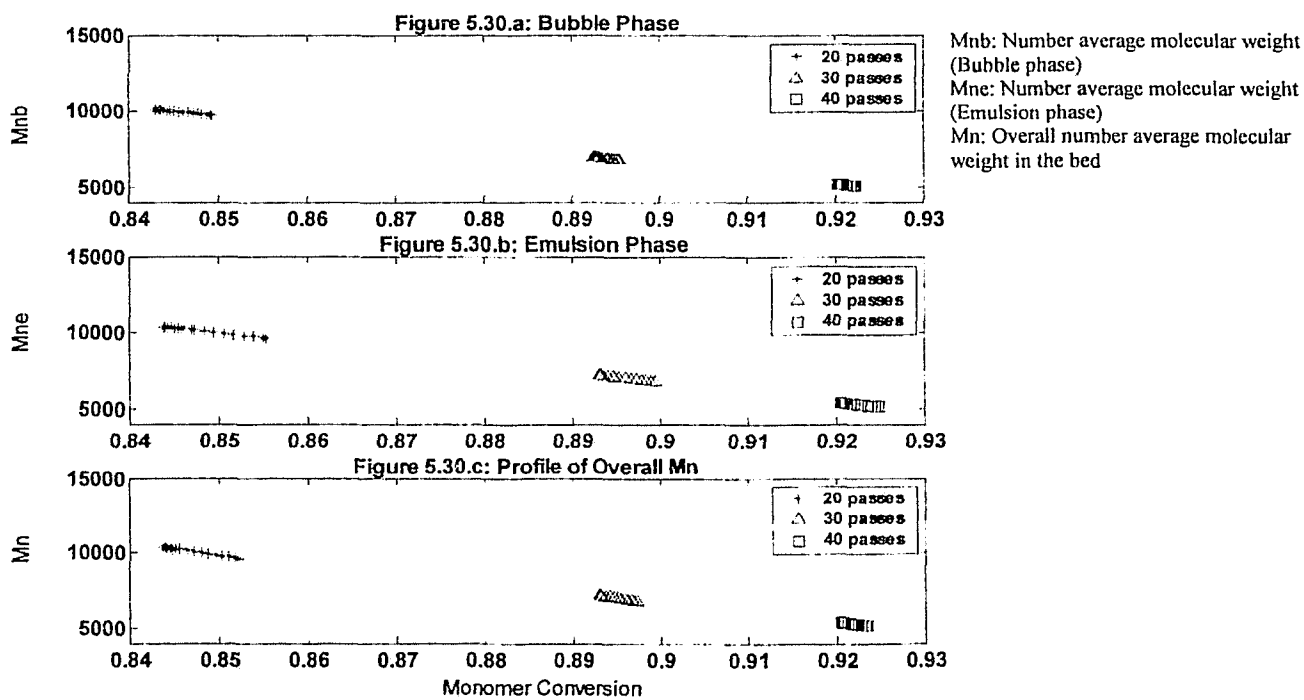
Figure 5.31: The effect of recycle stream on profile of weight average molecular weight of polymer versus conversion

Figure 5.31.a: Bubble Phase

Mwb: Weight average molecular weight (Bubble phase)
Mwe: Weight average molecular weight (Emulsion phase)
Mw: Overall weight average molecular weight in the bed

Figure 5.31.b: Emulsion Phase

Figure 5.31.c: Profile of Overall Mw

Monomer Conversion
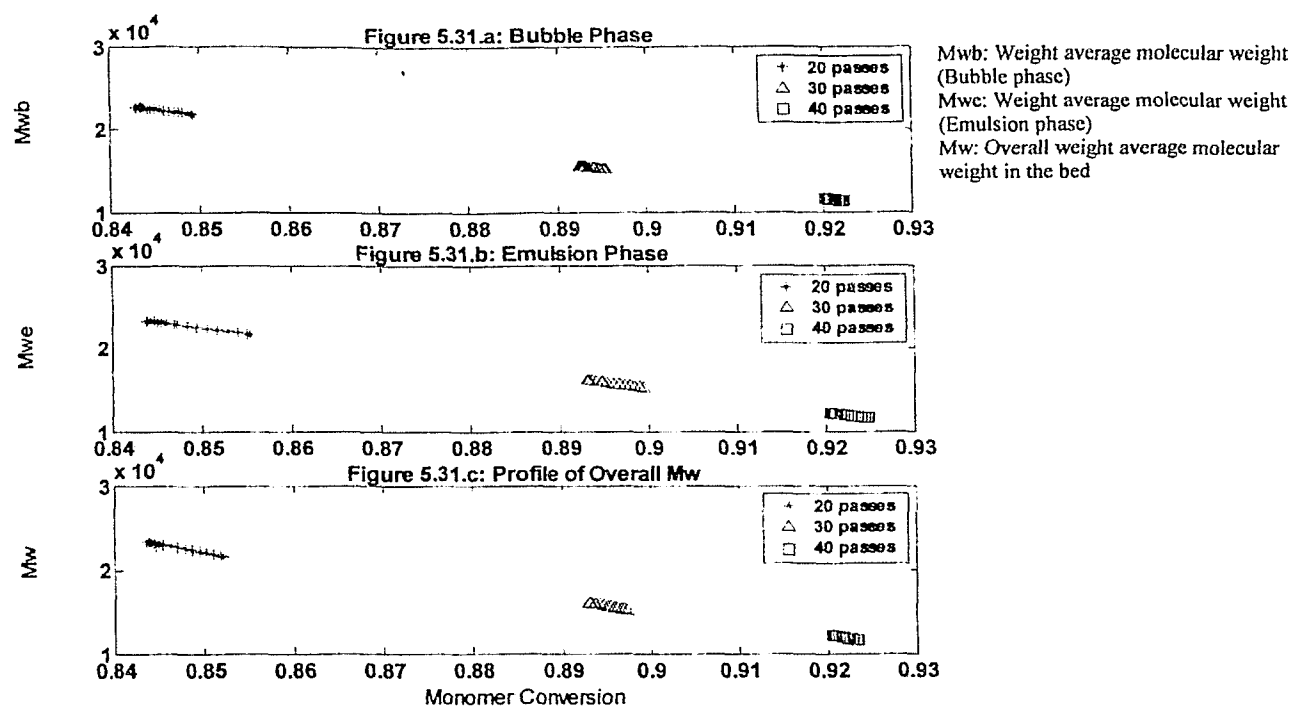
Figure 5.32: The effect of recycle stream on profile of polydispersity index versus conversion

Figure 5.32.a: Polydispersity Index (Bubble Phase)

PDIb: Polydispersity index (Bubble phase)
PDIe: Polydispersity index (Emulsion phase)
PDI: Overall polydispersity index the bed

Figure 5.32.b: Polydispersity Index (Emulsion Phase)

Figure 5.32.c: Profile of Ovarall Polydispersity Index

Conversion

73
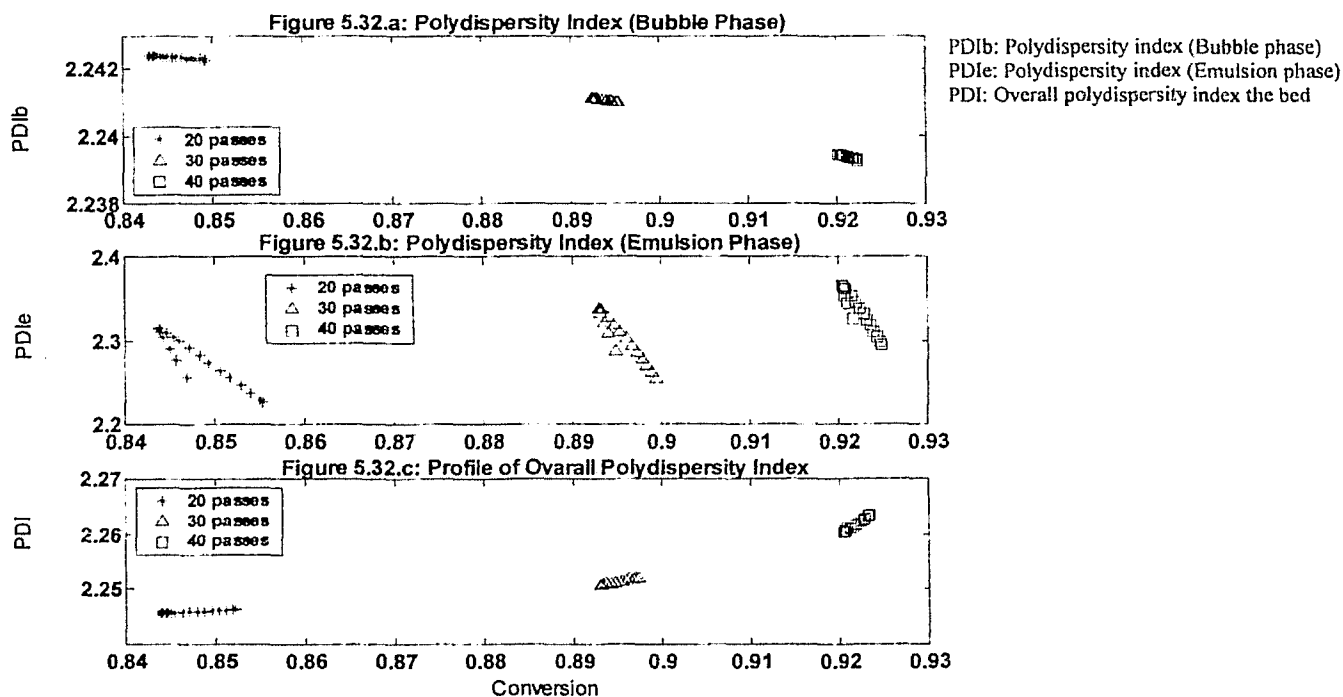
Figure 5.34 describes the reactor temperature profile in the bubble and emulsion phases when a recycle line is added to the system. It is observed that the temperature in both phases decreases with increasing number of passes.

In Figure 5.33, the effect of changing number of cycles on the molecular weight distribution is illustrated. Clearly, reducing the number of passes broadens the molecular weight distribution of polyethylene. The explanation is that as temperature increases, the rate of propagation increases, but the rate of termination goes up to a greater extent, since chain terminations reactions have greater activation energies than propagation reactions. The rate constants of termination are less affected by a temperature increase. Consequently, the ratio of the rate of propagation to that of terminations decreases, since the denominator of Equation (5.1) increases more rapidly than its numerator for an increase in the temperature. The overall result is a decrease in the degree of polymerization and hence the average molecular weight.

$$\overline{X_n} = \frac{k_p[M]}{k_{tfm}[M] + k_{tfA}[A] + k_{tfH}[H_2] + k_{tfs} + ...} \tag{5.1}$$

$\overline{X_n}$ is the number average degree of polymerization in terms of Ziegler-Natta kinetics and is essentially the ratio of the rate of propagation to that of termination.

The effects of adding a recycle stream on monomer conversion are better quantified in Figure 5.35. There is a relatively high increase in monomer conversion from 3 passes to 15 passes, whereas after that monomer conversion increases gradually by the addition of cycles. Furthermore, the simulation demonstrates that the monomer conversion can go up to 96 % after about 50 passes.

Figure 5.33: The effect of recycle stream on profile of molecular weight distribution (MWD) of polymer at the exit of bed

Figure 5.33.a: Profile of MWD (Bubble Phase)

Figure 5.33.b: Profile of MWD (Emulsion Phase)
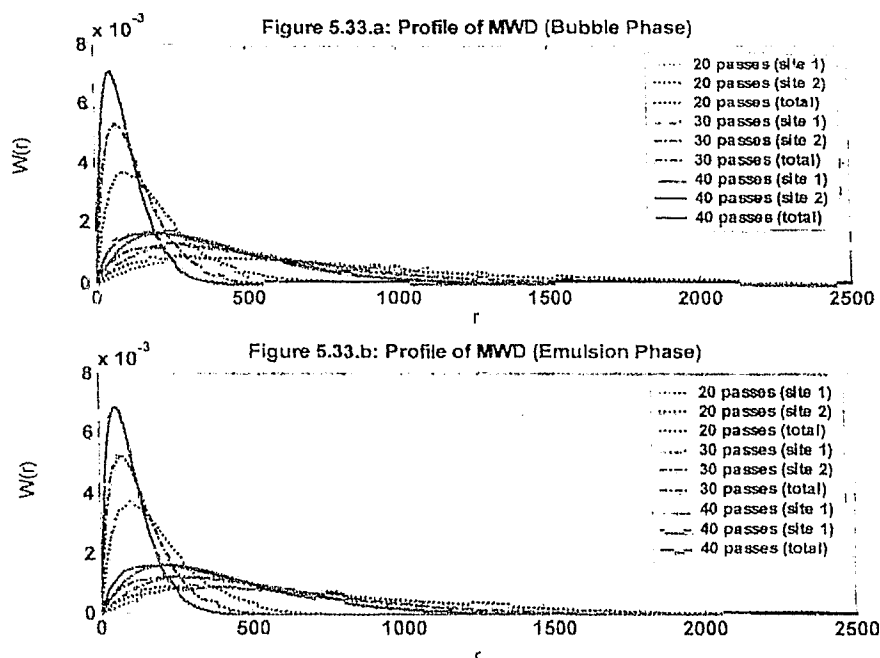
Figure 5.34: The effect of recycle stream on profile of reactor temperature versus reactor axial position

Figure 5.34.a: Bubble phase

Figure 5.34.b: Emulsion phase

75
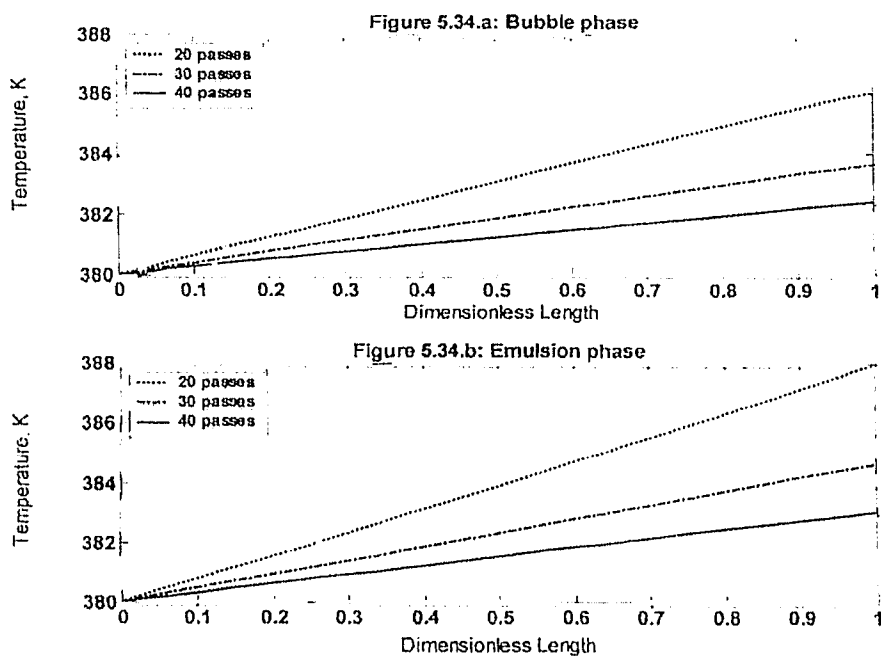
Figure 5.35: Profile of monomer conversion at the exit of the bed versus number of cycles

Figure 5.35.a: Profile of Conversion versus Cycle (Bubble phase)

Figure 5.35.b: Profile of Conversion versus Cycle (Emulsion Phase)

Figure 5.35.c: Profile of Overall Conversion versus Cycle
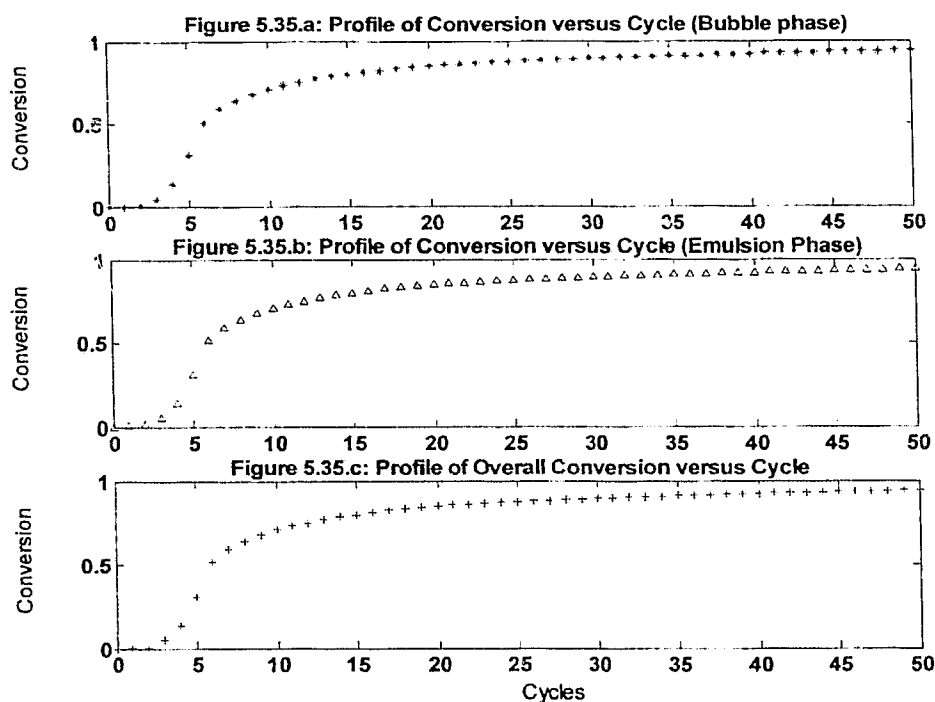
5.2.6 Chain Transfer Agent

Hydrogen is well known as a good chain transfer agent for lowering molecular weight when producing polymer with Ziegler-Natta catalyst. If we assume that transfer to hydrogen is the only significant reaction controlling molecular weight, it is evident that catalyst systems with higher hydrogen concentration produce shorter chains. Besides, chain transfer to hydrogen prevents other chain growth reactions from producing longer chains. As a result shorter chains with lower molecular weight are produced. Figure 5.36 shows the significant variation of the number average molecular weights with hydrogen concentration. Similar trend is predicted for weight average molecular weights of the polymer.

Furthermore, high hydrogen concentration favours *PDI* in the bubble phase only, but it has no significant effect on the *PDI* in the emulsion phase. The overall *PDI* in the bed has similar trends as in the bubble phase. Also as illustrated in Figure 5.38, higher hydrogen content in the gas feed produces narrower molecular weight distribution in both phases, for both site one and two and the total distribution of molecular weight in each phase. This is due to the increase in the rate of transfer reactions to the propagation reaction.

76

Figure 5.36: The effect of chain transfer agent concentration on profile of number average molecular weight of polymer versus conversion

Figure 5.36.a: Bubble Phase

Figure 5.36.b: Emulsion Phase

Figure 5.36.c: Profile of overall Mn

Mnb: Number average molecular weight (Bubble phase)
Mne: Number average molecular weight (Emulsion phase)
Mn: Overall number average molecular weight in the bed
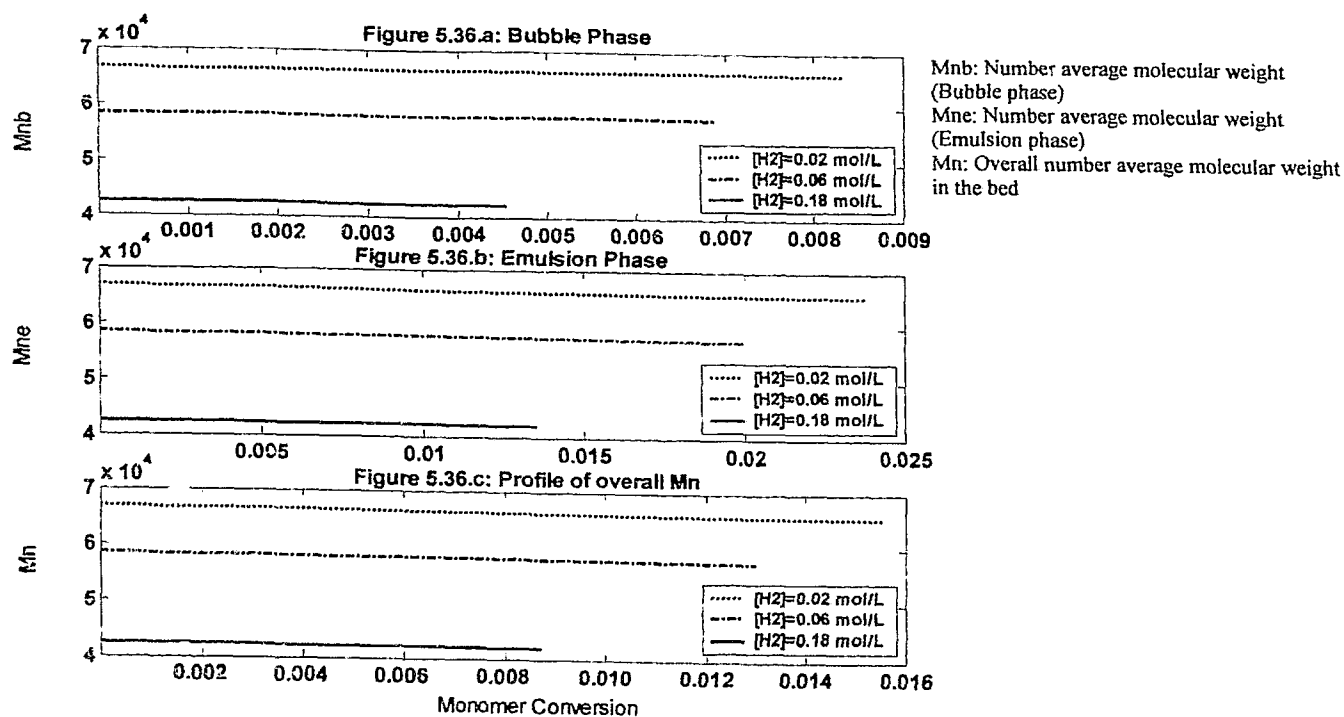
Figure 5.37: The effect of chain transfer agent concentration on profile of polydispersity index versus conversion

Figure 5.37.a: Polydispersity Index (Bubble Phase)

Figure 5.37.b: Polydispersity Index (Emulsion Phase)

Figure 5.37.c: Profile of Overall Polydispersity Index

PDIb: Polydispersity index (Bubble phase)
PDIe: Polydispersity index (Emulsion phase)
PDI: Overall polydispersity index the bed

77
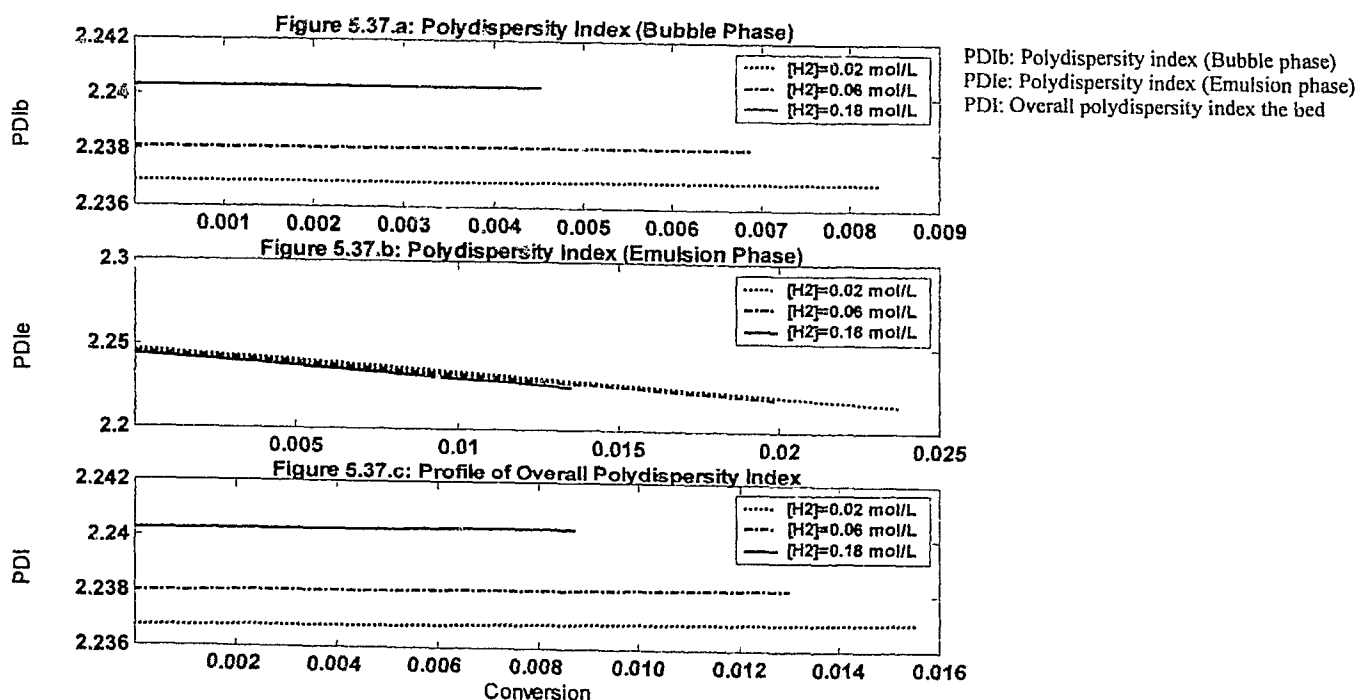
Figure 5.38: The effect of chain transfer agent concentration on profile of molecular weight distribution (MWD) of polymer at the exit of bed

Figure 5.38.a: Profile of MWD (Bubble Phase)

Figure 5.38.b: Profile of MWD (Emulsion Phase)
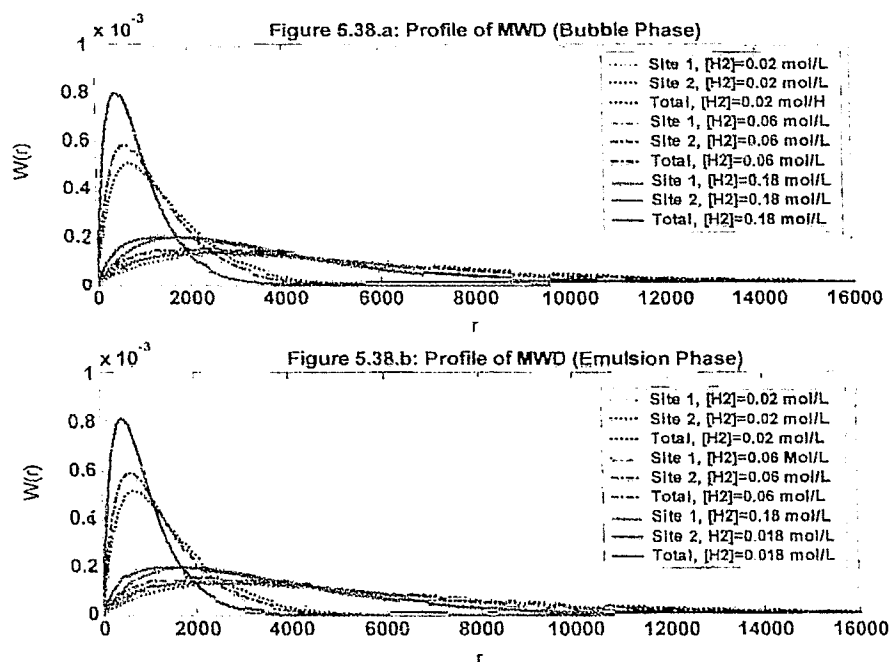
5.3 Dynamic Model

The dynamic model describes variations of monomer, catalyst, cocatalyst, chain transfer agent and polymer chains with axial position in the reactor and polymerization time. The model has been solved by improved first order Finite Difference method. The model is capable of predicting reactants profile at each position in the bed with respect to time. Also sixty grid points has been used in solving the sets of partial differential equations.

For instance, Figure 5.39 shows the profile of monomer conversion versus time in both bubble and emulsion phases at the reactor exit. Monomer conversion reaches 99% in nearly one hour. At this time the average catalyst concentration decreases from 0.05 mol/L to 4.45×10^{-2} mol/L and cocatalyst concentration from 0.7 mol/L to 0.694 mol/L (Figures D.1 and D.2).

The number average molecular weight is reduced significantly from about 60000 to 5000 when conversion reaches 97% (Figure 5.40). Similarly, $\overline{M_w}$ of the polymer decreases from 135600 to about 10000 (Figure 5.41).

78

Evolution of the *PDI* in the reactor is illustrated in Figure 5.42, giving a *PDI* value of 2.24. As shown in this diagram, polydispersity index increases slightly in the bubble phase and decreases after the conversion reaches about 85% due to the reduction in the second moments of polymer. Similarly in emulsion phase at conversion about 90% polydispersity index decreases from 2.24 to about 1.8. At this region almost all of monomer is consumed.

The profile of polymerization rate is shown in Figure D.4. As shown in this diagram polymerization rate in both phases have its highest values at about 25% monomer conversion that is attributed to the increase in formation of active sites. Above this point polymerization reduces gradually until all monomer is converted to polymer. Moreover, according to the simulation results, polymerization is above 30 times higher in the emulsion phase than in the bubble phase.

Figure 5.39: Profile of monomer conversion versus time at the exit of the bed (one pass and isothermal)

Figure 5.39.a: Monomer Conversion (Bubble phase)

Figure 5.39.b: Monomer Conversion (Emulsion phase)

Figure 5.39.c: Profile of Overall Monomer Conversion

79
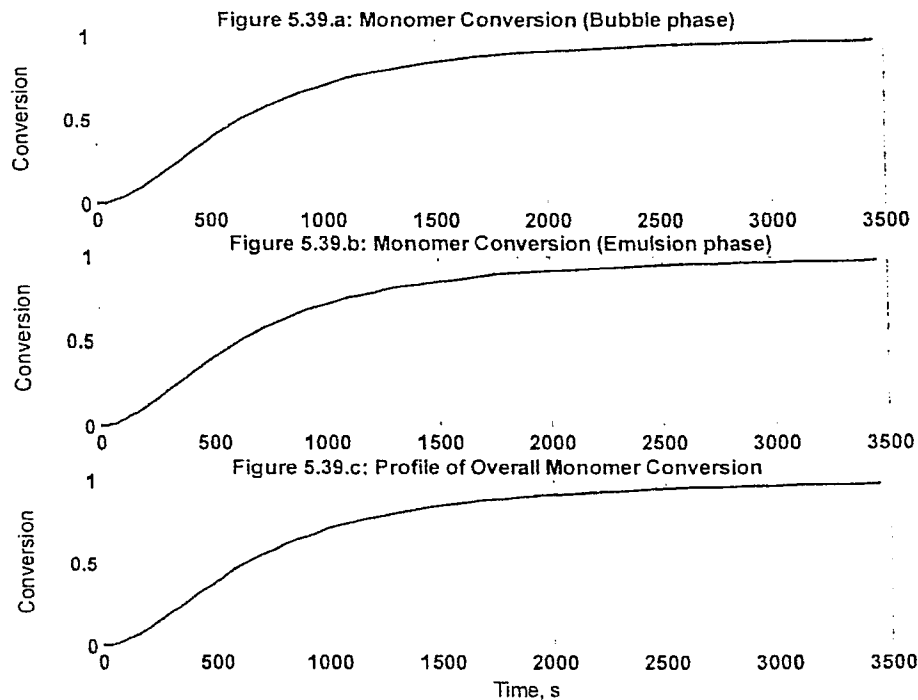
Figure 5.40: Dynamic profile of number average molecular weight of polymer versus conversion at the exit of the bed (one pass and isothermal)

Figure 5.40.a: Bubble Phase

Figure 5.40.b: Emulsion Phase

Figure 5.40.c, Profile of Overall Mn

Monomer Conversion

Mnb: Number average molecular weight (Bubble phase)
Mne: Number average molecular weight (Emulsion phase)
Mn: Overall number average molecular weight in the bed
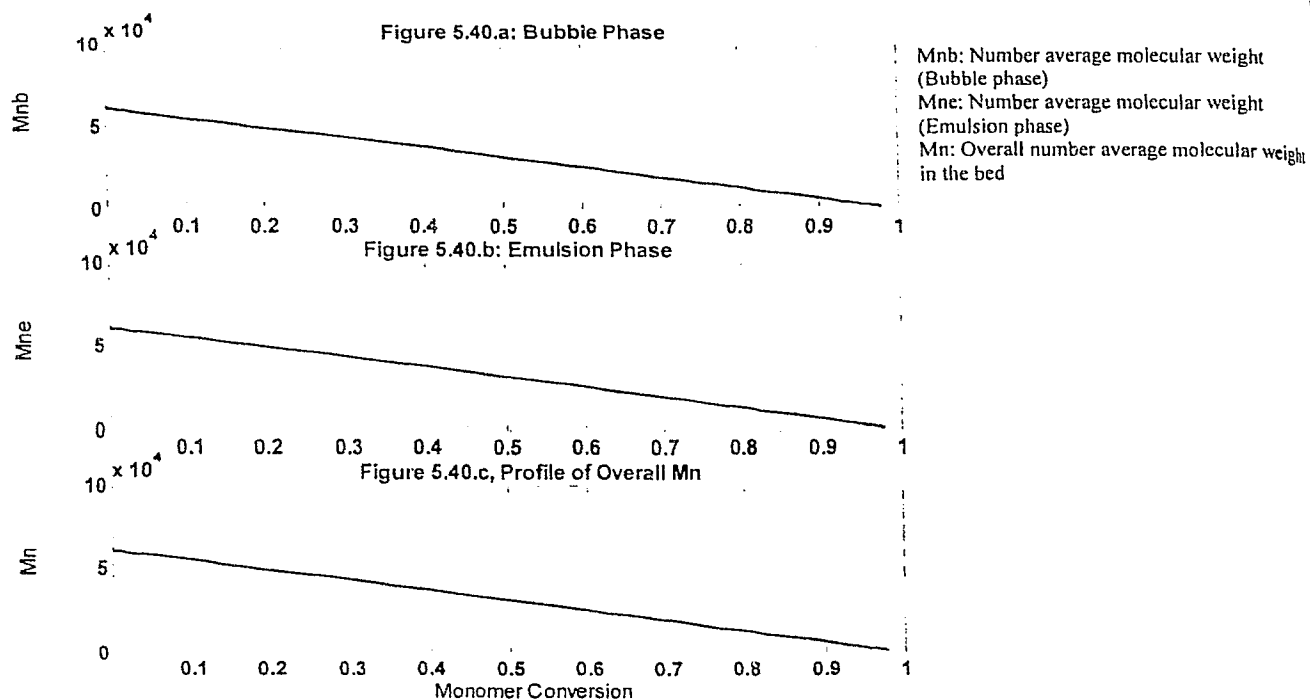
Figure 5.41: Dynamic profile of weight average molecular weight of polymer versus conversion (one pass and isothermal)

Figure 5.41.a: Bubble Phase

Figure 5.41.b: Emulsion Phase

Figure 5.41.c: Profile of Overall Mw

Monomer Conversion

Mwb: Weight average molecular weight (Bubble phase)
Mwe: Weight average molecular weight (Emulsion phase)
Mw: Overall weight average molecular weight in the bed

80
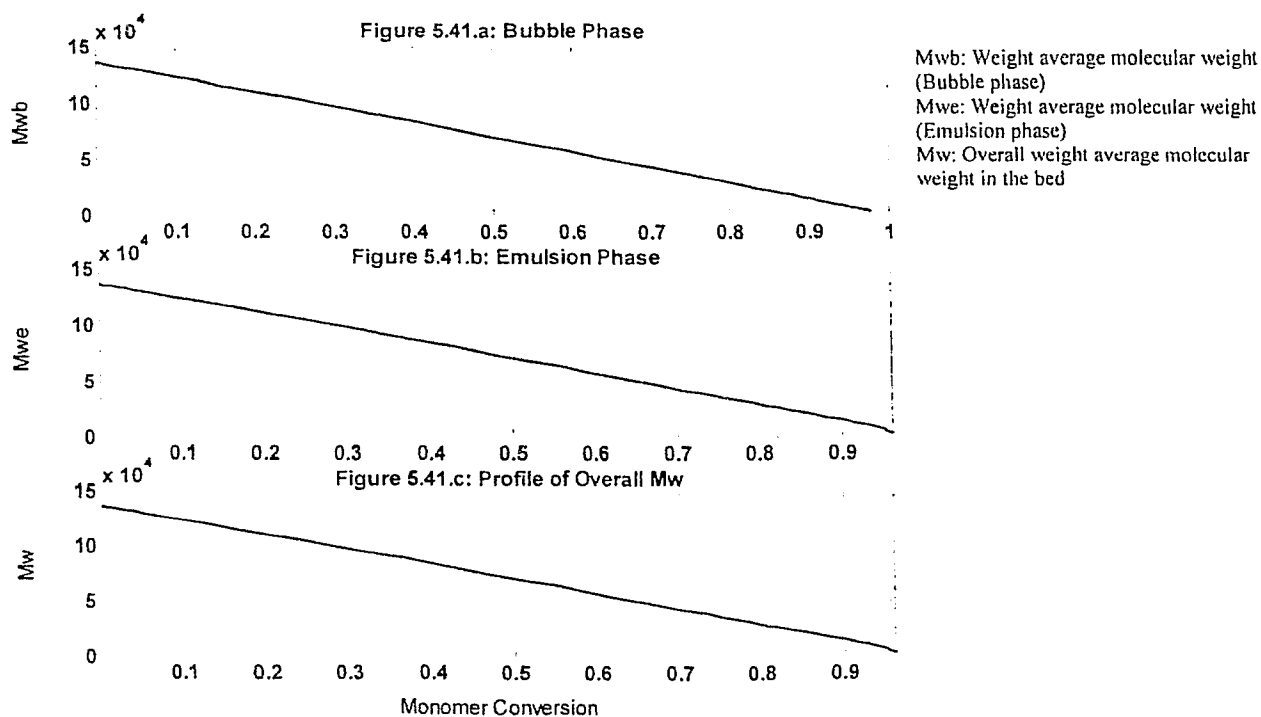
Figure 5.42: Dynamic profile of polydispersity index versus conversion at the exit of the bed (one pass and isothermal)

Figure 5.42.a: Polydispersity Index (Bubble Phase)

Figure 5.42.b: Polydispersity Index (Emulsion Phase)

Figure 5.42.c: Profile of Overall Polydispersity Index

Monomer Conversion

PDIb: Polydispersity index (Bubble phase)
PDIe: Polydispersity index (Emulsion phase)
PDI: Overall polydispersity index the bed
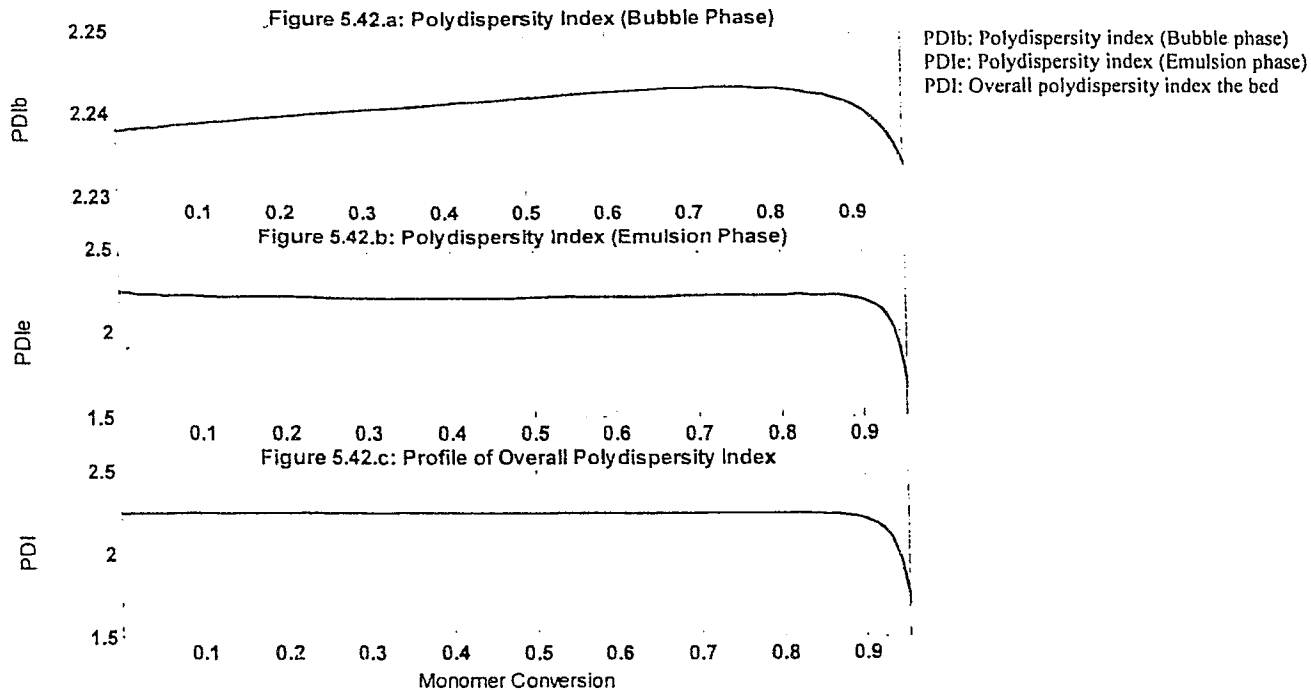
Figure 5.43: Dynamic profile of molecular weight distribution of polymer at the exit of bed (one pass and isothermal)

Figure 5.43.a: Profile of MWD (Bubble phase)

Figure 5.43.b: Profile of MWD (Emulsion phase)

Figure 5.40.c: Profile of Overall MWD in the bed

81
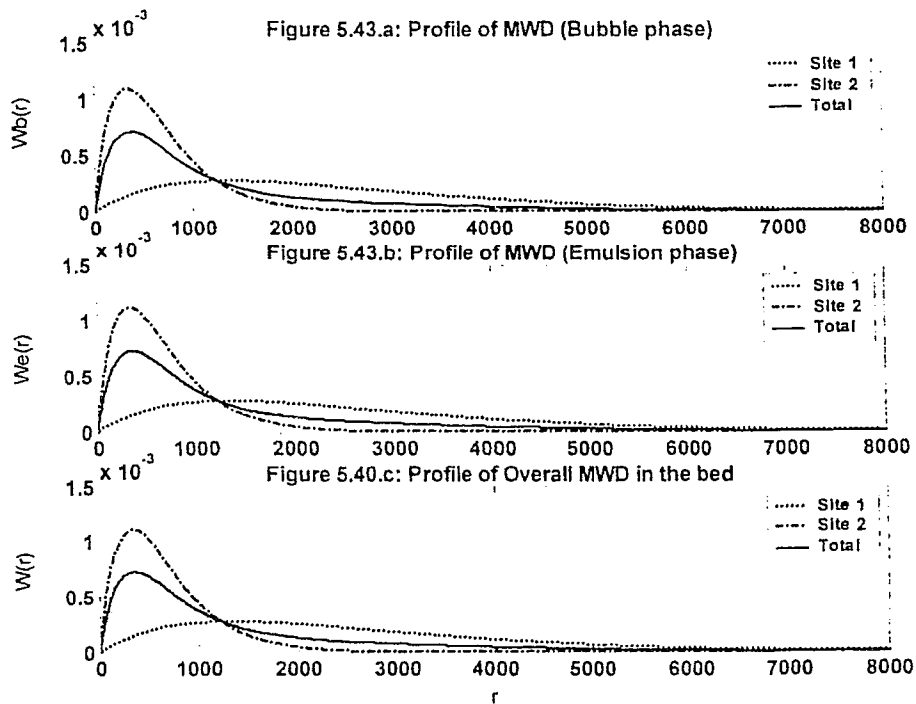
CHAPTER 6: CONCLUDING REMARKS AND RECOMMENDATIONS

a) Concluding Remarks

A kinetic model has been derived from molar balances of the main components in ethylene polymerization using multiple sites Ziegler-Natta catalysts. The kinetic scheme accounts for the formation, initiation and deactivation of active sites as well as for spontaneous transfer and transfer reactions to hydrogen, monomer and cocatalyst. A two-phase flow structure was employed to takes into account the hydrodynamics of particles inside the bubble phase and the dynamics of particle concentration in the emulsion phase, in terms of the superficial gas velocity in the reactor.

The hydrodynamic and kinetic models were integrated together to make a comprehensive PDE model describing the dynamics the HDPE production along the gas-phase FBR reactor. The model takes into account the variation of bubble size and bubble and emulsion velocity along the reactor height. It is capable of predicting profiles of the main polymerizing components (monomer, hydrogen, potential active sites and cocatalyst) and also of predicting of the properties of the polymer such as average molecular weights, polydispersity index and molecular weight distribution. Hence, the PDE model was integrated using an improved first order Finite Difference method. The predictive capabilities of the model are tested through extensive simulation runs that were carried out in order to assess the relative effects of the main process parameters.

Sensitivity analyses of the operating conditions showed that an inlet gas temperature rise favours monomer conversion and number and weight average molecular weights of polymer per one pass in the bed. Higher hydrogen content in the gas feed produces polymers with lower molecular weight and narrower molecular weight distribution in both bubble and emulsion phases. Also reducing superficial gas velocity by half almost doubles the conversion of monomer in the bed. Further, the reactor temperature goes up rapidly with lower superficial gas velocities in both phases and results in higher $\overline{M_n}$ and $\overline{M_w}$. With a decreasing bubble growth size in the bed. higher monomer conversion and reactor temperature in the bubble

phase were predicted. However, simulation tests have shown that the bubble size is not a critical parameter as claimed by Hatzantonis et al. (2000) and it has little effect on the overall $\overline{M_n}$, $\overline{M_w}$, MWD and PDI.

With a recycle stream, monomer conversion can go over 90% in 40 passes. Increasing number of cycles further resulted in lowering the number and weight average molecular weights of polymer. Although no data are available to validate the model, the simulation profiles for monomer conversion and molecular properties of polymer show that the model provides qualitatively reasonable results, based using proper-patented data only. In particular, the model confirms a broadened molecular weight distribution, which is typical of commercial high-density polyethylene.

b) Recommendations

This work can be extended to investigate effects of impurities in the system and modified further for copolymerization of ethylene. Application of an optimization technique can also provide more information on the process. Also the model can be further modified to take into account the jet penetration region and the disengagement zone in the fluidized bed reactor.

In the jetting region, mass and heat transfer rates are expected to be very high and therefore significantly affect the behaviour of the system in this region. Furthermore, due to the wide range of particle size in the bed (from small catalyst particles to large polymer particles) a particle population balance can be employed to predict the particle size distribution in the bed.

83

References

Abrahamson, A. R. and D. Geldart, "Behavior of Gas-Fluidized Beds of Fine Powders. Part I. Voidage of the Dense Phase in Bubbling Beds", Powder Technol. **26**, 47-55 (1980).

Alizadeh, M., N. Mostoufi, S. Pourmahdian, and R. Sotudeh-Gharabagh, "Modeling of Fluidized Bed Reactor of Ethylene Polymerization", Chem. Eng. J. **97** (1), 27-35 (2004).

Boor, J. J., "Ziegler-Natta Catalyst and Polymerizations", Academic Press. Inc., New York (1979)

Broadhurst, J. E., and H. A. Becker, "Onset of Fluidization and Slugging in Beds of Uniform Particles", AIChE J. **21**, 238 (1975).

Chaouki, J., A. Gonzalez, C. Guy, and D. Klvana, "Two Phase Model for a Catalytic Turbulent Fluidized Bed reactor: Application to Ethylene Synthesis", Chem. Eng. Sci. **54** (13&14), 2039-2045 (1999).

Chapra, S. C. and R. P. Canale, "Numerical methods for Engineers", Second edition, McGraw-Hill, New York (1988).

Chien, J. C. W., J. C. Wu and C. I. Kuo, "Magnesium-Chloride Supported High-Mileage Catalysts for Olefin Polymerization. 1. Chemical Composition and Oxidation-States of Titanium", J. Polym. Sci. Pol. Chem. **20** (8), 2019-2032 (1982).

Chien, J. C. W., "Advances in Polyolefins", R. B. Seymeur and T. Cheng, Eds., Plenum Press, New York (1987), pp. 255.

Choi, K. Y. and W. H. Ray, "The Dynamic Behaviour of Fluidized Bed Reactors for Solid Catalyzed Gas Phase Olefin Polymerization", Chem. Eng. Sci. **40** (12), 2261-2279 (1985).

Cui, H., N. Mostoufi, and J. Chaouki, "Characterization of Dynamic Gas-Solid Distribution in Fluidized Beds", Chem. Eng. J. **79**, 133-143 (2000).

de Carvalho, A. B., P. E. Gloor and A. E. Hamielec, "A Kinetic Mathematical Model for Heterogeneous Ziegler-Natta Copolymerisation", Polymer **30**, 280-296 (1989).

Davidson, J. F. and D. Harrison, "Fluidized Particles", Cambridge University Press, Cambridge (1963).

Davidson, J. F., "The Two-Phase Theory of Fluidization: Successes and Opportunities", AIChE Symposium Series **87**, 1-12 (1992).

Dusseault, J. J. A. and C. C. Hsu, "MgCl$_2$-Supported Ziegler-Natta Catalysts for Olefin Polymerization: Basic Structure, Mechanism and Kinetic Behaviour", Macromol. Chem. Phys. **33** (2), 103-145 (1993).

Felorzabihi, N., N. Ghadi and R. Dhib, "Differential Geometry Control of a Polymer Reactor", 2003 International Conference "Physics and Control" Proceedings, Eds., (PHYSCON'03), Saint Petersburg, Russia, Aug. 20-22, 2003a.

Felorzabihi, N. and R. Dhib, "Modeling of a Bubbling Fluidized Bed Reactor for Ammoxidation of Propane to Acrylonitrile", 53rd Canadian Chemical Engineering & PRES'03 Conference", Hamilton, ON, Canada, Oct. 26-29, 2003b.

Felorzabihi, N., "Modeling of Ethylene Polymerization with Ziegler-Natta Catalyst in a Bubbling Fluidized Bed Reactor", Internal report, Chem. Eng., Ryerson University, December 30, 2003c.

Felorzabihi, N. and R. Dhib, "Modeling and Simulation of Gas Phase Ethylene Polymerization with Ziegler-Natta Catalysts in a Bubbling Fluidized Bed Reactor, in "Proc. IPR Symposium", Waterloo, ON, Canada, May 11-12, 2004.

Fernandes, F. A. N. and L. M. F. Lona, "Fluidized Bed Reactor for Polyethylene Production. The Influence of Polyethylene Prepolymerization", Braz. J. Chem. Eng. **17** (2), 163-170 (2000).

Fernandes, F. A. N. and L. M. F. Lona, "Fluidized Bed Reactor Modeling for Polyethylene Production", J. Appl. Polym. Sci. **81**, 321-332 (2001a).

Fernandes, F. A. N. and L. M. F. Lona, "Heterogeneous Modeling for Fluidized-Bed Polymerization Reactor", Chem. Eng. Sci. **56**, 963-969 (2001b).

Fernandes, F. A. N. and L. M. F. Lona, "Heterogeneous Modeling of Fluidized-Bed Polymerization Reactors. Influence of Mass Diffusion into the Polymer Particle", Comput. Chem. Eng. **26**, 841 (2002).

Flory, P. J., "Principles of Polymer Chemistry", The George Fisher Baker Non-Resident Lectureship in Chemistry at Cornell University, Ithaca, Cornell University Press (1953).

Fryer, C. and O. E. Potter, "Experimental Investigation of Models for Fluidized-Bed Catalytic Reactors", AIChE J. **22** (1), 38-47 (1976).

Geldart, D., "Types of Gas Fluidization", Powder Technol. **7** (5), 285-292 (1973).

Grace, J. R., "Modeling and Simulation of Two-Phase Fluidized Bed Reactors", In H. I. De Lasa, Chemical Reactor Design and Technology, Martinus Nijhoff, Dordrecht, Netherlands (1986).

Haider, A. and O. Levenspiel, "Drag Coefficient and Terminal Velocity of Spherical and Nonspherical Particles", Powder Technol. **58**, 63 (1989).

Hatzantonis, H. and C. Kiparissides, "The Effect of Mean Particle Size on the Dynamic Behaviour of Catalyzed Olefin Polymerization Fluidized Bed Reactors", Comput. Chem. Eng. 22, Suppl., pp. S127-S134 (1998).

Hatzantonis, H., H. Yiannoulakis, A. Yiagopoulos, and C. Kiparissides, "Recent Developments in Modeling Gas-Phase Catalyzed Olefin Polymerization Fluidized-Bed Reactors: The Effect of Bubble Size Variation on the Reactor's Performance", Chem. Eng. Sci. 55, 3237-3259 (2000).

Hilligardt, K. and J. Werther, "Local Bubble-Gas Hold-Up and Expansion of Gas Solid Fluidized Beds", Ger. Chem. Eng. 9 (4), 215-221 (1986).

Horio, M. and A. Nonaka, "A Generalized Bubble Diameter Correlation for Gas-Solid Fluidized Beds", AIChE J. 33, 1865 (1987).

Jorgensen, R. J., G. L. Goeke and F. J. Karol, "Catalyst Composition for Copolymerisation Ethylene", U.S. Patent 4,349,648 (1982).

Karol, F. J., "Studies with High Activity Catalyst for Olefin Polymerization", Catal. Rev. 26 (3-4), 557-595 (1984).

Kato, K. and C. Y. Wen, "Bubble Assemblage Model for Fluidized Bed Catalytic Reactors", Chem. Eng. Sci. 24, 1351 (1969).

Keii, T., Y. Doi, E. Suzuki, M. Tamura, M. Murata, and K. Soga, "Propene Polymerization with a Magnesium Chloride-Supported Ziegler Catalyst. 2. Molecular Weight Distribution", Macromol. Chem. Phys. 185 (8), 1537-1557 (1984).

Kunii, D. and O. Levenspiel, "Bubbling Bed Model for Kinetic Processes in Fluidized Beds-Gas Solid Mass and Heat Transfer and Catalytic Reactions", Ind. Eng. Chem. Proc. DD. 7 (4), 481 (1968).

Kunii, D. and O. Levenspiel, "Fluidization Engineering", Wiley, New York (1969).

Kunii D. and O. Levenspiel, "Fluidized Reactor Models. 1. For the Bubbling Beds of Fine, Intermediate, and Large Particles, 2. For the Lean Phase: Free Board and Fast Fluidization", Ind. Eng. Chem. Res. **29**, 1226-1234 (1990).

Kunii, D. and O. Levenspiel, "Fluidization Engineering", Second Edition, Butterworth-Heinemann Publishers, London (1991).

Li, J., L. Wen, G. Qian, H. Cui and M. Kwauk, "Structure Heterogeneity, Regime Multiplicity and Nonlinear Behaviour in Particle-Fluid Systems", Chem. Eng. Sci. **51** (11), 2693-2698 (1996).

Lucas, A., J. Arnaldos, J. Casal and L. Puigjaner, "Improved Equation for the Calculation of Minimum Fluidization Velocity", Ind. Eng. Chem. Proc. DD. **25**, 426 (1986).

Lynch, D. T. and S. E. Wanke, "Reactor Design and Operation for Gas Phase Ethylene Polymerization Using Ziegler-Natta Catalyst", Can. J. Chem. Eng. **69**, 332 (1991).

McAuley, K. B., J. F. MacGregor and A. E. Hamielec, "A Kinetic Model for Industrial Gas-Phase Ethylene Copolymerization", AIChE J. **36**, 837-850 (1990).

McAuley, K. B., J. P. Talbot and T. J. Harris, "A Comparison of Two-Phase and Well-Mixed Models for Fluidized Bed Polyethylene Reactors", Chem. Eng. Sci. **49** (13), 2035-2045 (1994).

Mori, S. and C. Y. Wen, "Estimation of Bubble Diameter in Gaseous Fluidized Beds", AIChE J. **21**, 109 (1975).

Mostoufi, N., H. Cui, and J. Chaouki, "A Comparison of Two-and Single-Phase Models for Fluidized Bed Reactors", Ind. Eng. Chem. Res. **40**, 5526-5532 (2001).

Odian, G. "Principles of Polymerization", Third Edition, John Wiley and Sons Publishers, New York (1991).

Shaw, B. M., K. B. McAuley and D. W. Bacon, "Simulating Joint Chain Length and Composition Fractions from Semi-Batch Ethylene Copolymerisation Experiments", Polym. React. Eng. **6** (2), 113-142 (1998).

Soares, J. B. P. and A. E. Hamielec, "General Dynamic Mathematical Modeling of Heterogeneous Ziegler-Natta and Metallocene Catalyzed Copolymerisation with Multiple Site Types and Mass and Heat Transfer Resistances", Polym. React. Eng. **3** (3), 261-324 (1995).

Soares, J. B. P. and A. E. Hamielec, "Copolymerisation of Olefins in a Series of Continuous Stirred-Tank Slurry-Reactors Using Heterogeneous Ziegler-Natta and Metallocene Catalysts. I. General Dynamic Mathematical Model", Polym. React. Eng. **4** (2&3), 153-191 (1996).

Toomey, R. D. and H. F. Johnstone, "Gaseous Fluidization of Solid Particles", Chem. Eng. Prog. **48** (5), 220-226 (1952).

Treybal, R. E., "Mass transfer operations", McGraw-Hill College, June (1980).

Usami, T., Y. Gotoh and S. Takayama, "Generation Mechanism of Short-Chain Branching Distribution in Linear Low-Density Polyethylenes", Macromolecules **19**, 2722-2726 (1986).

Wagner, B. E., G. L. Goeke and F. J. Karol, "Process for the Preparation of High-Density Polymers in Fluid Bed Reactors", U.S. Patent 4,303,771 (1981).

Werther, J., "Hydrodynamics and Mass Transfer Between Bubble and Emulsion Phase in Fluidized Beds of Sand and Cracking Catalyst", in "Fluidization", Vol. IV, D. Kunii and R. Toei, Eds., Engineering Foundations, New York (1983).

Wu, S. Y. and J. Baeyens, "Segregation by Size Difference in Gas Fluidized Beds", Powder Technol. **98**, 139-150 (1998).

Xie, T., K. McAuley, J. Hsu and D. W. Bacon, "Gas Phase Ethylene Polymerization: Production Process, Polymer Properties, and Reactor Modeling", Ind. Eng. Chem. Res. **33**, 449-479 (1994).

Yang, W. C., " Hand Book of Fluidization and Fluid-Particle Systems", Marcel Dekker Inc., New York (2003).

Yiagopoulos, A., H. Yiannoulakis, V. Dimos and C. Kiparissides, "Heat and Mass Transfer Phenomena During the Early Growth of a Catalyst Particle in Gas-Phase Olefin Polymerization: The Effect of Prepolymerization Temperature and Time", Chem. Eng. Sci. **56**, 3979-3995 (2001).

Zucchini, U. and G. Cecchin, "Control of Molecular Weight Distribution in Polyolefins Synthesized with Ziegler-Natta Catalytic Systems", Adv. Polym. Sci. **51**, 101-153 (1983).

Appendices

Appendix A: Discretized Model for Catalyst, Active Sites, Moments of Dead Polymer and Temperature

Discretized model equations for catalyst, active sites, moments of dead polymer and reactor temperature can be written as:

For zeroth moment of dead polymer at site one in the bubble phase:

For case $i = \dfrac{6n}{m} + 1$:

$$\frac{d\mu_{01,b,i}}{dt} = -u_b \frac{-\mu_{01,b,i+2} + 4\mu_{01,b,i+1} - 3\mu_{01,b,i}}{2dz} + \frac{(1-\varepsilon_b)}{\varepsilon_b} R_{\mu 01,b,i} \qquad (A.1)$$

For case $i = \dfrac{7n}{m}$ (n: $N_{gridpt} \times m$ and m: Number of equations):

$$\frac{d\mu_{01,b,i}}{dt} = -u_b \frac{3\mu_{01,b,i} - 4\mu_{01,b,i-1} + \mu_{01,b,i-2}}{2dz} + \frac{(1-\varepsilon_b)}{\varepsilon_b} R_{\mu 01,b,i} \qquad (A.2)$$

For other values of i $(\dfrac{6n}{m} + 1 < i < \dfrac{7n}{m})$:

$$\frac{d\mu_{01,b,i}}{dt} = -u_b \frac{\mu_{01,b,i+1} - \mu_{01,b,i-1}}{2dz} + \frac{(1-\varepsilon_b)}{\varepsilon_b} R_{\mu 01,b,i} \qquad (A.3)$$

For zeroth moment of dead polymer at site two in the bubble phase:

For case $i = \dfrac{7n}{m} + 1$:

$$\frac{d\mu_{02,b,i}}{dt} = -u_b \frac{-\mu_{02,b,i+2} + 4\mu_{02,b,i+1} - 3\mu_{0,b,i}}{2dz} + \frac{(1-\varepsilon_b)}{\varepsilon_b} R_{\mu 02,b,i} \qquad (A.4)$$

For case $i = \dfrac{8n}{m}$:

$$\frac{d\mu_{02,b,i}}{dt} = -u_b \frac{3\mu_{02,b,i} - 4\mu_{02,b,i-1} + \mu_{02,b,i-2}}{2dz} + \frac{(1-\varepsilon_b)}{\varepsilon_b} R_{\mu 02,b,i} \qquad (A.5)$$

For other values of i $(\dfrac{7n}{m} + 1 < i < \dfrac{8n}{m})$:

91

$$\frac{d\mu_{02,h,i}}{dt} = -u_h \frac{\mu_{02,h,i+1} - \mu_{02,h,i-1}}{2dz} + \frac{(1-\varepsilon_h)}{\varepsilon_h} R_{\mu 02,h,i} \qquad (A.6)$$

For zeroth moment of dead polymer at site one in the emulsion phase:

For case $i = \dfrac{8n}{m} + 1$:

$$\frac{d\mu_{01,e,i}}{dt} = -u_e \frac{-\mu_{01,e,i+2} + 4\mu_{01,e,i+1} - 3\mu_{01,e,i}}{2dz} + \frac{(1-\varepsilon_e)}{\varepsilon_e} R_{\mu 01,e,i} \qquad (A.7)$$

For case $i = \dfrac{9n}{m}$ (n: $N_{gridpt} \times m$ and m: Number of equations):

$$\frac{d\mu_{01,e,i}}{dt} = -u_h \frac{3\mu_{01,e,i} - 4\mu_{01,e,i-1} + \mu_{01,e,i-2}}{2dz} + \frac{(1-\varepsilon_e)}{\varepsilon_e} R_{\mu 01,e,i} \qquad (A.8)$$

For other values of i ($\dfrac{8n}{m} + 1 < i < \dfrac{9n}{m}$):

$$\frac{d\mu_{01,e,i}}{dt} = -u_h \frac{\mu_{01,e,i+1} - \mu_{01,e,i-1}}{2dz} + \frac{(1-\varepsilon_e)}{\varepsilon_e} R_{\mu 01,e,i} \qquad (A.9)$$

For zeroth moment of dead polymer at site two in the emulsion phase:

For case $i = \dfrac{9n}{m} + 1$:

$$\frac{d\mu_{02,e,i}}{dt} = -u_h \frac{-\mu_{02,e,i+2} + 4\mu_{02,e,i+1} - 3\mu_{0,e,i}}{2dz} + \frac{(1-\varepsilon_e)}{\varepsilon_e} R_{\mu 02,e,i} \qquad (A.10)$$

For case $i = \dfrac{10n}{m}$:

$$\frac{d\mu_{02,e,i}}{dt} = -u_h \frac{3\mu_{02,e,i} - 4\mu_{02,e,i-1} + \mu_{02,e,i-2}}{2dz} + \frac{(1-\varepsilon_e)}{\varepsilon_e} R_{\mu 02,e,i} \qquad (A.11)$$

For other values of i ($\dfrac{9n}{m} + 1 < i < \dfrac{10n}{m}$):

$$\frac{d\mu_{02,e,i}}{dt} = -u_h \frac{\mu_{02,e,i+1} - \mu_{02,e,i-1}}{2dz} + \frac{(1-\varepsilon_e)}{\varepsilon_e} R_{\mu 02,e,i} \qquad (A.12)$$

92

The same procedure can be used for the first and second moments of dead polymer produced at each active site and in each phase. The grid points that have been selected for numerical solution of these moments are tabulated in Table A.1.

Table A.1 Grid points selected for numerical solution of moments of dead polymer

Moments of dead polymer	Site number	Reaction rate	Phase	Grid number, i
Zero	One	$R_{\mu01,b,i}$	Bubble	(6n/m)+1 to 7n/m
Zero	Two	$R_{\mu02,b,i}$	Bubble	(7n/m)+1 to 8n/m
Zero	One	$R_{\mu01,e,i}$	Emulsion	(8n/m)+1 to 9n/m
Zero	Two	$R_{\mu02,e,i}$	Emulsion	(9n/m)+1 to 10n/m
First	One	$R_{\mu11,b,i}$	Bubble	(10n/m)+1 to 11n/m
First	Two	$R_{\mu12,b,i}$	Bubble	(11n/m)+1 to 12n/m
First	One	$R_{\mu11,e,i}$	Emulsion	(12n/m)+1 to 13n/m
First	Two	$R_{\mu12,e,i}$	Emulsion	(13n/m)+1 to 14n/m
Second	One	$R_{\mu21,b,i}$	Bubble	(14n/m)+1 to 15n/m
Second	Two	$R_{\mu22,b,i}$	Bubble	(15n/m)+1 to 16n/m
Second	One	$R_{\mu21,e,i}$	Emulsion	(16n/m)+1 to 17n/m
Second	Two	$R_{\mu22,e,i}$	Emulsion	(17n/m)+1 to 18n/m

For potential active site of type one in the bubble phase:

For case $i = \dfrac{18n}{m}+1$:

$$\frac{d[C^*(1)]_{h,i}}{dt} = -u_h \frac{-[C^*(1)]_{h,i+2} + 4[C^*(1)]_{h,i+1} - 3[C^*(1)]_{h,i}}{2dz} + \frac{(1-\varepsilon_h)}{\varepsilon_h} R_{c^*(1),h,i} \qquad (A.13)$$

For case $i = \dfrac{19n}{m}$ (n: $N_{gridpt} \times m$ and m: Number of equations):

$$\frac{d[C^*(1)]_{h,i}}{dt} = -u_h \frac{3[C^*(1)]_{h,i} - 4[C^*(1)]_{h,i-1} + [C^*(1)]_{h,i-2}}{2dz} + \frac{(1-\varepsilon_h)}{\varepsilon_h} R_{c^*(1),h,i} \qquad (A.14)$$

For other values of $i (\dfrac{18n}{m}+1 < i < \dfrac{19n}{m})$:

$$\frac{d[C^*(1)]_{h,i}}{dt} = -u_h \frac{[C^*(1)]_{h,i+1} - [C^*(1)]_{h,i-1}}{2dz} + \frac{(1-\varepsilon_h)}{\varepsilon_h} R_{c^*(1),h,i} \qquad (A.15)$$

93

The same procedure can be used for potential active two produced in bubble phase and emulsion phase. The grid points that have been selected for numerical solution of these components are tabulated in Table A.2.

Table A.2 Grid points selected for numerical solution of potential active sites

Potential active site/ Site number	Reaction rate	Phase	Grid number
$C^{\bullet}(1)_b$ / One	$R_{C^{\bullet}(1),b}$	Bubble	(18n/m)+1 to 19n/m
$C^{\bullet}(2)_b$ / Two	$R_{C^{\bullet}(2),b}$	Bubble	(19n/m)+1 to 20n/m
$C^{\bullet}(1)_e$ / One	$R_{C^{\bullet}(1),e}$	Emulsion	(20n/m)+1 to 21n/m
$C^{\bullet}(2)_e$ / Two	$R_{C^{\bullet}(2),e}$	Emulsion	(21n/m)+1 to 22n/m

For uninitiated sites of type one produced by formation reactions in the bubble phase:

For case $i = \dfrac{22n}{m} + 1$:

$$\frac{d[R^{\bullet}(0,1)]_{b,i}}{dt} = -u_b \frac{-[R^{\bullet}(0,1)]_{b,i+2} + 4[R^{\bullet}(0,1)]_{b,i+1} - 3[R^{\bullet}(0,1)]_{b,i}}{2dz} + \frac{(1-\varepsilon_b)}{\varepsilon_b} R_{R^{\bullet}(0,1),b,i} \qquad (A.16)$$

For case $i = \dfrac{23n}{m}$ *(n:* $N_{gridpt} \times m$ *and m: Number of equations):*

$$\frac{d[R^{\bullet}(0,1)]_{b,i}}{dt} = -u_b \frac{3[R^{\bullet}(0,1)]_{b,i} - 4[R^{\bullet}(0,1)]_{b,i-1} + [R^{\bullet}(0,1)]_{b,i-2}}{2dz} + \frac{(1-\varepsilon_b)}{\varepsilon_b} R_{R^{\bullet}(0,1),b,i} \qquad (A.17)$$

For other values of $i\,(\dfrac{22n}{m} + 1 < i < \dfrac{23n}{m})$:

$$\frac{d[R^{\bullet}(0,1)]_{b,i}}{dt} = -u_b \frac{[R^{\bullet}(0,1)]_{b,i+1} - [R^{\bullet}(0,1)]_{b,i-1}}{2dz} + \frac{(1-\varepsilon_b)}{\varepsilon_b} R_{R^{\bullet}(0,1),b,i} \qquad (A.18)$$

The grid points used for numerical solution of uninitiated sites produced by formation reactions are tabulated in Table A.3.

94

Table A.3 Grid points selected for numerical solution of uninitiated sites produced by formation reactions

Uninitiated site/ Sites number	Reaction rate	Phase	Grid number
$R^{\bullet}(0,1)_h$/One	$R_{R^{\bullet}(0,1),h,i}$	Bubble	(22n/m)+1 to 23n/m
$R^{\bullet}(0,2)_h$/Two	$R_{R^{\bullet}(0,2),b,i}$	Bubble	(23n/m)+1 to 24n/m
$R^{\bullet}(0,1)_e$/One	$R_{R^{\bullet}(0,1),e,i}$	Emulsion	(24n/m)+1 to 25n/m
$R^{\bullet}(0,2)_e$/Two	$R_{R^{\bullet}(0,2),e,i}$	Emulsion	(25n/m)+1 to 26n/m

For reactor temperature in the bubble phase:

For case $i = \dfrac{26n}{m} + 1$:

$$\frac{dT_{h,i}}{dt} = -u_h \frac{-T_{h,i+2} + 4T_{h,i+1} - 3T_{h,i}}{2dz} + \frac{H_{be}(T_{e,i} - T_{h,i})}{Cp_g^{\bullet} \varepsilon_h [M]_{h,i} + (1 - \varepsilon_h)\rho_{polym} Cp_{polym}} \tag{A.19}$$

$$+ \frac{R_{p,h,i}(1 - \varepsilon_h)(-\Delta H)Mw}{Cp_g^{\bullet} \varepsilon_h [M]_{h,i} + (1 - \varepsilon_h)\rho_{polym} Cp_{polym}} + \frac{Cp_g^{\bullet} K_{be}([M]_{e,i} - [M]_{h,i})(T_{e,i} - T_{h,i})}{Cp_g^{\bullet} \varepsilon_h [M]_{h,i} + (1 - \varepsilon_h)\rho_{polym} Cp_{polym}}$$

For case $i = \dfrac{27n}{m}$

$$\frac{dT_{h,i}}{dt} = -u_h \frac{3T_{h,i} - 4T_{h,i-1} + T_{h,i-2}}{2dz} + \frac{H_{be}(T_{e,i} - T_{h,i})}{Cp_g^{\bullet} \varepsilon_h [M]_{h,i} + (1 - \varepsilon_h)\rho_{polym} Cp_{polym}} \tag{A.20}$$

$$+ \frac{R_{p,h,i}(1 - \varepsilon_h)(-\Delta H)Mw}{Cp_g^{\bullet} \varepsilon_h [M]_{h,i} + (1 - \varepsilon_h)\rho_{polym} Cp_{polym}} + \frac{Cp_g^{\bullet} K_{be}([M]_{e,i} - [M]_{h,i})(T_{e,i} - T_{h,i})}{Cp_g^{\bullet} \varepsilon_h [M]_{h,i} + (1 - \varepsilon_h)\rho_{polym} Cp_{polym}}$$

For other values of i ($\dfrac{26n}{m} + 1 < i < \dfrac{27n}{m}$):

$$\frac{dT_{h,i}}{dt} = -u_h \frac{3T_{h,i+1} - T_{h,i-1}}{2dz} + \frac{H_{be}(T_{e,i} - T_{h,i})}{Cp_g^{\bullet} \varepsilon_h [M]_{h,i} + (1 - \varepsilon_h)\rho_{polym} Cp_{polym}} \tag{A.21}$$

$$+ \frac{R_{p,h,i}(1 - \varepsilon_h)(-\Delta H)Mw}{Cp_g^{\bullet} \varepsilon_h [M]_{h,i} + (1 - \varepsilon_h)\rho_{polym} Cp_{polym}} + \frac{Cp_g^{\bullet} K_{be}([M]_{e,i} - [M]_{h,i})(T_{e,i} - T_{h,i})}{Cp_g^{\bullet} \varepsilon_h [M]_{h,i} + (1 - \varepsilon_h)\rho_{polym} Cp_{polym}}$$

95

For reactor temperature in the emulsion phase:

For case $i = \dfrac{27n}{m} + 1$:

$$\frac{dT_{e,i}}{dt} = -u_e \frac{-T_{e,i+2} + 4T_{e,i+1} - 3T_{e,i}}{2dz} + \frac{\delta H_{he}(T_{b,i} - T_{e,i})}{(1-\delta)\{Cp_g^* \varepsilon_e [M]_{e,i} + (1-\varepsilon_e)\rho_{polym} Cp_{polym}\}} \qquad (A.22)$$

$$+ \frac{R_{p,e,k}(1-\varepsilon_e)(-\Delta H)Mw}{Cp_g^* \varepsilon_e [M]_{e,k} + (1-\varepsilon_e)\rho_{polym} Cp_{polym}} + \frac{\delta Cp_g^* K_{he}([M]_{b,i} - [M]_{e,k})(T_{e,u} - T_{b,i})}{(1-\delta)\{Cp_g^* \varepsilon_e [M]_{e,k} + (1-\varepsilon_e)\rho_{polym} Cp_{polym}\}}$$

For case $i = \dfrac{28n}{m}$:

$$\frac{dT_{e,i}}{dt} = -u_e \frac{3T_{e,i} - 4T_{e,i-1} + T_{e,i-2}}{2dz} + \frac{\delta H_{he}(T_{b,i} - T_{e,i})}{(1-\delta)\{Cp_g^* \varepsilon_e [M]_{e,i} + (1-\varepsilon_e)\rho_{polym} Cp_{polym}\}} \qquad (A.23)$$

$$+ \frac{R_{p,e,i}(1-\varepsilon_e)(-\Delta H)Mw}{Cp_g^* \varepsilon_e [M]_{e,i} + (1-\varepsilon_e)\rho_{polym} Cp_{polym}} + \frac{\delta Cp_g^* K_{he}([M]_{b,i} - [M]_{e,i})(T_{e,i} - T_{b,i})}{(1-\delta)\{Cp_g^* \varepsilon_e [M]_{e,i} + (1-\varepsilon_e)\rho_{polym} Cp_{polym}\}}$$

For other values of i $(\dfrac{27n}{m} + 1 < i < \dfrac{28n}{m})$:

$$\frac{dT_{e,i}}{dt} = -u_e \frac{3T_{e,i+1} - T_{e,i-1}}{2dz} + \frac{\delta H_{he}(T_{b,i} - T_{e,i})}{(1-\delta)\{Cp_g^* \varepsilon_e [M]_{e,i} + (1-\varepsilon_e)\rho_{polym} Cp_{polym}\}} \qquad (A.24)$$

$$+ \frac{R_{p,e,i}(1-\varepsilon_e)(-\Delta H)Mw}{Cp_g^* \varepsilon_e [M]_{e,i} + (1-\varepsilon_e)\rho_{polym} Cp_{polym}} + \frac{\delta Cp_g^* K_{he}([M]_{b,i} - [M]_{e,i})(T_{e,i} - T_{b,i})}{(1-\delta)\{Cp_g^* \varepsilon_e [M]_{e,i} + (1-\varepsilon_e)\rho_{polym} Cp_{polym}\}}$$
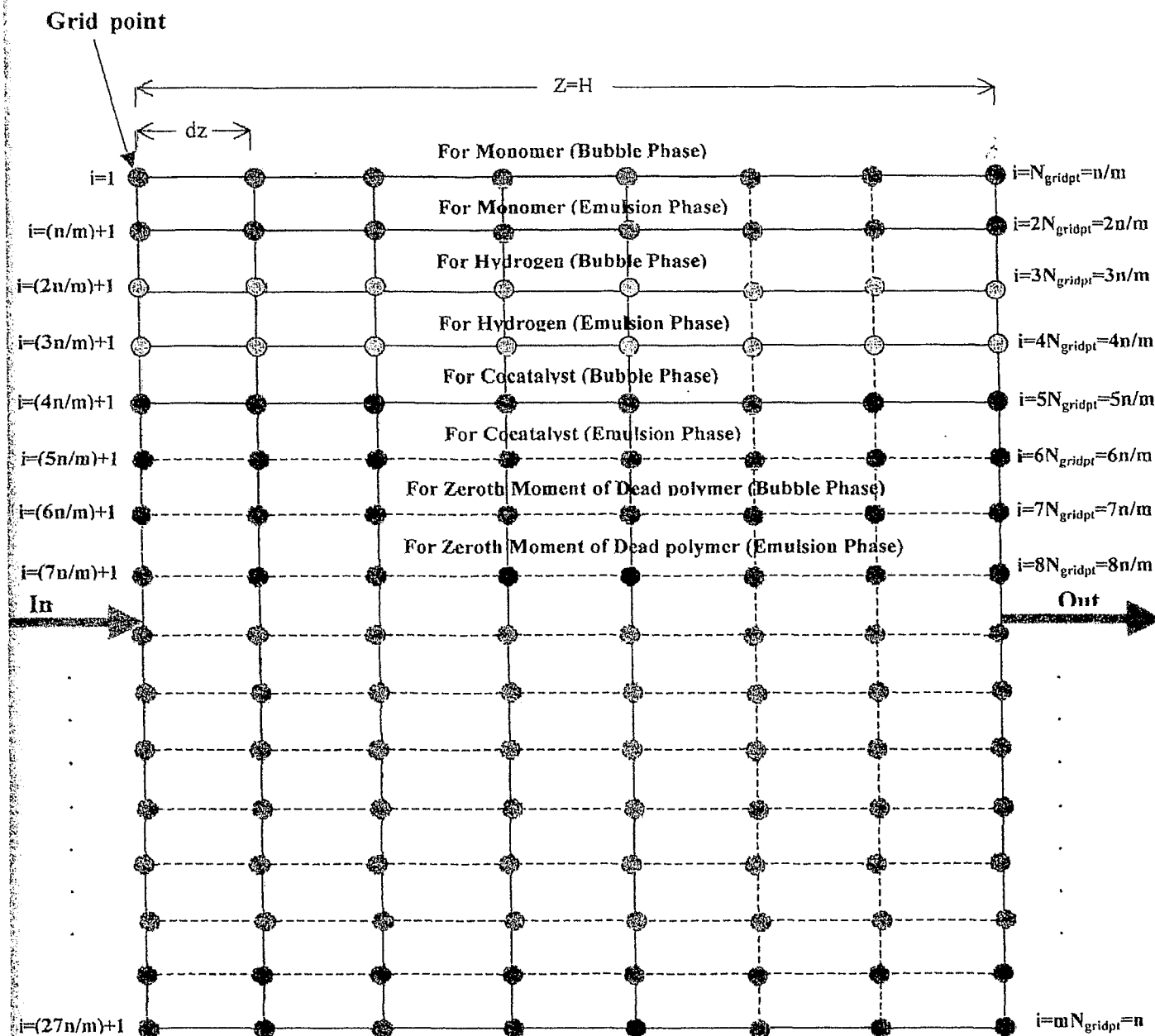
96

Figure A.1: Schematic Diagram of the Numerical Solution Algorithm

Figure A.1: Schematic Diagram of the Numerical Solution Algorithm

97

Appendix B: Steady-State Model Supplementary Figures

Figure B.1: Profile of catalyst concentration versus reactor axial position (isothermal)

Figure B.1.a: Catalyst Concentration (Bubble Phase)

Figure B.1.b: Catalyst Concentration (Emulsion Phase)

Figure B.2: Profile of cocatalyst concentration versus reactor axial position (isothermal)

Figure B.2.a: Cocatalyst Concentration (Bubble Phase)

Figure B.2.b: Cocatalyst Concentration (Emulsion Phase)

Figure B.2.c: Profile of Overall Cocatalyst Concentration

Ccocatb: Cocatalyst concentration (Bubble phase)
Ccocate: Cocatalyst concentration (Emulsion phase)
Ccocat: Overall cocatalyst concentration in the bed

98
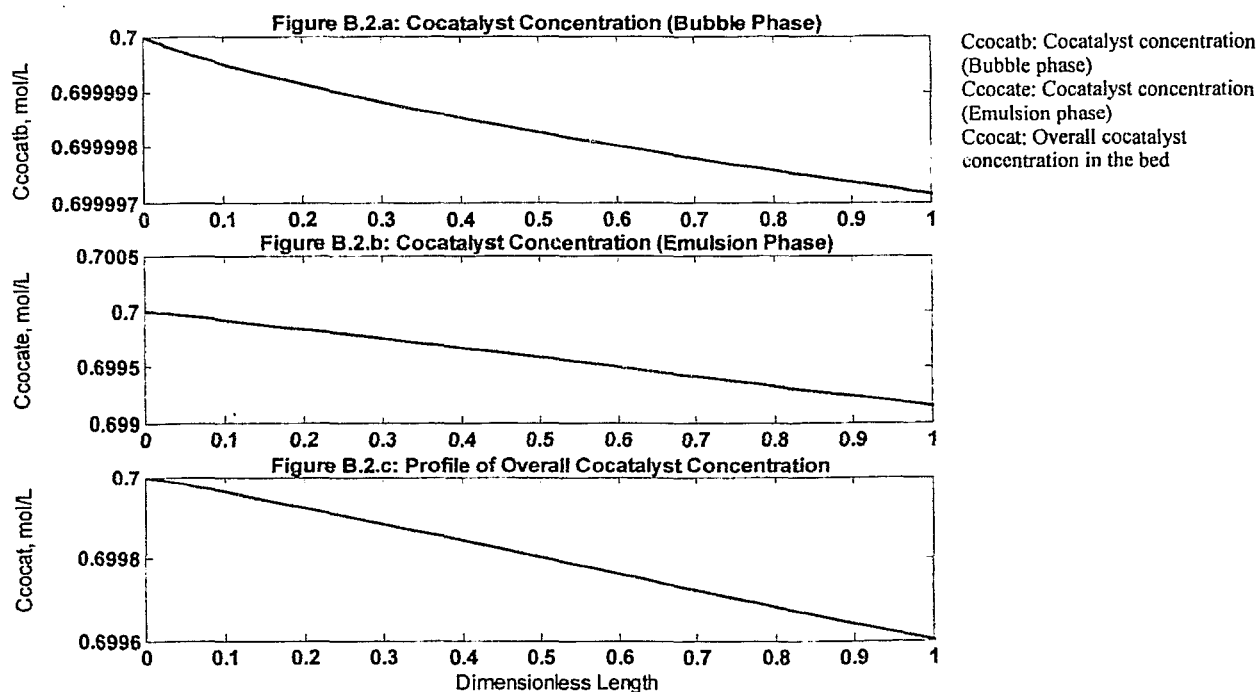
Figure B.3: Profile of chain transfer agent concentration versus reactor axial position
(isothermal)

Figure B.3.a: H2 Concentration (Bubble Phase)

CH2b: H2 concentration (Bubble phase)
CH2e: H2 concentration (Emulsion phase)
CH2: Overall H2 concentration

Figure B.3.b: H2 Concentration (Emulsion Phase)

Figure B.3.c: Profile of Overall H2 Concentration
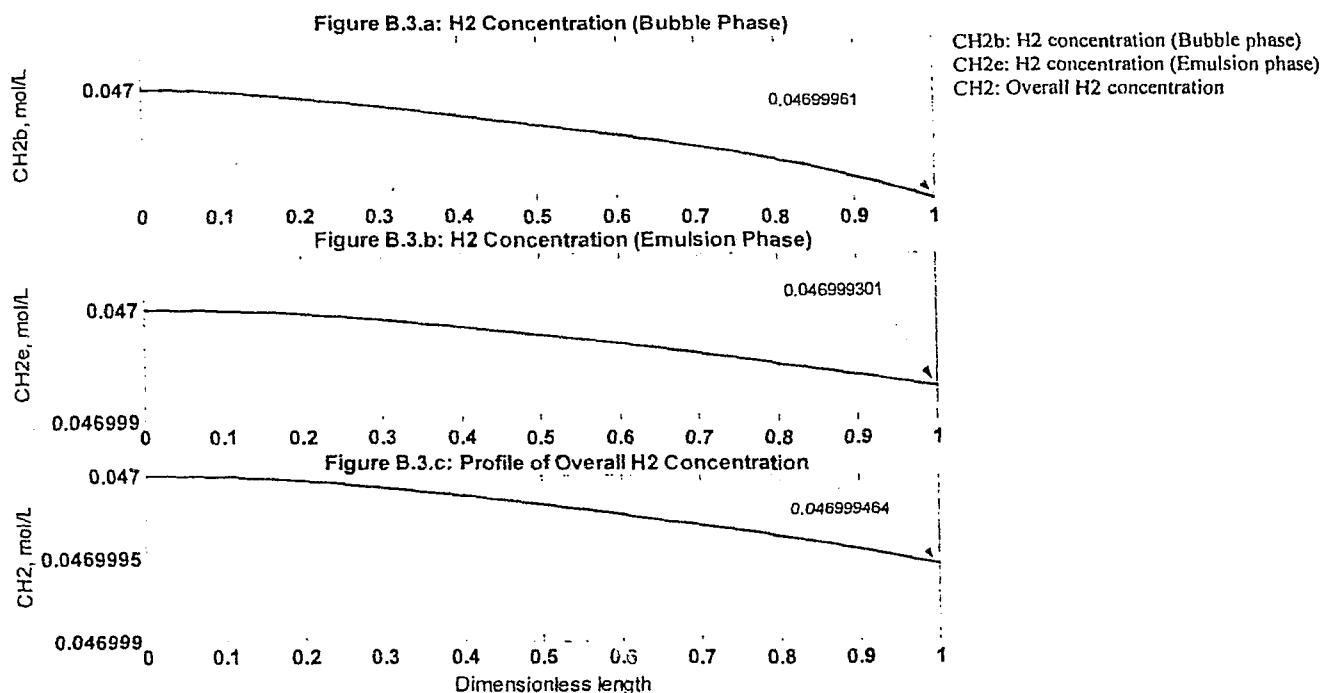
Figure B.4: Profile of polymerization rate versus conversion (isothermal)

Figure B.4.a: Polymerization Rate (Bubble Phase)

Rpb: Polymerization rate (Bubble phase)
Rpe: Polymerization rate (Emulsion phase)

Figure B.4.b: Polymerization Rate (Emulsion Phase)

99

Figure B.5: Profile of bubble growth versus reactor axial position (isothermal)

Figure B.5: Profile of Bubble Size Along The Bed
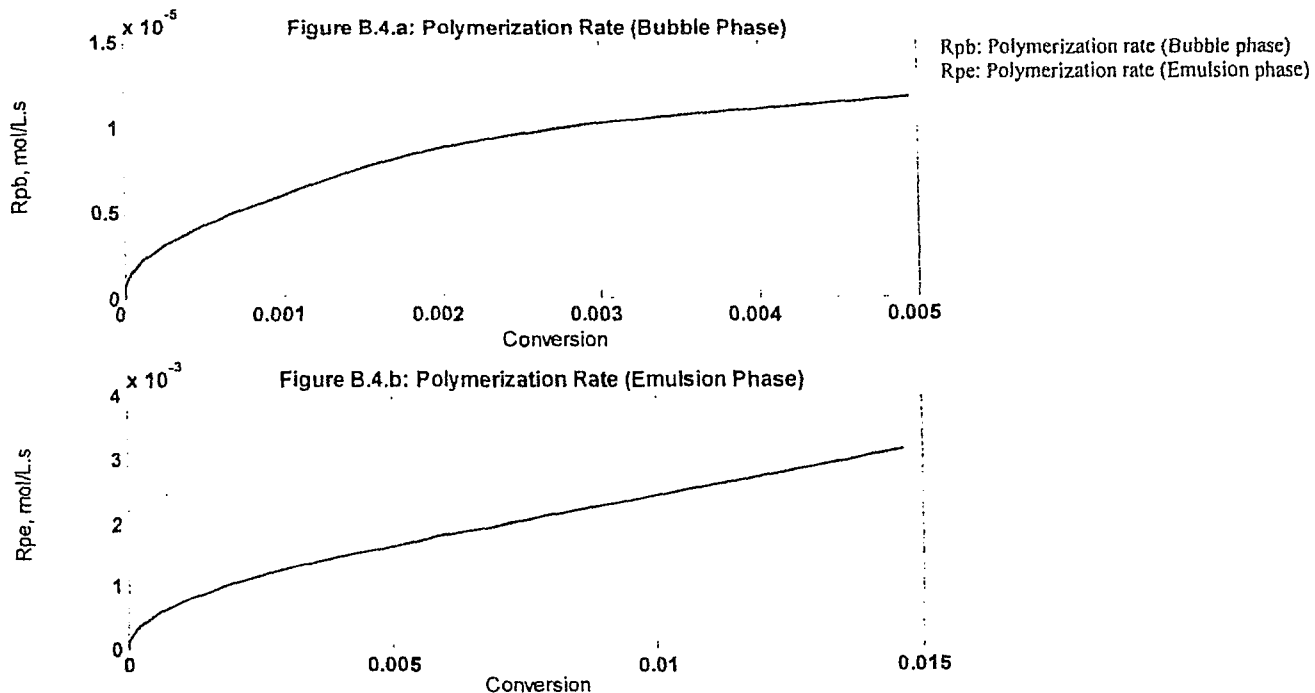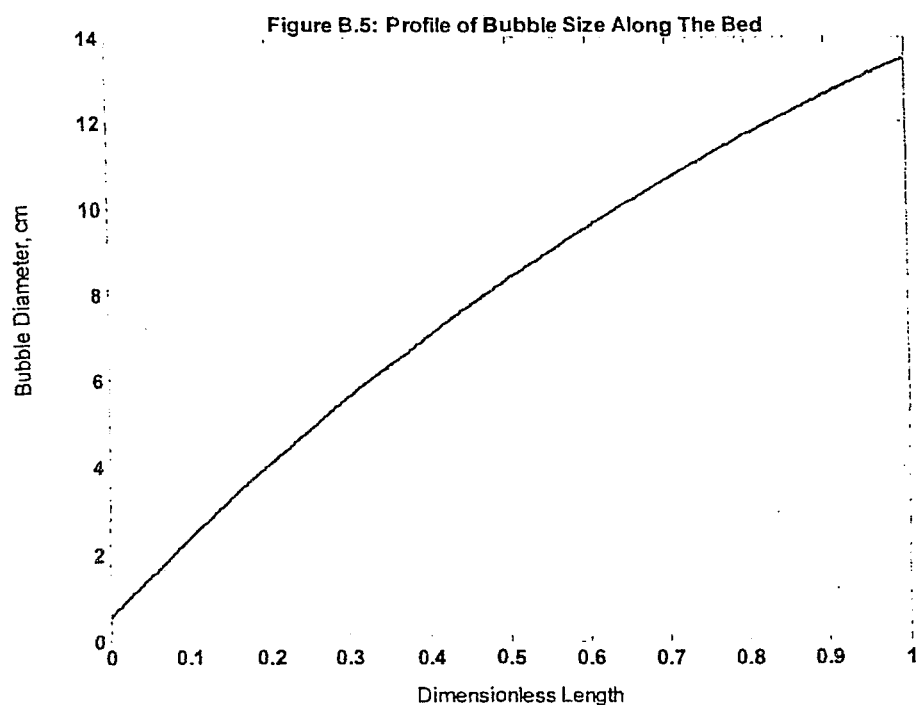
Figure B.6: Profile of catalyst concentration versus reactor axial position (non-isothermal)

Figure B.6.a: Catalyst Concentration (Bubble Phase)
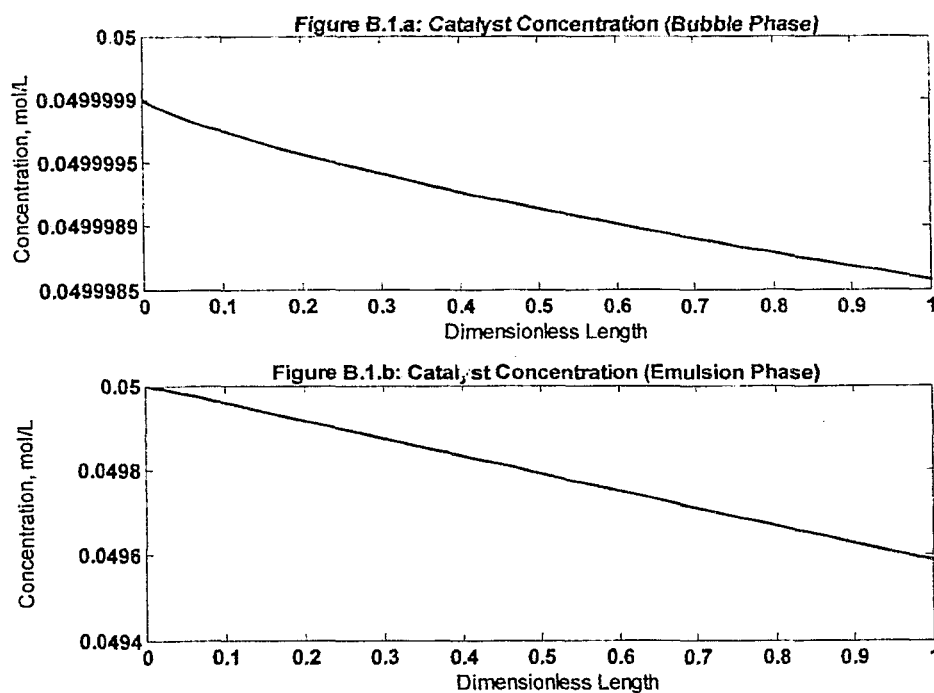

Figure B.12.b: Catalyst Concentration (Emulsion Phase)

100
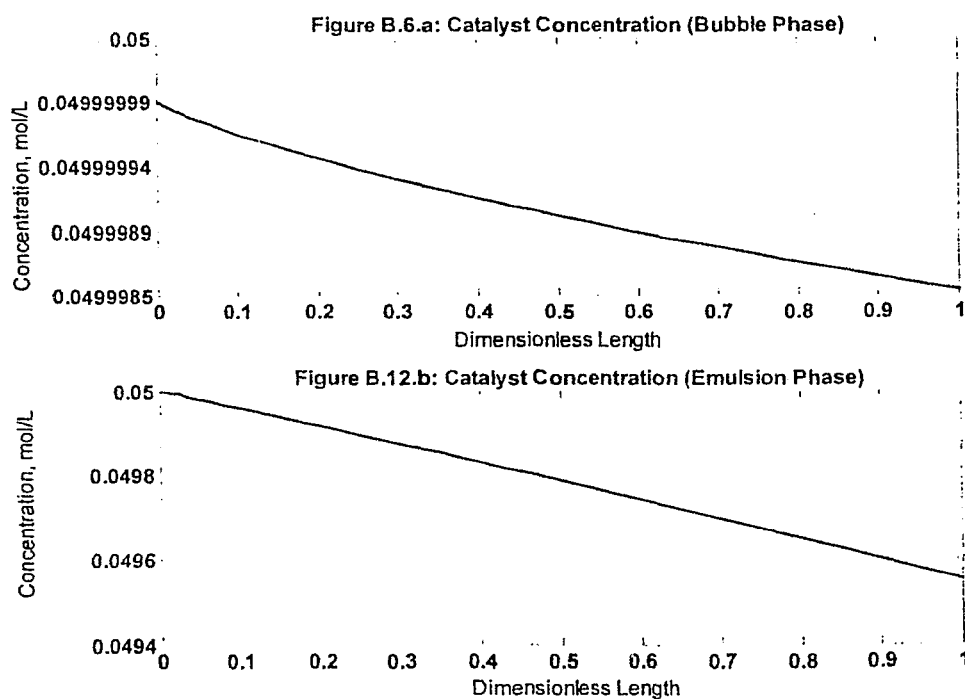
Figure B.7: Profile of cocatalyst concentration versus reactor axial position (non-isothermal)

Figure B.7.a: Cocatalyst Concentration (Bubble Phase)

Figure B.7.b: Cocatalyst Concentration (Emulsion Phase)

Figure B.7.c: Profile of Overall Cocatalyst Concentration

Ccocatb: Cocatalyst concentration (Bubble phase)
Ccocate: Cocatalyst concentration (Emulsion phase)
Ccocat: Overall cocatalyst concentration in the bed
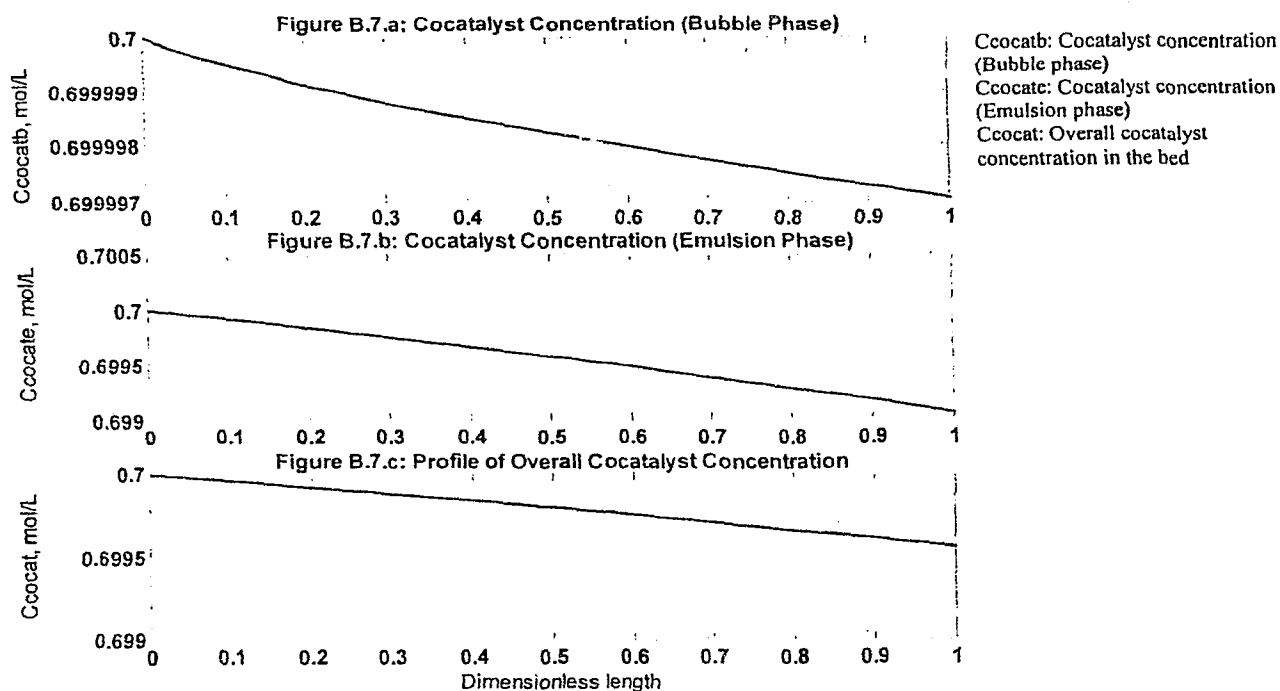
Figure B.8: Profile of hydrogen concentration versus reactor axial position (non-isothermal)

Figure B.8.a: H2 Concentration (Bubble Phase)

Figure B.8.b: H2 Concentration (Emulsion Phase)

Figure B.8.c: Profile of Overall H2 Concentration

CH2b: H2 concentration (Bubble phase)
CH2e: H2 concentration (Emulsion phase)
CH2: Overall H2 concentration

101
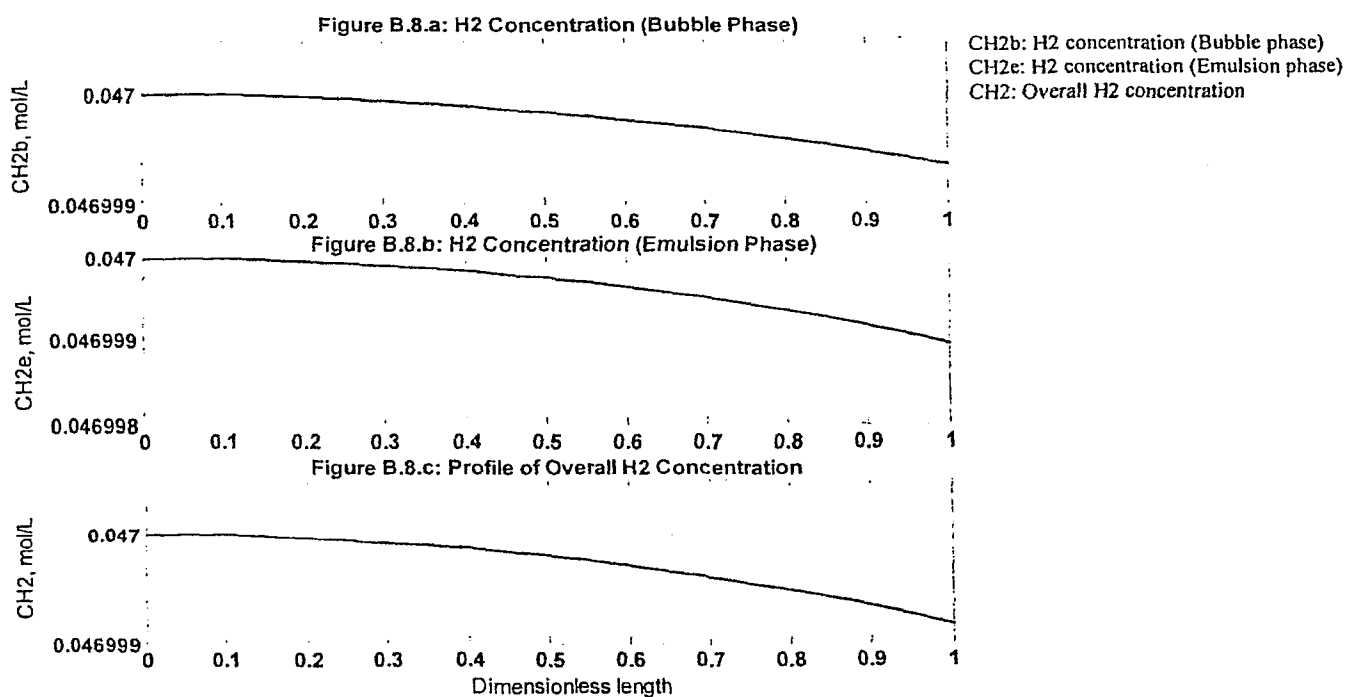
Figure B.9: Profile of polymerization rate versus conversion (non-isothermal)

Figure B.9.a: Polymerization Rate (Bubble Phase)

Rpb: Polymerization rate (Bubble phase)
Rpe: Polymerization rate (Emulsion phase)

Figure B.9.b: Polymerization Rate (Emulsion Phase)

102
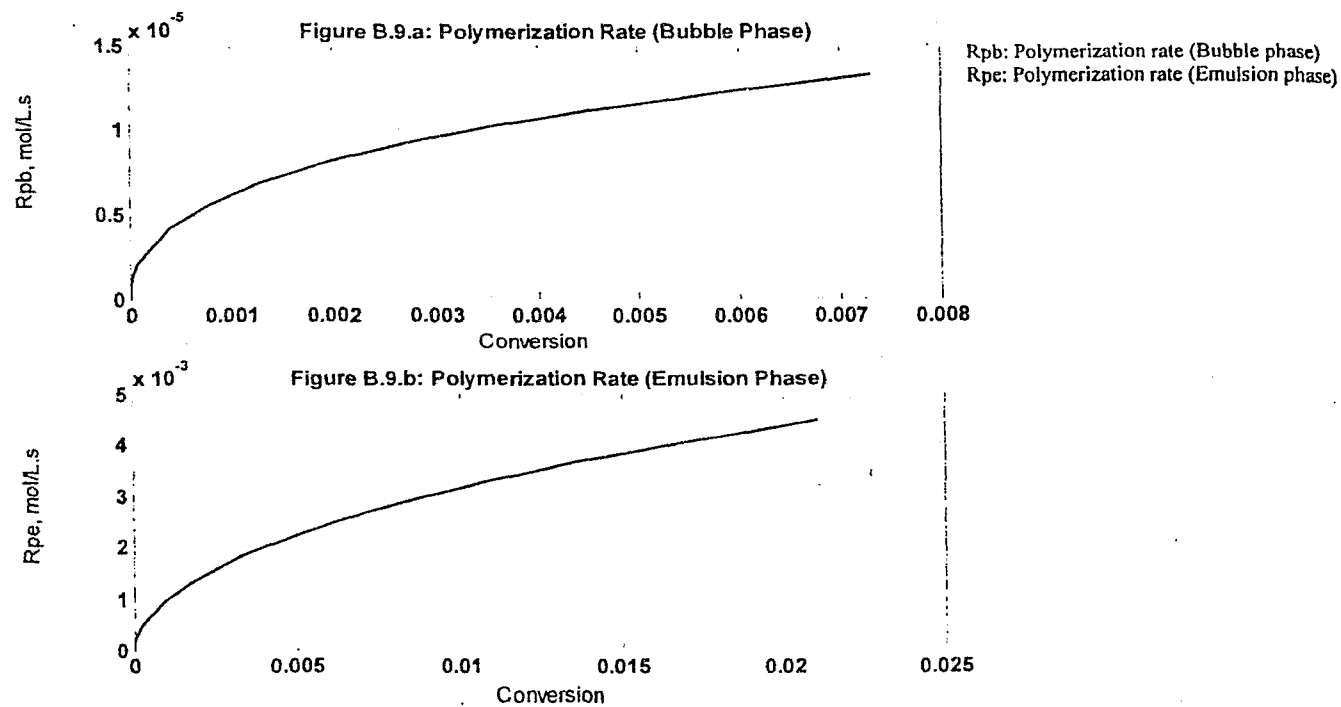
Appendix C: Parametric Study Supplementary Figures

Figure C.1: The effect of superficial gas velocity on profile of catalyst concentration versus reactor axial position

Figure C.1.a: Catalyst Concentration (Bubble Phase)

Figure C.1.b: Catalyst Concentration (Emulsion Phase)
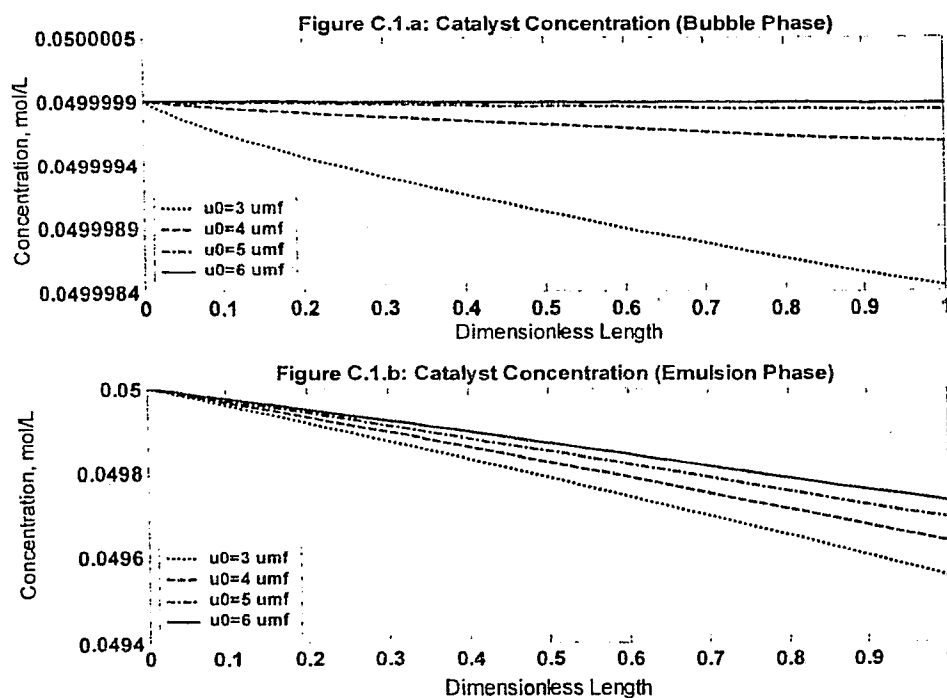
Figure C.2: The effect of superficial gas velocity on profile of cocatalyst concentration

Figure C.2.a: Cocatalyst Concentration (Bubble Phase)

Ccocatb: Cocatalyst concentration (Bubble phase)
Ccocate: Cocatalyst concentration (Emulsion phase)
Ccocat: Overall cocatalyst concentration in the bed

Figure C.2.b: Cocatalyst Concentration (Emulsion Phase)

Figure C.2.c: Profile of Overall Cocatalyst Concentration

103
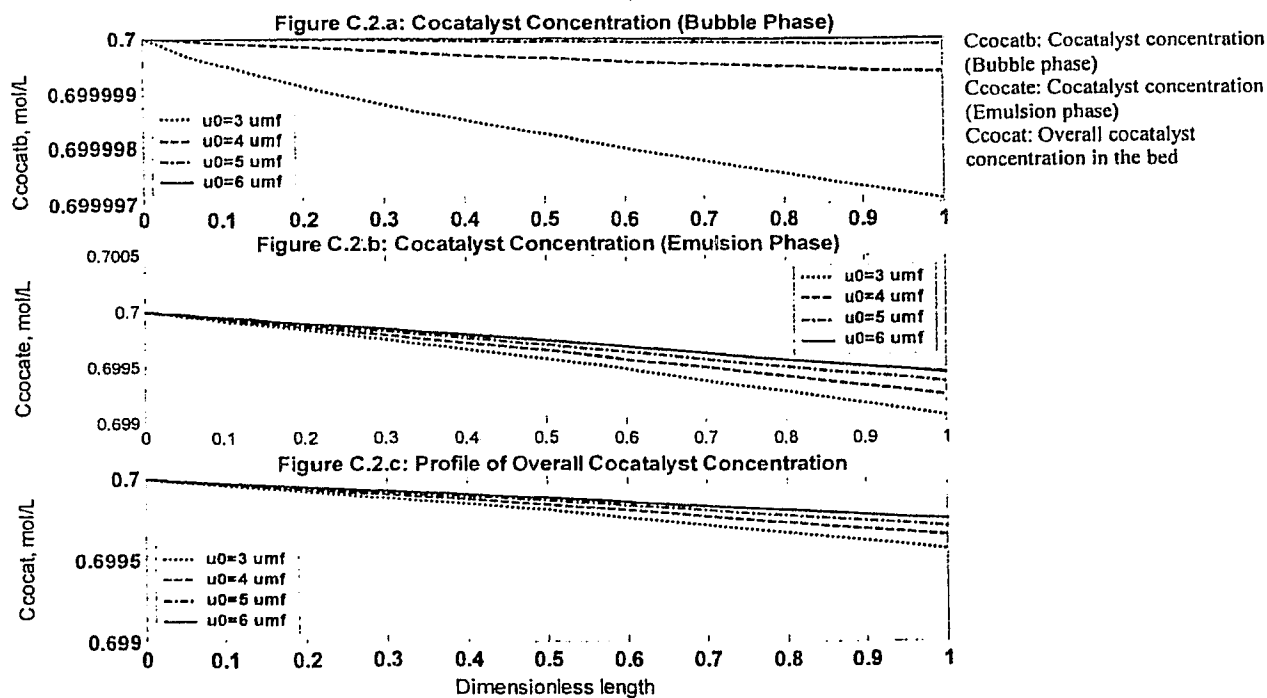
Figure C.3: The effect of superficial g s velocity on profile of hydrogen concentration versus reactor axial position

Figure C.3.a: H2 Concentration (Bubble Phase)

CH2b: H2 concentration (Bubble phase)
CH2e: H2 concentration (Emulsion phase)
CH2: Overall H2 concentration

Figure C.3.b: H2 Concentration (Emulsion Phase)

Figure C.3.c: Profile of Overall H2 Concentration

Dimensionless length

Figure C.4: The effect of superficial gas velocity on Profile of polymerization rate versus conversion

Figure C.4.a: Polymerization Rate (Bubble Phase)

Rpb: Polymerization rate (Bubble phase)
Rpe: Polymerization rate (Emulsion phase)

Conversion
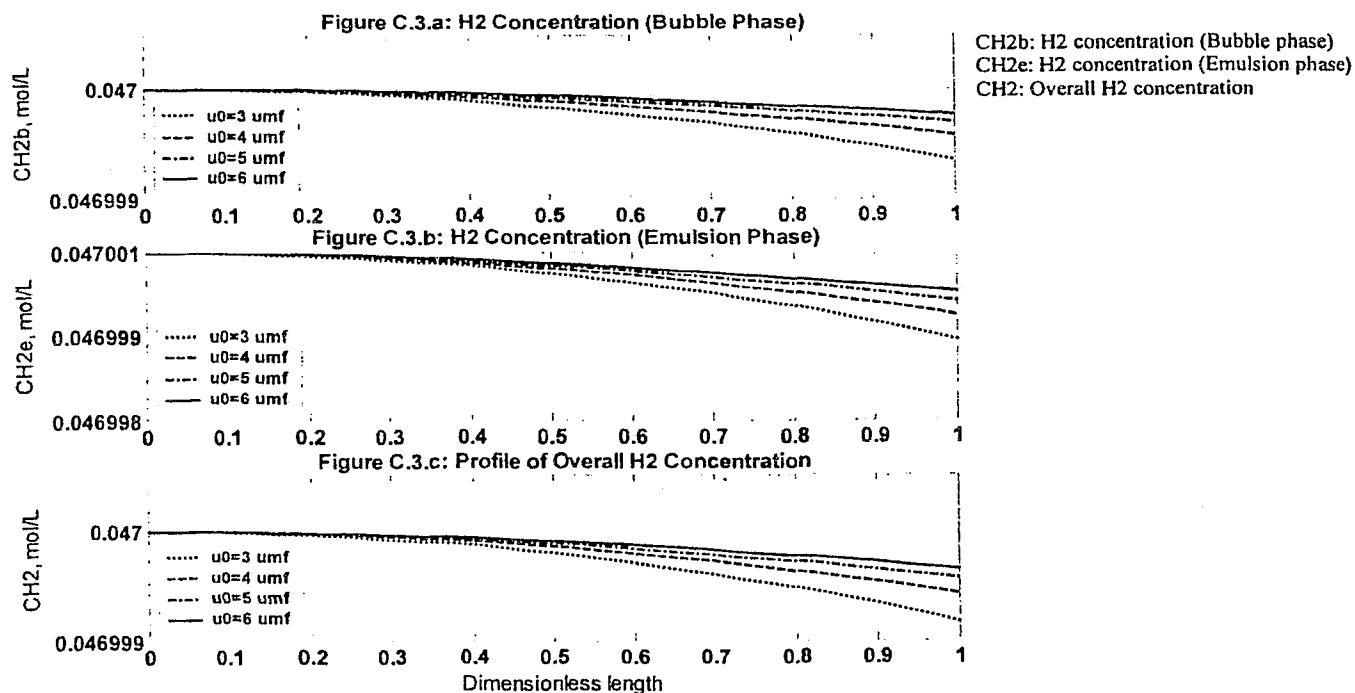
Figure C.4.b: Polymerization Rate (Emulsion Phase)

Conversion

104
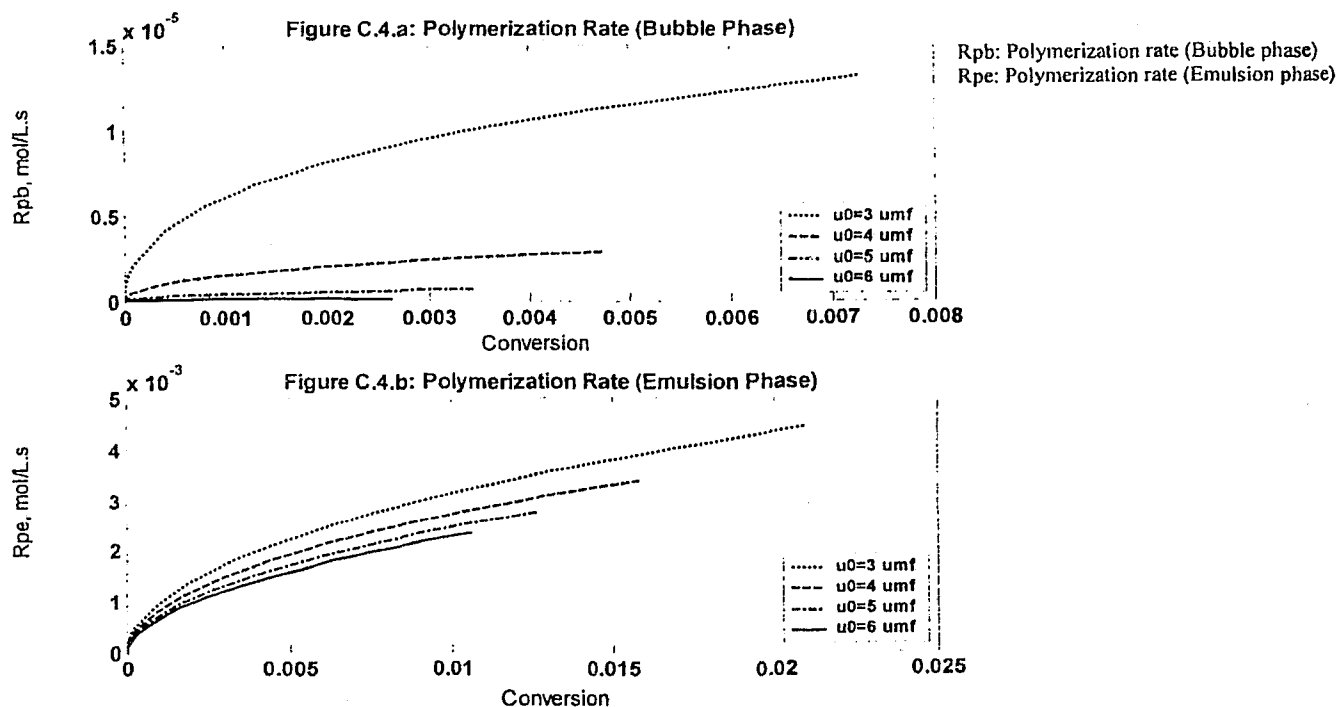
Figure C.5: The effect of superficial gas velocity on profile of bubble growth versus reactor axial position
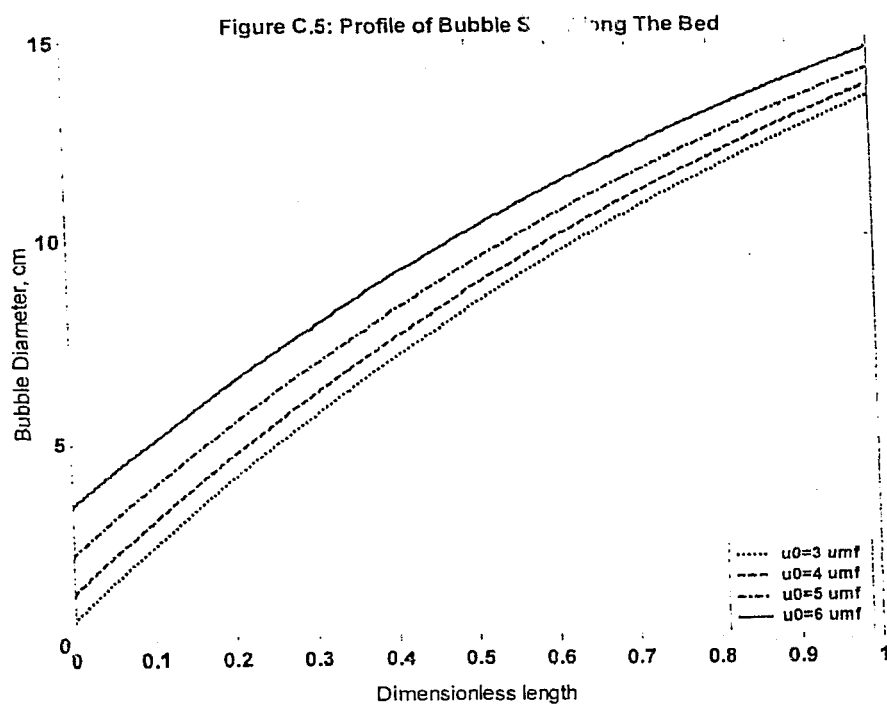
Figure C.5: Profile of Bubble S   ong The Bed

Figure C.6: The effect of mean particle size on profile of catalyst concentration along the bed height

Figure C.6.a: Catalyst Concentration (Bubble Phase)
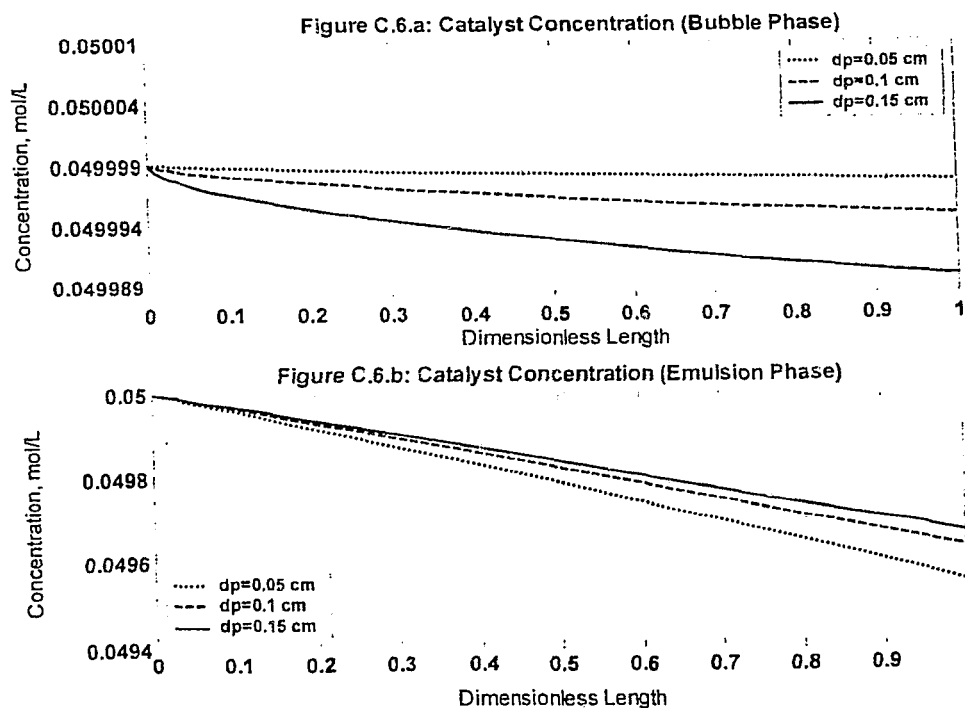

Figure C.6.b: Catalyst Concentration (Emulsion Phase)

105

Figure C.7: The effect of mean particle size on profile of cocatalyst concentration versus reactor axial position

Figure C.7.a: Cocatalyst Concentration (Bubble Phase)
Figure C.7.b: Cocatalyst Concentration (Emulsion Phase)
Figure C.7.c: Profile of Overall Cocatalyst Concentration

Ccocatb: Cocatalyst concentration (Bubble phase)
Ccocate: Cocatalyst concentration (Emulsion phase)
Ccocat: Overall cocatalyst concentration in the bed
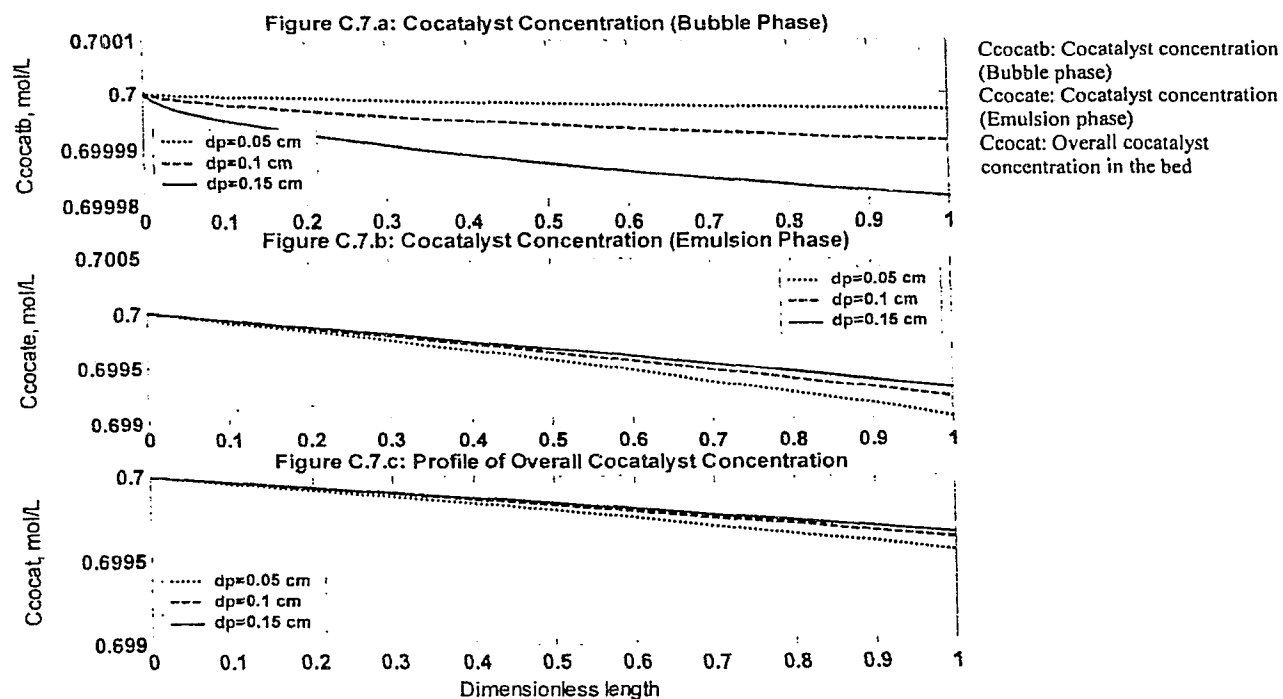
Figure C.8: The effect of mean particle size on profile of hydrogen concentration versus reactor axial position

Figure C.8.a: H2 Concentration (Bubble Phase)
Figure C.8.b: H2 Concentration (Emulsion Phase)
Figure C.8.c: Profile of Overall H2 Concentration

CH2b: H2 concentration (Bubble phase)
CH2e: H2 concentration (Emulsion phase)
CH2: Overall H2 concentration

106
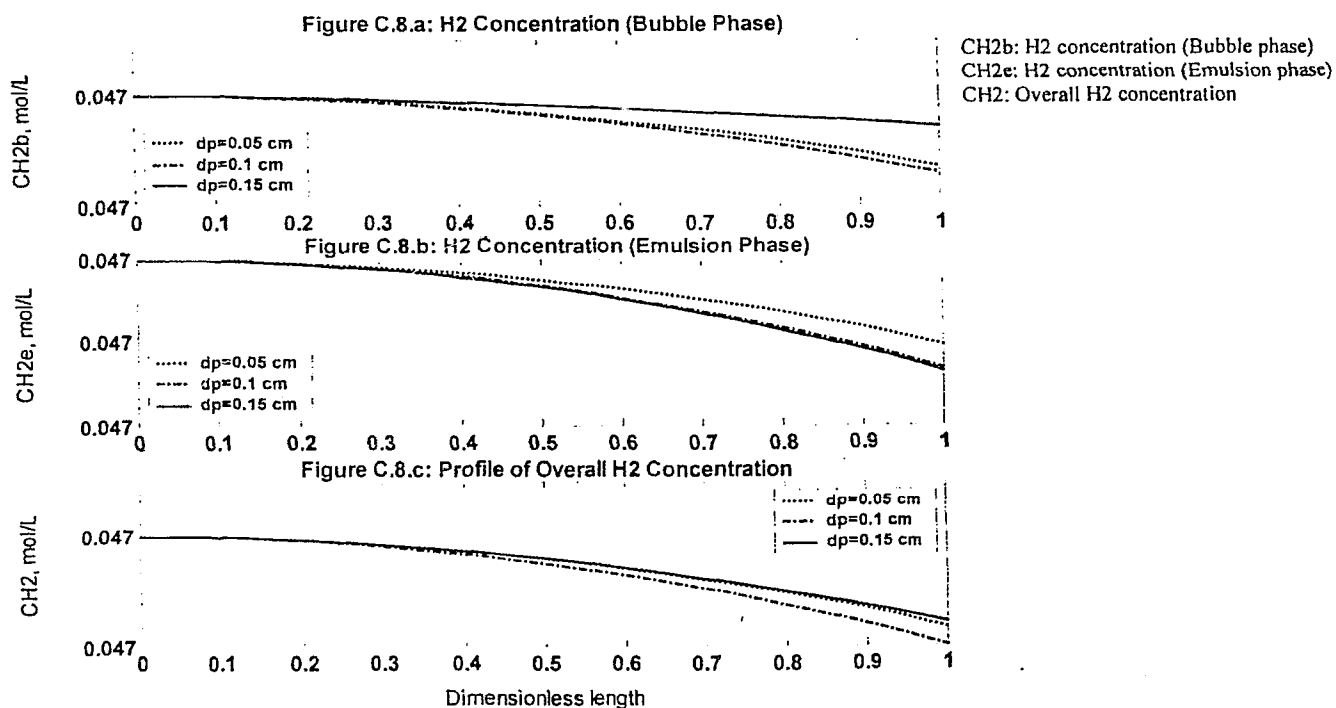
Figure C.9: The effect of mean particle size on profile of polymerization rate versus conversion

Figure C.9.a: Polymerization Rate (Bubble Phase)
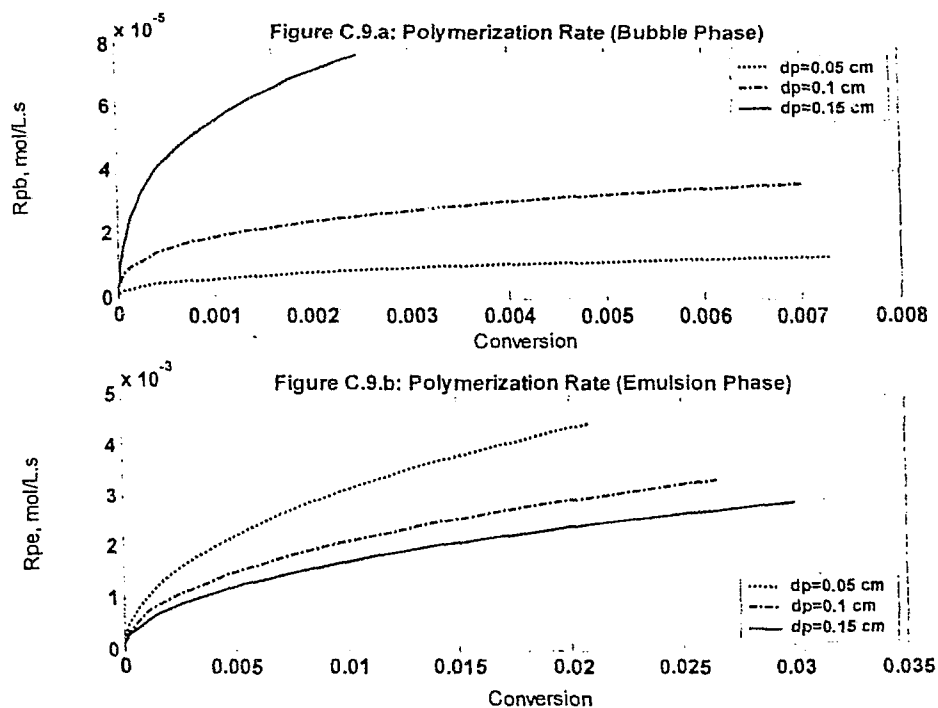

Figure C.9.b: Polymerization Rate (Emulsion Phase)

Figure C.10: The effect of mean particle size on Profile of bubble growth versus reactor axial position

Figure C.10: Profile of Bubble Size Along The Bed

107

Figure C.11: The effect of gas feed temperature on profile of catalyst concentration versus reactor axial position

Figure C.11.a: Catalyst Concentration (Bubble Phase)

Figure C.11.b: Catalyst Concentration (Emulsion Phase)
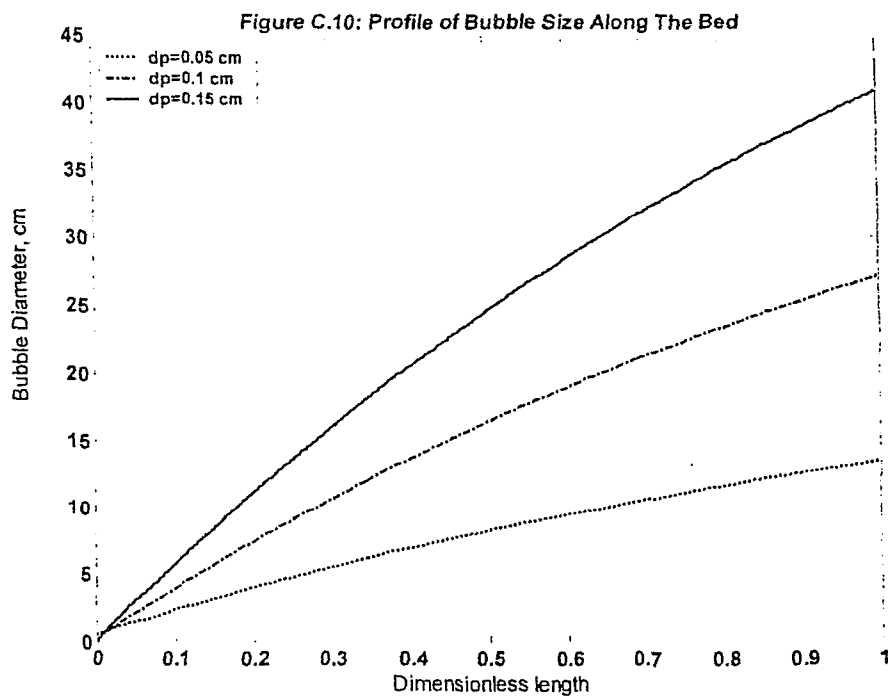
Figure C.12: The effect of gas feed temperature on profile of cocatalyst concentration versus reactor axial position

Figure C.12.a: Cocatalyst Concentration (Bubble Phase)

Figure C.12.b: Cocatalyst Concentration (Emulsion Phase)

Figure C.12.c: Profile of Overall Cocatalyst Concentration

Ccocatb: Cocatalyst concentration (Bubble phase)
Ccocate: Cocatalyst concentration (Emulsion phase)
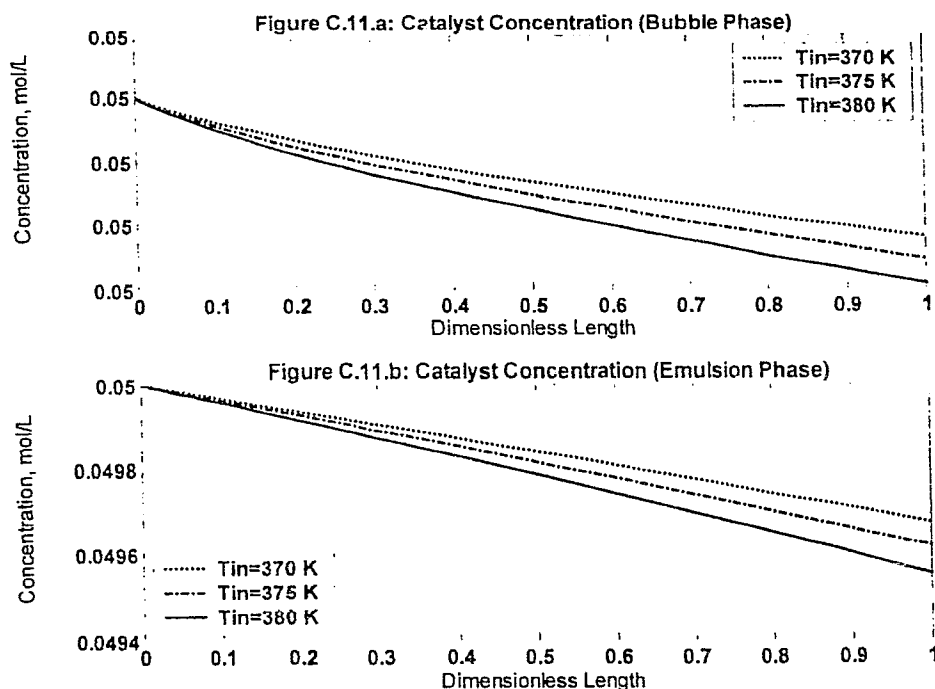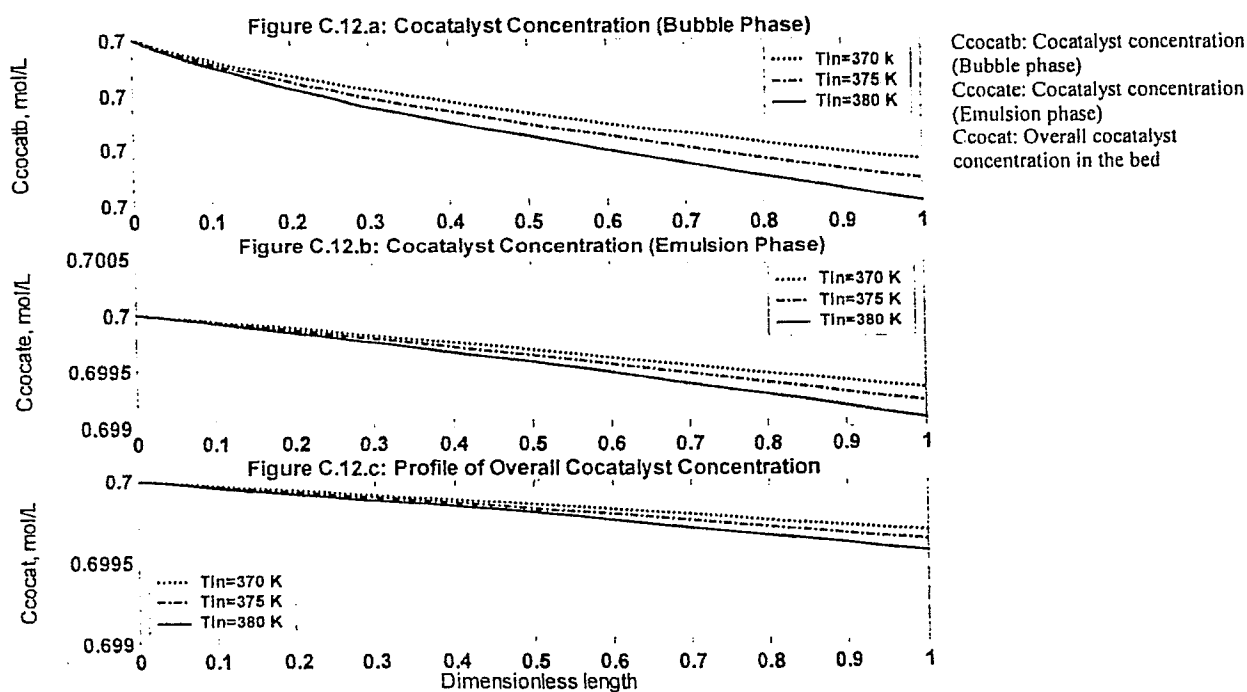Ccocat: Overall cocatalyst concentration in the bed

108

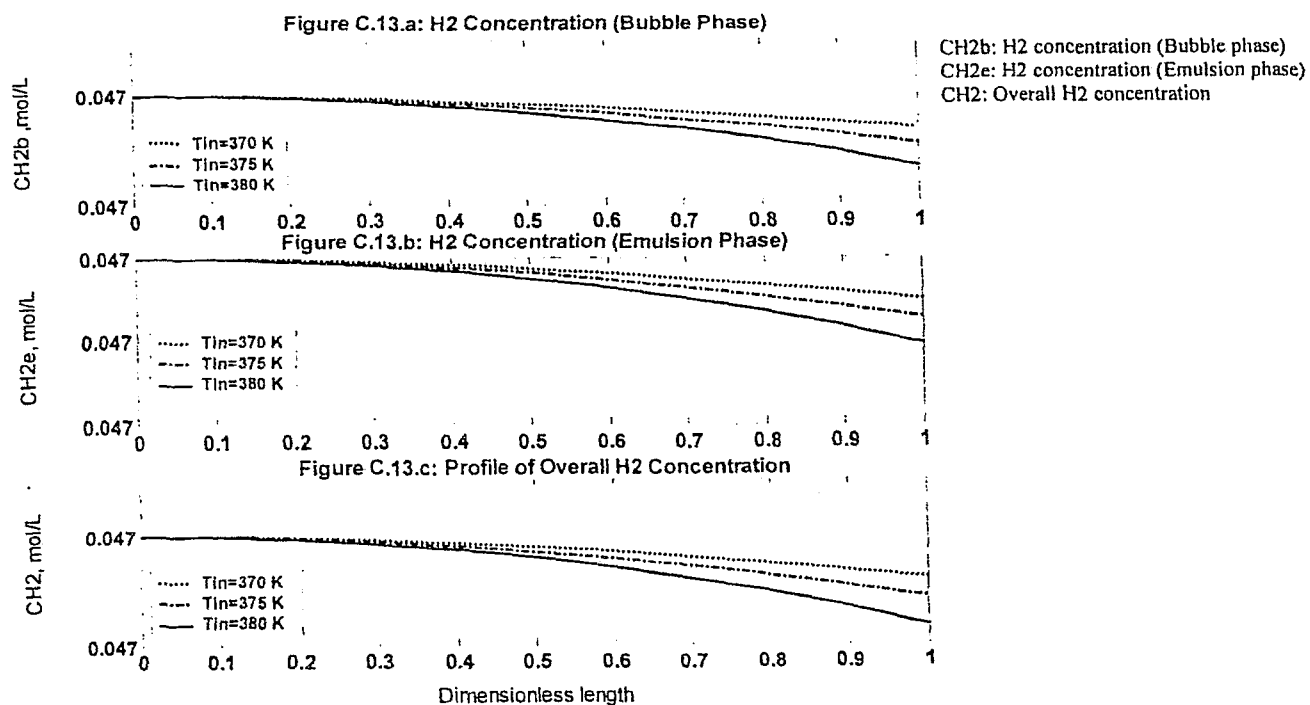Figure C.13: The effect of gas feed temperature on profile of hydrogen concentration versus reactor axial position

Figure C.13.a: H2 Concentration (Bubble Phase)

CH2b: H2 concentration (Bubble phase)
CH2e: H2 concentration (Emulsion phase)
CH2: Overall H2 concentration

Figure C.13.b: H2 Concentration (Emulsion Phase)

Figure C.13.c: Profile of Overall H2 Concentration

Figure C.14: The effect of gas feed temperature on profile of polymerization rate versus conversion

Figure C.14.a: Polymerization Rate (Bubble Phase)

Rpb: Polymerization rate (Bubble phase)
Rpe: Polymerization rate (Emulsion phase)

Figure C.14.b: Polymerization Rate (Emulsion Phase)

109

Figure C.15: The effect of bubble size on profile of catalyst concentration versus reactor axial position

Figure C.15.a: Catalyst Concentration (Bubble Phase)
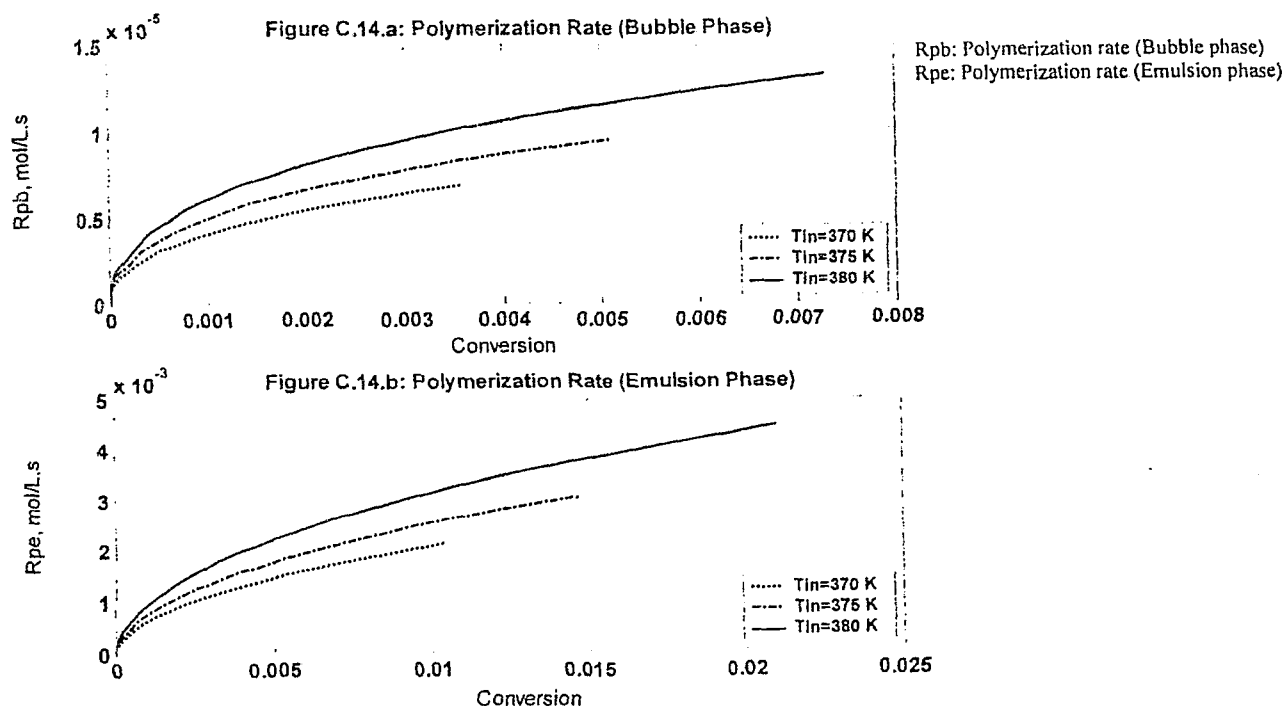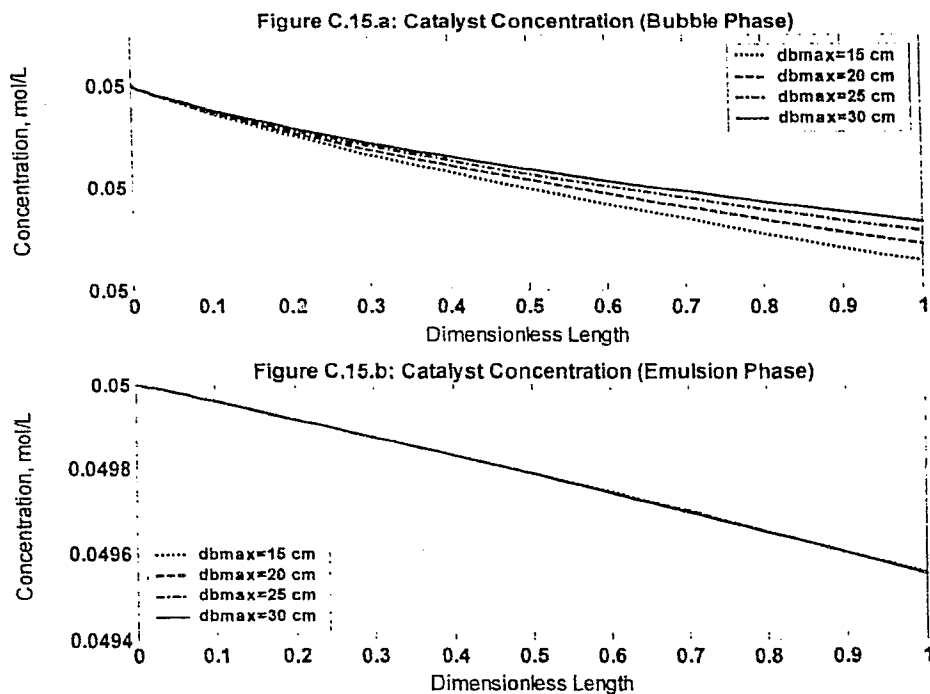
Figure C.15.b: Catalyst Concentration (Emulsion Phase)

Figure C.16: The effect of bubble size on profile of cocatalyst concentration versus reactor axial position

Figure C.16.a: Cocatalyst Concentration (Bubble Phase)

Figure C.16.b: Cocatalyst Concentration (Emulsion Phase)

Figure C.16.c: Profile of Overall Cocatalyst Concentration

Ccocatb: Cocatalyst concentration (Bubble phase)
Ccocate: Cocatalyst concentration (Emulsion phase)
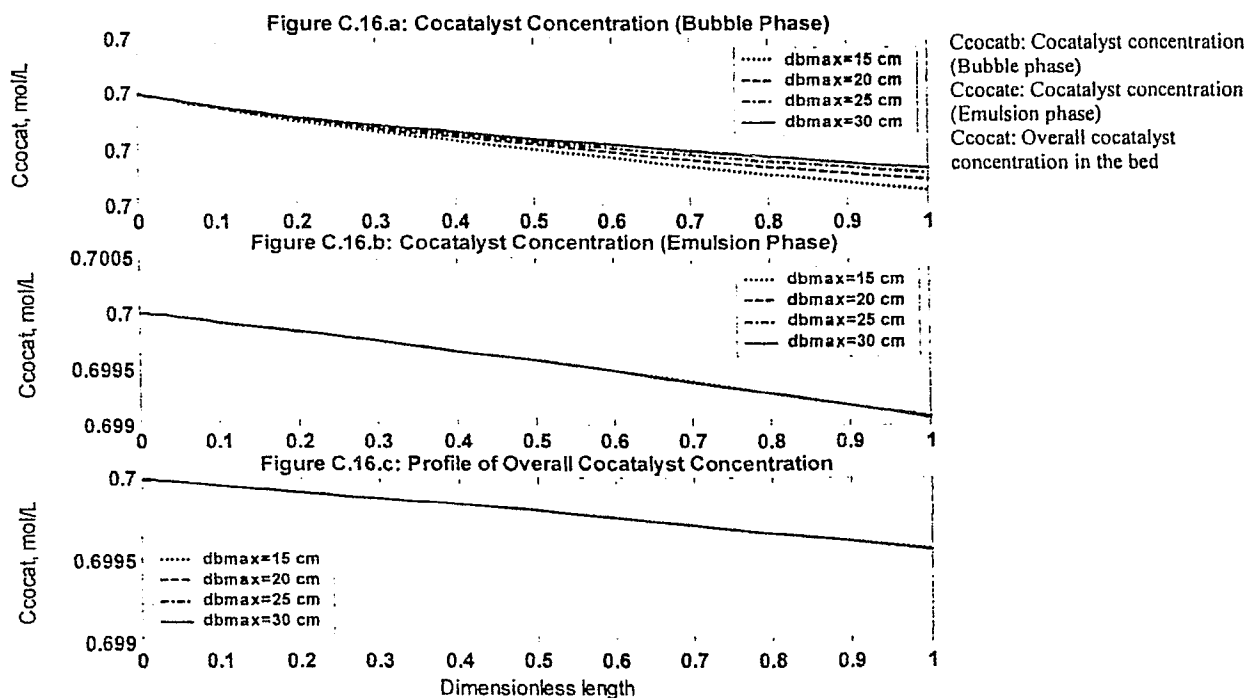Ccocat: Overall cocatalyst concentration in the bed

110

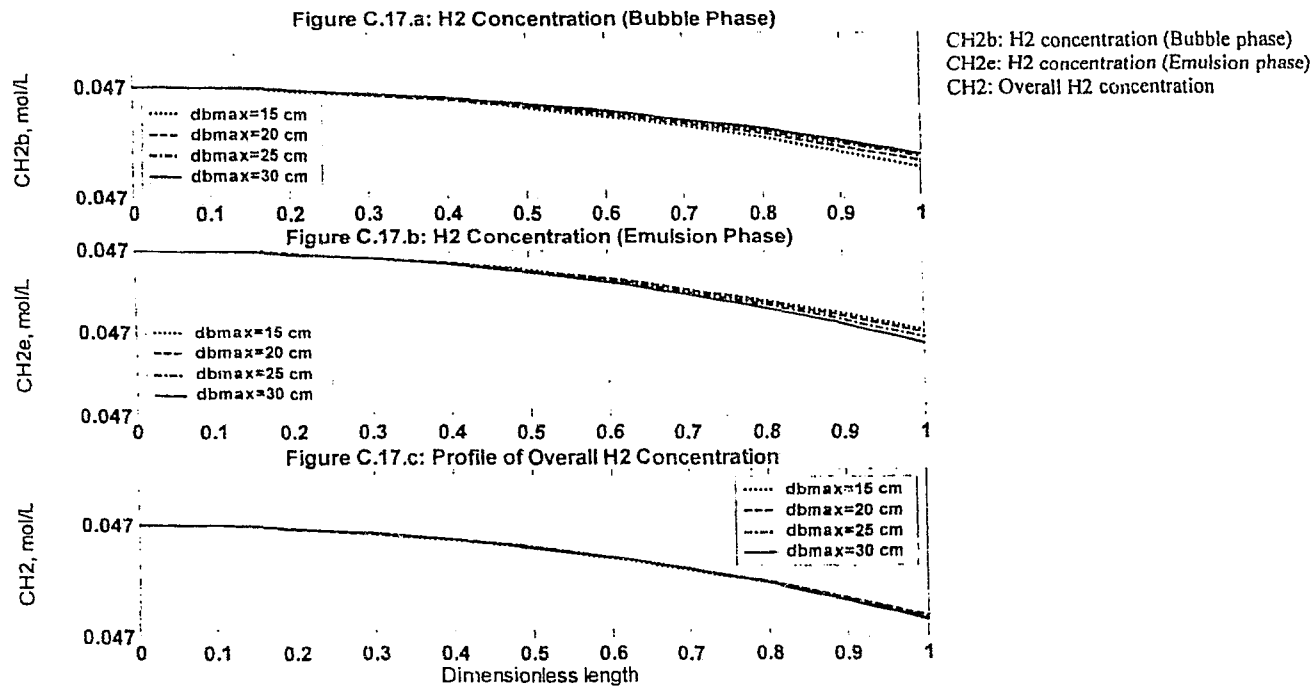Figure C.17: The effect of bubble size on profile of hydrogen concentration versus reactor axial position

Figure C.17.a: H2 Concentration (Bubble Phase)

CH2b: H2 concentration (Bubble phase)
CH2e: H2 concentration (Emulsion phase)
CH2: Overall H2 concentration

Figure C.18: The effect of bubble size on profile of bubble growth versus reactor length

Figure C.18: Profile of Bubble Size Along the Bed

Figure C.19: The effect of recycle stream on profile of catalyst concentration versus reactor axial position

Figure C.19.a: Catalyst Concentration (Bubble Phase)
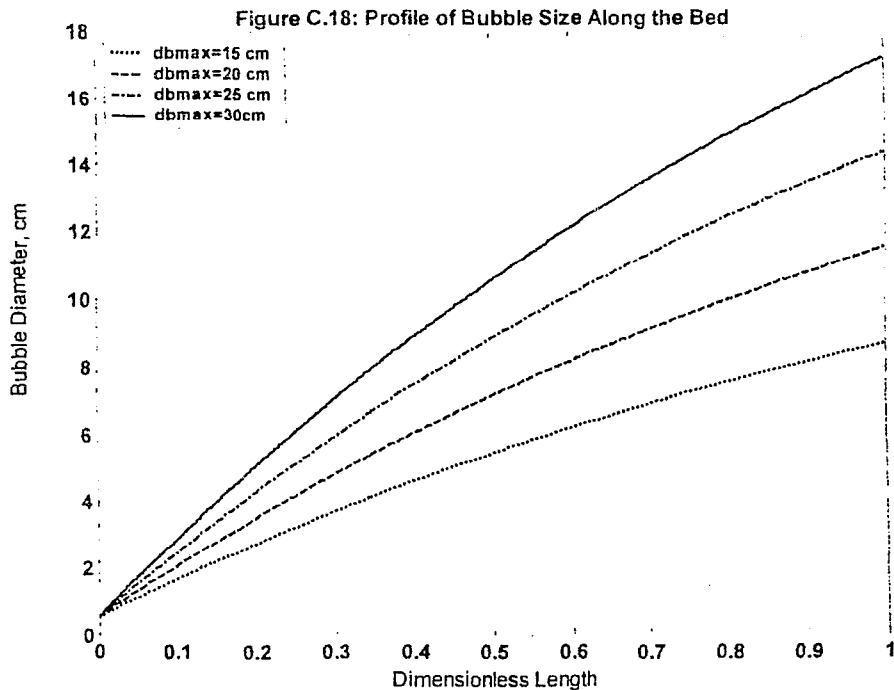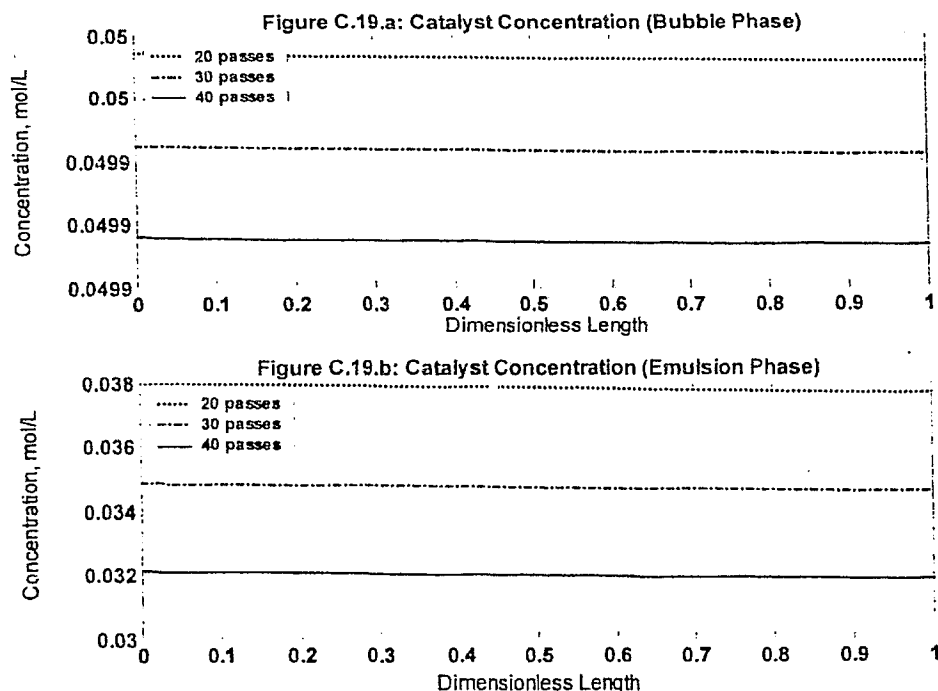
Figure C.19.b: Catalyst Concentration (Emulsion Phase)

Figure C.20: The effect of recycle stream on profile of cocatalyst concentration versus reactor axial position

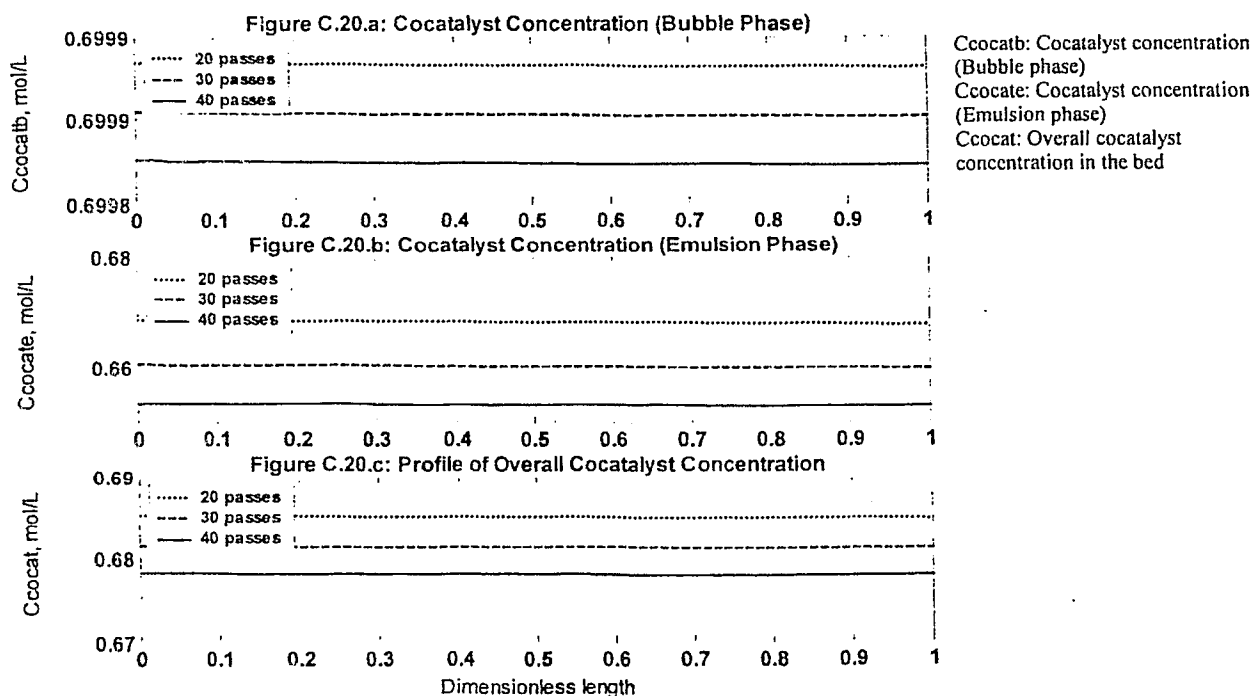Figure C.20.a: Cocatalyst Concentration (Bubble Phase)

Figure C.20.b: Cocatalyst Concentration (Emulsion Phase)

Figure C.20.c: Profile of Overall Cocatalyst Concentration

Ccocatb: Cocatalyst concentration (Bubble phase)
Ccocate: Cocatalyst concentration (Emulsion phase)
Ccocat: Overall cocatalyst concentration in the bed

112

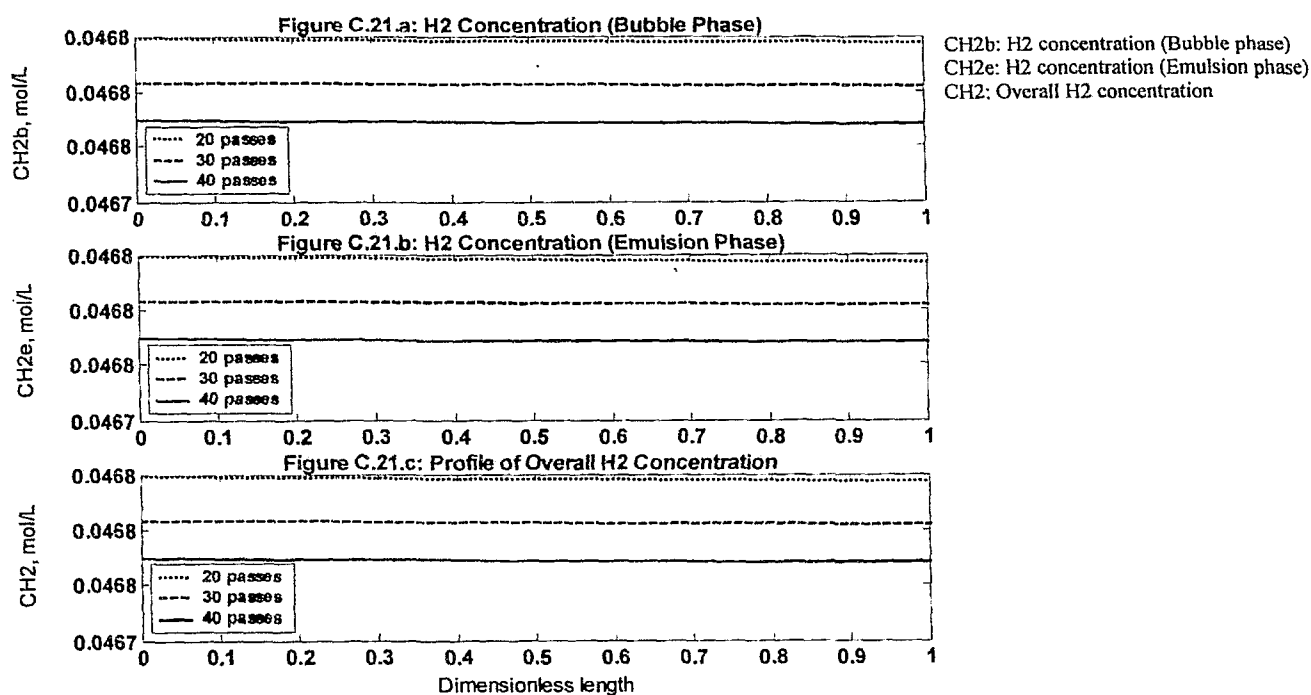Figure C.21: The effect of recycle stream on profile of hydrogen concentration versus reactor axial position

CH2b: H2 concentration (Bubble phase)
CH2e: H2 concentration (Emulsion phase)
CH2: Overall H2 concentration

Figure C.22: The effect of recycle stream on profile of polymerization rate versus conversion

Rpb: Polymerization rate (Bubble phase)
Rpe: Polymerization rate (Emulsion phase)

113
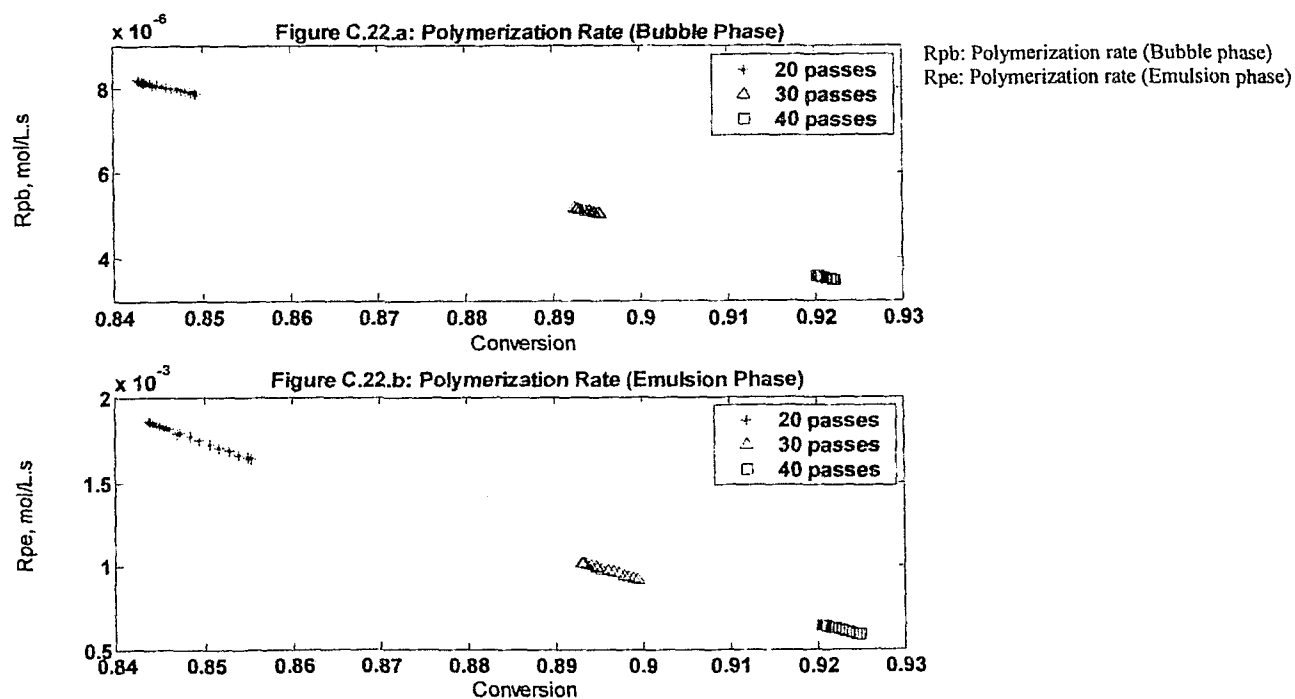
Appendix D: Dynamic Model Supplementary Figures

Figure D.1: Profile of catalyst concentration versus time at the exit of the bed (one pass and isothermal)
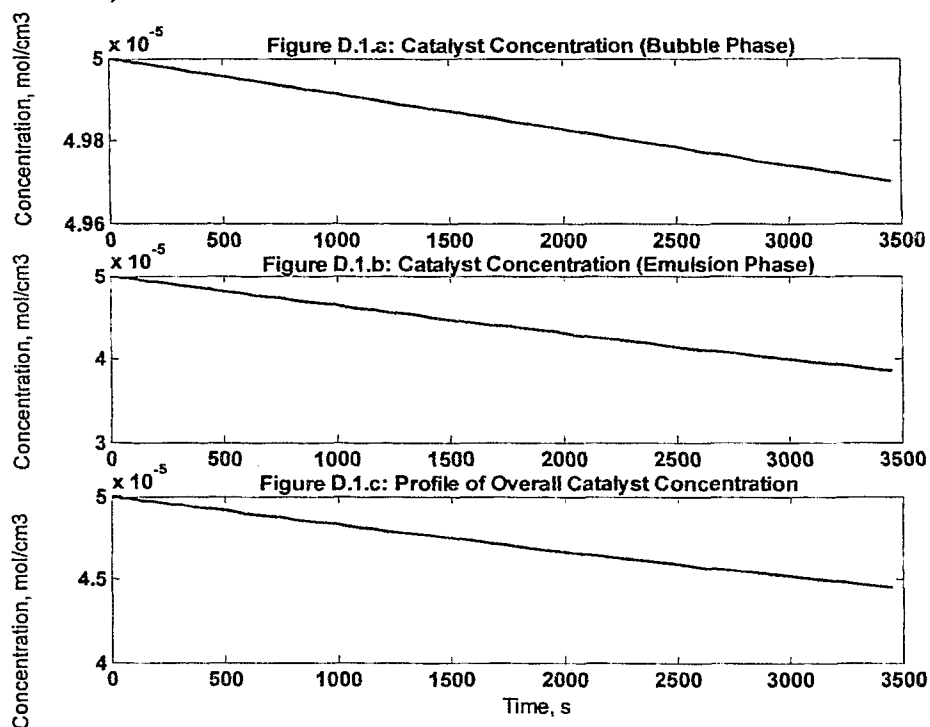

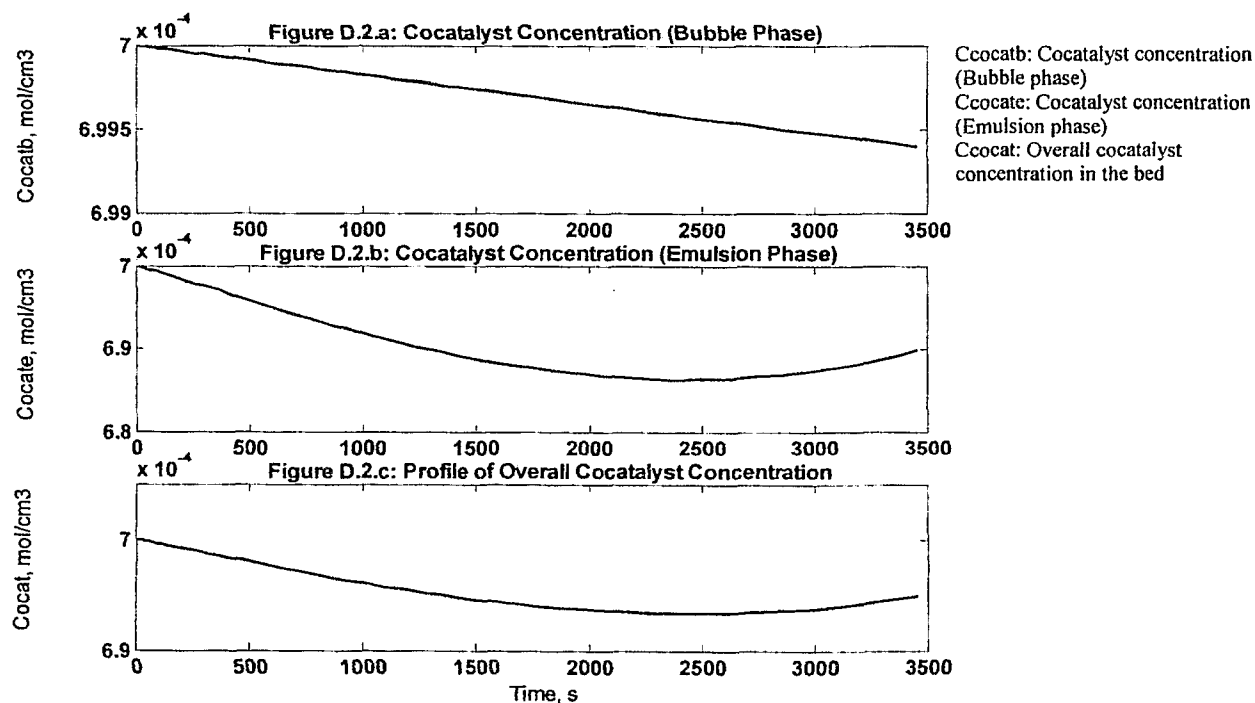Figure D.2: Profile of cocatalyst concentration versus reactor axial position (one pass)

Ccocatb: Cocatalyst concentration
(Bubble phase)
Ccocate: Cocatalyst concentration
(Emulsion phase)
Ccocat: Overall cocatalyst
concentration in the bed

114

Figure D.3: Profile of hydrogen concentration versus reactor axial position (one pass and isothermal)

Figure D.3.a: H2 Concentration (Bubble Phase)
Figure D.3.b: H2 Concentration (Emulsion Phase)
Figure D.3.c: Profile of Overall H2 Concentration

CH2b: H2 concentration (Bubble phase)
CH2e: H2 concentration (Emulsion phase)
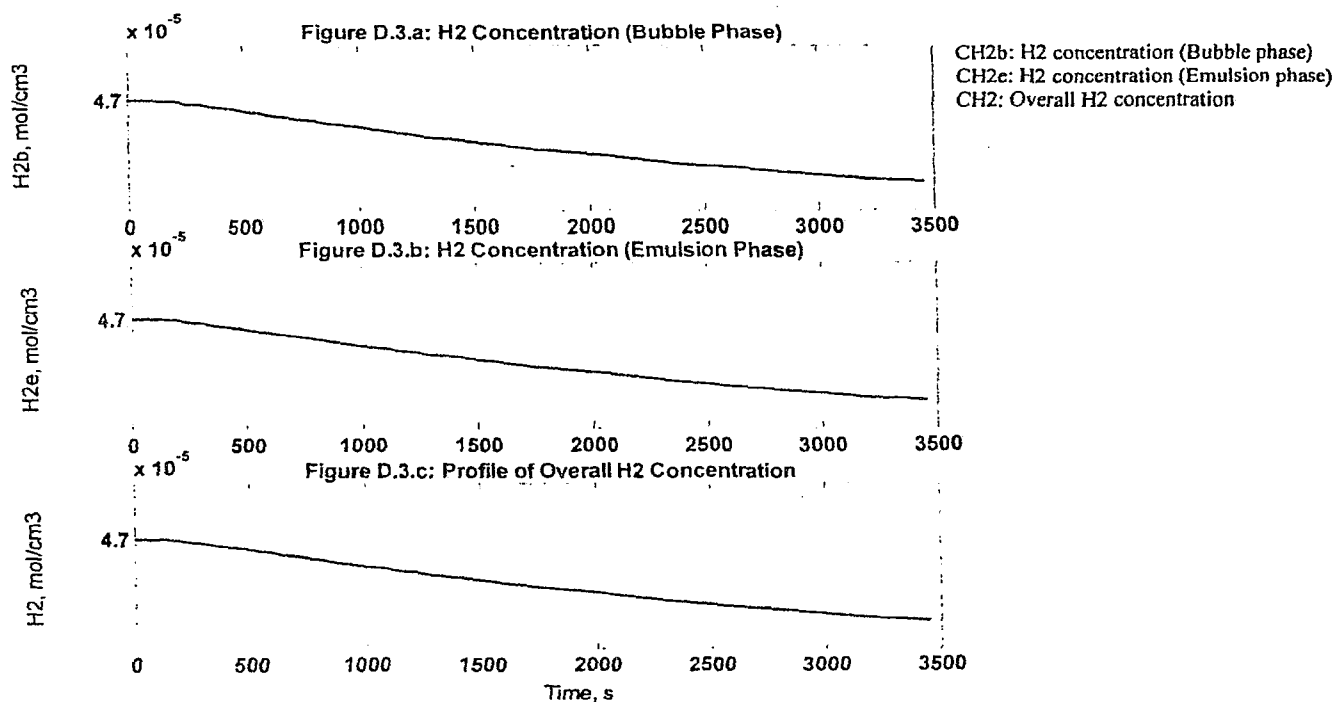CH2: Overall H2 concentration

Figure D.4: Profile of polymerization rate versus conversion (one pass and isothermal)

Figure D.4.a: Polymerization Rate (Bubble Phase)
Figure D.4.b: Polymerization Rate (Emulsion Phase)

Rpb: Polymerization rate (Bubble phase)
Rpe: Polymerization rate (Emulsion phase)

115